Republic of Iraq
Ministry of Higher Education
and Scientific Research
University of Babylon

Fluid – Solid Interaction on the Mixed Convection of Nanofluid flow with Hexagonal Solid in Open Cavity

A Thesis

Submitted to the College of Engineering, University of Babylon in Partial Fulfillment of the Requirements for the Degree of Master of Science \ Engineering\ Mechanical Engineering \ Power

By

Haider Najem Obaid Hajwel

Supervised By

Assist. Prof. Dr. Hameed K. Hamzah

2021 A.D ***1443 A.H***

بسم الله الرحمن الرحيم

اقْرَأْ بِاسْمِ رَبِّكَ الَّذِي خَلَقَ ﴿١﴾ خَلَقَ
الْإِنْسَانَ مِنْ عَلَقٍ ﴿٢﴾ اقْرَأْ وَرَبُّكَ الْأَكْرَمُ
﴿٣﴾ الَّذِي عَلَّمَ بِالْقَلَمِ ﴿٤﴾ عَلَّمَ الْإِنْسَانَ
مَا لَمْ يَعْلَمْ ﴿٥﴾

صَدقَ ٱللَّهُ العلي العَظيم

سورة العلق

Certification

I certify that this thesis entitled **" Fluid – Solid Interaction (FSI) of Elastic – Step Type Corrugation Effects on the Mixed Convection of Nanofluid with Hexagonal Solid in Open Cavity with Magnetic Field "** has been prepared by "***Haider Najem Obaid Hajwl***" under my supervision at the department of Mechanical Engineering, College of Engineering, University of Babylon as a partial fulfillment of the requirements for the Degree of Master of Science in Mechanical Engineering / Power.

I recommend that this thesis be forwarded for examination in accordance with the regulation of the University of Babylon.

Signature

Assist. Prof. Dr. Hameed K. Hamzah
Department of Mechanical Engineering
College of Engineering
University of Babylon/Iraq

Data: / / 2021

Dedication

*To the owner of the big heart, the reason for my existence, and the crown of time, **(my dear father)**, may God have mercy on him ….*

*To my dear angel, house of mercy and warm embrace, **(my mother)** , may God prolong her life and make her a tent for us .....*

*To the companion of the path and life, to my firm rib that does not tilt. Aba Haider, **(Dr. Amir Najm)**, may God have mercy on you, my brother ….*

*To the light that illuminates my life, the strong bond, and the spring with which I drink love and tenderness, my brothers **(Wesam + Firas)** ….*

*To whom I looked at her, she made me happy, and if I commanded her, she obeyed me, to my second half, my wife and the mother of my children **(Safaa)** ….*

*To the family treasure, two pieces from my father and mother, my dear sisters **(Enas + Sally)** ….*

*To **my pulse** ….*

Haider 2021

Acknowledgments

Praise be to Allah for the mercy, blessing and assistance during the preparation of this work.

I would like to express my deep thanks to my supervisor ***Assist. Prof. Dr. Hameed K. Hamzah*** *for his scientific and moral support, everlasting guidance and endless inspiration. His assistance and sage advice have been invaluable to be of significant inputs to this study.*

I would like also to submit my thanks to all staff members of the Department of Mechanical Engineering at University of Babylon, Head of the Department ***Prof. Dr. Samer Mohammed****, for his constructive contribution to this study .*

My thanks also are extended to all my colleague ***M.Sc. students****, with a special feeling of gratitude.*

Finally, I owe all my successes to ***my family****, with a special feeling of gratitude given to* ***my father****, may God have mercy on him, my brother* ***Dr. Amir Najem****, may God have mercy on him.* ***my mother****, my brothers* ***(Wesam and Firas)****, my wife* ***(Safaa)****, sisters* ***(Enas and Sally)*** *and my children* ***(Amir, Reda and Dura)****, may God grant them long life for their encouraging and persevering words in my ears.*

Haider 2021

Abstract

This study numerically investigates a solid-fluid reaction (FSI) in the control of mixed convection within a square cavity using gradient hot flexible walls in the form of steps. Also the effects of magnetic field angle, and hexagonal shape at different locations in the nanofluid (CNT-water) with Prandtl number (Pr=6.9), the two-dimensional flow, Newtonian, incompressible, laminar was assumed and the study was achieved under unstable condition.

The governing differential equations governing fluid and structure were solved using the finite element method (Galerkin) within the Arbitrary Lagrangian-Eulerian (ALE) using the software (COMSOL Multiphysics ver. 5.5). The study criteria represented the effect of Re = (100 and 500), magnetic inclination angle ɣ= (0° and 90°), Hartmann number Ha = (0 and 60), concentration of nanofluids φ = (0 to 6%) and modulus of elasticity E = (10^4 and 10^8) where the Rayleigh number was constant for all study is Ra=10^5.

In this position of the results showed that the best position of the solid body at (x = 0.5, y = 0.7). The cavity contains the largest value of Nusselt number, where the percentage was 5% more than the cavity that does not contain a solid body, and the effect of increasing the average Nusselt number with the increase in the concentration of nanofluids. And the best magnetic inclination angle was when it was zero, because the magnet is in the direction of the flow and this leads to the smashing of the vortices. When the Hartmann number increases, the heat transfer becomes more efficient.

When using a flexible hot wall works to improve heat transfer, so that the improvement in the average Nnsselt number when using a flexible hot wall at conditions (Re=300, Ha= 25, φ=0.02 and E=10^4) is about more than

22% compared to in the solid wall, it was also found that the average Nusselt number increases with the elasticity of the elastic hot wall.

The establishment of the entropy and the alpha number for different cases is investigated. Sgen,μ decreases with increasing E due to decreased fluid mobility. While Sgen,T decreases with increasing E due to the increase of convective heat transfer.

Nomenclatures

Symbol	Meaning	Unit
$u_\circ$	Uniform velocity	m^2
T	Temperature	k
H	Length cavity	M
w	Ports sizes	M
h_1	Size of wall below the inlet port	M
N	Number of steps corrugation	---
a	Length of hexagonal solid	M
l	Height of hexagonal solid	M
k	Thermal conductivity	$W/m.^0c$
h	Convection heat transfer coefficient	$W/m^2.^0c$
$B_\circ$	Magnetic field strength	$\frac{v.s}{m^2}$--
v	volt	
E	Young's modulus	N/m^2
u , v	x-y velocity components	m/s
Q	Heat transfer rate	J\S
S	Entropy	J
c_p	Specific heat at constant presure	J/kg.k
p	Pressure	Pa
F	Force	N
n	normal vector	---
m	iteration number	---

Greek Symbols

Symbol	Meaning	Unit
μ	Dynamic viscosity	(Pa.s)
φ	Nanoparticles volume concentration	(%)
γ	Magnetic inclination angle	degree
β	Thermal diffusivity	m^2/s
θ	Non-dimensional temperature	----
ρ	Density	(kg/m^3)
ν	Kinematic viscosity of the fluid	m^2/s
α	Thermal diffusivity	m^2/s
σ	Stress tensor	N/m^2
∇	Cartesian coordinate vector	M
τ	Time period	sec
ξ	Independent variables	----

Subscripts

Symbol	Description
c	Cold fluid
h	Hot fluid
ave	Average
loc	Local
nf	Nanofluid
bf	Base fluid
p	Solid particle
s	Solid
v	Volume
f	Fluid
r	Density ratio
in	Input
eff	Effectiveness
Cond.	Conduction
conv.	Convection
i	Interface region
gen	Generation
m	Iteration number
$*$	Dimensional parameters

Abbreviations

Symbol	Description
CNT-water	Carbon-nanotube/water
FSI	Fluid-structure interactions
MHD	Magnto-Hydrodynamics
CFD	Computation Fluid Dynamic
ALE	Arbitrary Lagrangian Eulerian
MEMS	Micro-Electro-Mechanical Systems
FEM	Finite Element Method

Dimensionless Numbers

Symbol	Definition
Ri	Richardson number represents the ratio of natural convection to the forced convection.
Gr	Grashof number the ratio of the buoyancy force to the viscous forces acting on the fluid.
Re	Reynolds number represents the ratio of the inertia forces to friction forces in the fluid.
Ha	Hartmann number is the ratio" of electromagnetic "force to the viscous force.
Pr	Prandtl number is the ratio of kinematic viscosity to the thermal diffusivity.
Nu	Nusselt number is the ratio of convective to conductive heat transfer across a boundary.
Be	Bejan number is the ratio of heat transfer irreversibility to total irreversibility due to heat transfer and fluid friction

Table of Contents

CHAPTER ONE

INTRODUCTION

Chapter One :Introduction

1.1 Introduction

The heat transfer enhancement is a method of a great importance in the field of industry and technology. It expresses itself in various forms (conduction, convection, and radiation) **[1]**. The heat transfer by convection from one place to another is a 'heat transfer by fluid movement **[2]**. It is usually the dominant form of liquid heat transfer. While typically described as a distinct method of heat transfer, it does include combined processes of unknown' conduction and advection (the combined heat diffusion process). The types of convection heat transfer can be classified as in figure (1-1).

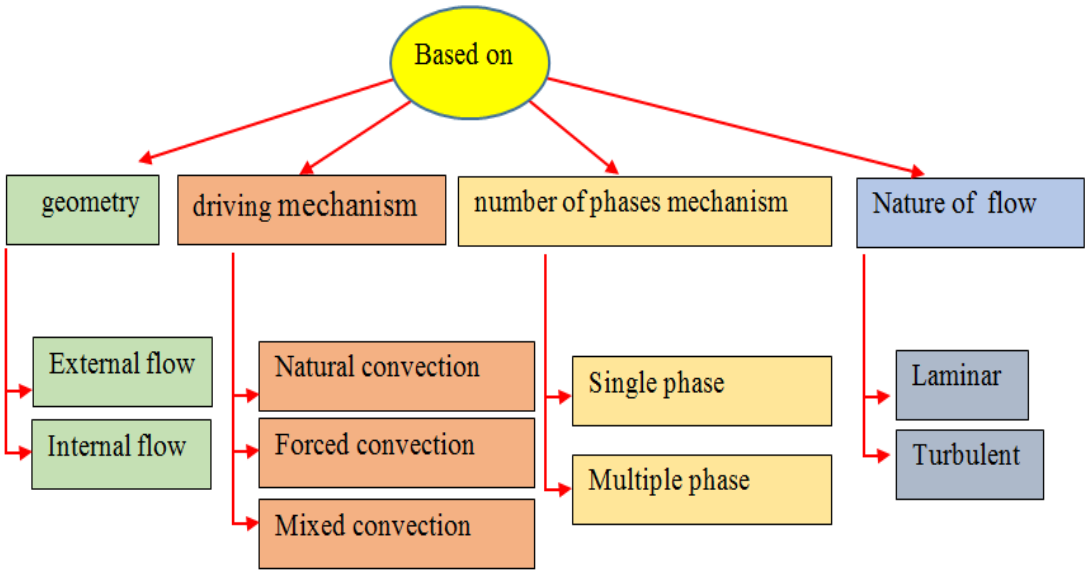

Figure (1- 1) classification of convection heat transfer

1.2 The classified according the driving mechanism into: -

Natural convection: It happens when the fluid movement is produced by the buoyancy forces resulting from density variation in fluid temperature variations **[3]** .

Forced convection: It happens when a fluid is forced to flow over the surface from an external source such as pumps and fans creating a convectional current artificially created.

Mixed convection: It happens both when the natural and the forced convection happen simultaneously **[4]**.

1.3 Mixed Convection Heat Transfer in Cavity

The mixed convection cavity, which have been the subject of interest in numerous research studies. This type can be constructed by a combination for both free and forced convection. In another word, when the pumping force effect on the buoyancy force. Also, that constructed by any external factor is represented by the movement one or more walls of the cavity, rotating the cylinder or any geometry inside the cavity and found the pump or fan that effects on the current flow. Under the interaction between the natural and forced convection, it essential to find an indication of the relative magnitudes of convection. In mixed convection flow in the cavity, Richardson number ($Ri = \frac{Gr}{Re^2}$) . This criterion is used to distinguish the following three flow regions inside the enclosure.

Ri >> 1 (Pure natural or free convection)

Ri = 1 (Mixed convection)

Ri << 1 (Pure forced convection)

In a ventilated cavity, where there are complex variations possible due to the interaction between the forced outer stream provided by the inlet and the buoyancy-driven flows caused by the heat source. As a result, understanding the fluid flow and heat transfer characteristics of mixed convection in a vented cavity is important.

1.3.1 Mixed Convection Applications.

Many researchers have been interested in studying the mixed convection heat transfer in different enclosures because of its wide applications in various systems such as cooling of electronic, solar collectors, heat exchangers and nuclear reactors, etc. as depicted in figure (1-2).

Figure (1- 2) Liquid cooled heat sink

Image from: https://www.electronics-cooling.com

1.4 Nanofluid Concept and Applications

A nanofluid is a new category of thermal transfer fluids developed with the scattering in conventional thermal transfer fluids with metallic/non-metallic nanoparticles of less than 100 nm. Nanofluids typically consist of metals, carbides, oxides or carbon nano-tubing, which are employed for the production of nanofluids. Basic fluids also include water, oil and other materials, bio-fluid, solutions for polymers, ethylene or triethylene and other coolants. **[5]**

Nanofluids, including fuel cells, medicinal, and hybrid-powered automobiles, engine vehicle cooling, refrigeration, heat exchanger types, Nano clastic and boiler flue gas temperature reductions as detailed by Xuan and Qiang **[5]**, are used in various applications.

Spherical nano particles grinding are mostly used in nanofluids preparation. Also, heat exchanger rod-shaped, tube-shaped and disk-shaped nanoparticles are used. When particles have rod or tube shape, they are always less than 100 nm in diameter but may have a micrometer length. And this particle can form size clusters according to description. **[6]**

Increasing nanofluid parameters such as thermal conductivity, density, and viscosity can increase the heat transfer process efficiency. The transfer of heat from a tube to the wall of a tube through forced convection is discussed when nanofluids flow in a tube. It is expected to be the same as the improvement in thermal conductivity of the nanofluid by utilizing a nanofluid. This is because the heat transfer factor and friction factor are increased.

1.4.1 Advantages and Disadvantages of Nanofluids

The main reasons to improve the heat transfer performance of the fluid by suspending nanoparticles in base fluids may be listed as follows. Advantages and disadvantage of nanofluids are tabulated in Table (1-1).

Table (1- 1) Main Advantages and Disadvantages of Nanofluids [5]

	Advantages	**Disadvantages**
1	The suspended nanoparticles in the main fluid increase, contact surface area, viscosity, density, and effective thermal of the fluid.	Low specific heat compared to main fluid.
2	The nanoparticle dispersion flattens and transverse temperature regression of the fluid.	Problems in the production process

3	The turbulence and mixing of oscillation of the fluid increase the temperature distribution of the main fluid.	The high cost of nanofluids, the high cost of producing nanofluids are among the reasons that may hamper the application of nanofluids in industry.
4	Breaking down the sub-layers that are created near the wall through the tube.	
5	Collision between the particles, the fluid and the wall surface increase the temperature distribution in the main fluids.	

1.4.2 Applications of Nanofluids

The followings are some applications of Nanofluids: **[5]**

1. Transportation (Engine cooling/vehicle thermal management).
2. Electronics cooling (Cooling of computers and servers with high performance).
3. Nuclear cooling systems (Primary water reactor coolant (PWR) and safety system emergency systems)
4. Reduction of boiler gas flow temperature Energy efficient cooling, building heating without additional heating, ventilation and air conditioning pumping power.
5. Enhance heat transfer in heat exchangers.
6. Industry of biomedicine. For example, traditional technique of cancer treatment kills cancer cells, radiation is drug-free and cools the brain.
7. Other applications (Fuel cell cooling, solar heating system, combustion system, Air condition and Refrigeration systems, …etc.)

1.5 Fluid-structure interaction (FSI)

The phenomenon of fluid –structure interaction is the combination of laws that describe fluid mechanics and structure mechanics. What distinguishes this phenomenon is the interference, which can be steady or

fluctuating between a flexible body or a moving structure and a fluid flow around or inside the flexible structure.

When the fluid circled around a flexible body or flow inside it, it exposes the body to stresses and strains that cause deformations. These distortions can be very enormous or very slight depending on several factors including fluid pressure and flow velocity as well as the material properties of the flexible structure.

If these abnormalities are very small and the change over time is relatively small, the boundary conditions of the fluid flow will not very have affected by those distortions and it can focus on the resultant stresses that get to the flexible structure only.

If these distortions are significant, the pressure and velocity fields will change and therefore this problem should be treated as dual effect, the fluid pressure and flow velocity affect the flexible structure causing deformations, in turn, the distortions that get to the flexible structure affect and change the boundary conditions of the fluid **[7]**.

1.5.1 Fundamental of fluid-structure interaction

Fluid-structure interaction is a multiphasic interface phenomena appear in systems where fluid influences distortion of a rigid structure which, in turn, changes the conditions of the fluid. Thereafter an elastic structure which is in contact with fluid flow is exposed to a force (pressure) that causes distortions in the solid structure. And in response, the distorted solid structure modifies conditions of the flow domain. Eventually, the changed fluid applies different pressure form on the solid structure. Thus, the procedure is repeated again. This form of interference is termed as Fluid-Structure Interaction (FSI). **[8]**

FSI can happen in numerous areas of engineering, and is an essential aspect in the manufacturing of numerous engineering systems. It is available in several forms, both in natural systems as well as in artificial systems. The interference such as branches of tree with wind and groundwater interference with the earth are characteristic models in nature. Fluid-structure interference for engineering systems occurs in simulation manner of offshore platforms with the ocean, flight features of airplanes, and dams with containers. Although there are different forms of interaction and different nature between the structure and fluid in the mentioned problems, all the problems drop within the Fluid-Structure Interaction. **[8]**

Another examples of fluid-structure interaction are; constancy and response wings of the aircraft in space engineering, blood flow through arteries and veins in medical applications has become a major concern these days, reaction constructions like high buildings and bridges to winds effect in civil engineering, and vibration of heat exchangers devices in nuclear manufacturing and pressure reservoir.

While all these interactions are significant in many domains of technology and production, due to their robust non-linearity and the multiphysical interaction nature, proper understanding of fluid structure interactions is still a true challenge. Furthermore, FSI issues are often not difficult to explain analytically and hence must be examined by numerical approaches. For instances in which empirical work is inefficient, reasonable and long-term, numerical approaches of these integrated applications are increasing.

These applications need big calculating period and also need a new steady and precise algorithm to resolve problems. During the recent years, due to the great technological development in the performance of computers

and algorithms has enabled it to solve such problems. Moreover, resolving several physical problems that were not reachable in the early times.

Using numerical methods can be useful to reduce the wasted time on empirical methods to compute a big number of manufacturing options. The best way to understand the problem is attained through a computational method since of augmented quantity of data assembled through calculation process. There is incessant study in the areas of fluid dynamics and structural mechanics. Therefore, it has reached a high level to assistance in resolving big manufacturing and engineering problems that were not reachable in the last years **[7].**

Find out how an elastic structure combines to its fluid flow environment may produce unique engineering visions, and aids enhance our find out of numerous natural phenomena. FSI can be steady or vibratory. In vibratory interference, the strain produced in the structure causes it to transfer such that the basis of strain is minimized, and the solid structure back to its original state merely for the procedure to repeat again.

1.6 Linear elastic materials

Linear elastic material describes each body that can bend without being broken or damaged. When a solid object is exposed to natural or forced forces, it causes deformities in the body, resulting in a change in the shape of the body. However, once these forces are removed, the body returns to its original form. Many scientific applications and engineering devices contain flexible parts including flexible fins in heat exchangers, microelectronic cooling systems, solar panels, and medical devices such as heart valves, blood pumps **[7].**

1.7 Magnetic Field (MHD)

The academic topic of Magneto-hydrodynamics (MHD) analyzes dynamics in electrical conduction areas. For example, plasmas, liquid metals and salt water are such fluids. The word Magneto-hydrodynamics (MHD) comes from a movement magneto that means magnetic field, hydro that means liquid and dynamics. Hannes Alfven established the field of MHD, for which the Novel Prize in physics was awarded in 1970. The notion of MHD is that magnetic fields can drive a flowing fluid, generating fluid forces and thereby altering the magnetic field. The set of MHD equations are a mix of fluid dynamic equations from Nevier-Stokes and Maxwell's electromagnetic equations. Simultaneously, analytically or numerically, these difference equations must be resolved. MHD is a continuum theory that cannot therefore handle kinetic phenomena, i.e., which are significant in terms of the existence of discrete particles or the distribution of non-thermal velocities. The simple version of MHD, ideal MHD, proposes that the fluid has so small levels of resistance that the perfect conductor may be treated. This is the end of the magnetic endless Lenz law specifies that the fluid is in some respect connected to magnetic field lines, as the Reynolds number is in ideal MHD. Some of the effects of MHD on specific sectors are now:

1. MHD can create force without connection between two different media.
2. MHD is the science branch that is involved in the flow of fluids in electricity and magnetism.
3. This electromagnetic force generated the same order of magnitude as the hydro-dynamical & inertia force. The equation of motion takes this force.
4. MHD applied to astrophysical and geophysical problems. Such as the motion of the sea induce magnetic field that perturb the earth’s magnetic field. The electromagnetic force due to the interaction of currents and earth’s magnetic field propels ocean movement.

5. Engineers make use of MHD in their design of the heat exchanger, pumps and flow metals etc.

1.8 Entropy Generation

Entropy in closed but changing systems, a system where energy transfer is carried out only to one direction, is defined as the degree of disorder. The criteria for the performance of engineering machinery include entropy generation, which is the irreversibility of a process. Thanks to entropy production, thermodynamic efficiency of the system is diminished. Entropic analysis shows us what section of the physical model or system energy is more dissipated. Bejan investigated the basics of minimizing entropy production. The influence of MHD on the transfer of heat as well as entropy in a cavity filled with nanofluid is mostly investigated. An increase in the volume percentage of nanoparticles has been shown to improve the average number of nutrients and entropy. It primarily depends on the magnetic field's strength and inclination angle. **[9]**

1.9 The aims of the thesis

The study of heat transfers within several engineering geometries (square, rectangle, triangle, etc.) that include ventilation openings has taken a large deal of interest of the researchers in recent years. When a flexible structure is immersed in a fluid, the fluid pressure forces impinge on the body and vary its shape temporarily. In line, the change of the structure generated by fluid flow also affects the flow field and adjustments the boundary conditions of the fluid domain. This interaction between the fluid and the solid structure is found in many applications of engineering, natural and industrialized. Therefore, this work was concentrated to analysis the heat transfers and fluid flow fields in a square cavity with two openings for towards the inside and leaving fluid and having a flexible elastic wall with different step installed to demonstrate and achieve the following objectives:

1. Utilize of flexible wall with free displacement to govern the mixed convection heat transfer rate in various engineering and industrial applications.
2. Study the effects of the fundamental flow parameters such as (Reynolds number, (modulus of elasticity), and (number of step) on the flow and heat transfer rate enhancement.
3. Study the effect of Hartman number and entropy generations on the flow and heat transfer rate enhancement.
4. Study the location of hexagonal in cavity and its effect on the flow and heat transfer rate enhancement.

1.10 Outline of the Thesis

This work is divided into five chapters.

Chapter One: provides an overview of the problem.

Chapter Two: deals with a review of the literature.

Chapter Three: focuses on theoretical and CFD analysis to compute the range of nano Fluids, the Hartmans (elasticity module) and the rates of flow of volume in space and temporal pressures, temperatures and speeds. The theoretical analysis is based on solution and computer program methods designed for the performance of all calculations.

Chapter Four: deals with result and discussion. In this chapter deals with (validations) comparison between the Results of recent researchers and theoretical results.

Chapter Five: discusses the findings of this study and the suggestions for further work.

CHAPTER TWO

LITERATURE REVIEW

Chapter Two: Literature Review

2.1 Introduction

In recent years, the nanofluid has been appeared as an alternative heat transfer fluid for heat transfer applications showing a significant possibility for the heat transfer enhancement. The fluid structure Interaction (FSI) convective heat transfer of nanofluids has relatively been less acclaimed in literature, therefore the number of the publications dealt with this subject were limited and exclusive. The purpose of the literature review is to summarize the previous work closely related to the present works. Their works mainly deal with the background on the enhancement of heat transfer coefficient, Nusselt number, velocity distribution, and physical properties by using nanofluids. It is presented in two main sections, the first is the numerical studies of heat transfer improvement by using nanofluids in mixed convection laminar flow through cavity and the second section is the numerical studies including the effect of entropy, Bejman number with FSI and Ha.

2.2 Previous Studies

Angirasa,2000 [11] explored Mixed convection flow in an isothermal vertical wall enclosure. Forced flow conditions are obtained by an inlet at the lower part of the isothermal surface and an airflow at the top that faces the intake. The differences in temperatures between the wall and the stream are responsible for buoyancy. Detailed examination is made of the interplay between buoyancy and forced flow. Temperature potentials are considered both positive and negative. The heat transfer rises at the lower Grashof values in either direction as the forced flow increases. The relationship becomes highly complex with greater absolute values of the Grashof number. The fluctuation of the ratio, Gr/Re^2, shows an anomalous

heat transfer behavior. The associated flux and thermal fields are discussed and local and average Nusselt number values are shown.

Iwai et al., 2000 [12] stimulated the effects of the aspect ratio of the duct, and flows across a reversal step at Reynolds low. Numerical results have been compared with other studies and the experimental data have been agreed satisfactorily. The pattern of the Nusselt number and of the coefficient of skin friction on the bottom wall have also been closely observed. A size ratio of AR = 16 was determined to be at least required for a 2D region near the center line in Re = 250. It was found, for the lower Reynolds, this 2D region has become wider. It was also determined that on the centerline but near the two side walls in each case the largest number of Nusselt appeared.

Abu-Mulaweh, 2003 [13] examined the result of the flow and heat transfer of the vertical, horizontal, and reclining backwards and forward-facing single-phase laminar mixed convection flow described in many open literature research. The aim of this study was to provide a complete review of the effects on stream flow and thermal fields downstream of various parameters, including step height, Reynolds number, Prandtl number, inclination angular, expansion ratio, temperature differential of a heated wall and free stream. The study also summarizes several correlation equations reported in many of these investigations to estimate the reattachment length of the recirculation areas, which can grow upstream and/or downstream.

Saeidi and Khodadadi, 2006 [14] examined the square cavity with inlet and outlet ports, a finite-volume calculation of steady laminar forced convection. The position of the outflow port was different along four walls of the cavity due to the fixed position of the input port. The ports have a width equivalent to 5%, 15% and 25% on the side. A total of 108 cases were analyzed when the exit ports were positioned at 9 places on the walls for

Re = 10, 40, 100 and 500 and Pr = 5. At the interface of the through flow and near to solid walls on both sides of the outflow port, regions with a high temperature gradient are regularly seen. The local Nusselt numbers were low at three corners when there was no outlet port adjacent, however on both sides of the outlet port there was an intense thermal transfer rate. The local Nusselt numbers might fluctuate greatly depending on the flow and the temperature fields between these minimum and maximal. The largest overall Nusselt number can be attained if the outlet port is placed on 3 corners at one end. The outlet port situated at the center of the walls ensures the minimal overall heat transfer of the cavity. If the outlet port was positioned on a dimensionless wall co-ordinate (+ 0,5W), a maximum heat transfers and the minimum pressure drop was observed.

Abbassi & Ben Nassrallah, 2007 [15] investigated The laminar flow of an electrically driving viscous fluid in a step backwards, under the usual premise of the magneto hydrodynamic (MHD). For the number of Reynolds less than Re = 380 within the range $0 \leq N \leq 0.2$ where N was the Stuart number or interaction parameter that was the ratio of the electromagnetic force with the inertia force, numerical simulations are carried out. The heat transmission of Prandtl from Pr from (0.022 – 7) to water was examined, corresponding to liquid metal. It was determined that the external magnetic field reduces the size of the recirculation zone by calculating the connection length. Velocity profiles demonstrate that the basic flow was dampened by the induced magnetic field outside the recirculation zone while the flow was accelerated close to the wall channel. In the case of high Prandtl fluids, heat transfer was considerably increased by the magnetic field.

Velazquez et al. 2008 [16] described the effect on the heat transfer rates behind a reverse face step of the unstable laminar 2-D system that the prescribed flow pulsation (defined by two control parameters: velocity

pulsation frequency and pressure gradient amplitude at the inlet section), has on the heat transfer rate behind a backward facing step in the unsteady laminar 2-D regime. The working fluid that we have considered was Water with temperature-dependent viscosity and thermal conductivity were the working fluid we considered. We observed that the time-averaged Nusselt number behind the step depends on the above two control parameter, and always was higher than in the steady-state case, for pressure gradients that prevent flow reversals at both the downstream and upstream boundary conditions. At Reynolds 100 and pulsating at the resonance frequency, the maximum Nusselt average time was 55 percent longer than in a steady-case, in the horizontal wall behind the step with a length of four times the step height. The time-averaged Nusselt number smoothly drops and comes near was constant state value apart from the resonant pulsation frequency.

Khanafer et al.,2008 [17] studied the laminar pulsatile mixed convection and heat transfer over the reverse channel step. A finite element approach based on the weighted residual Galerkin method was used to distinguish the governing equations. For different relevant dimensionless groups, temporary fluctuations were given in streamlines, isotherms and dimensional coefficient of skin friction and the Nusselt number. In the area of Reynolds number, Richardson number and dimensional oscillation frequency the following characteristics were explored: $100 \leq Re \leq 1000$, $1.78 \times 10^{-3} \leq Ri \leq 10$, and $0.1 \leq \pi \leq 5$. The following: The fluid flow and thermal transfer characteristics wre examined. During this experiment, the working fluid was given a Prandtl value of 0.71. Our results show that the Reynolds number, Richardson number and dimensionless oscillation frequency have a profound effect on the structure of fluid flow, heat transfer fields, and skin friction coefficient.

Khalil Khanafer 2014 [18] examined steady laminar, mixed convection flow and heat transfer In the driven cavity with a flexible heated bottom surface. The rectangular or sinusoidal wavy profiles for rigid wall analysis characterize the heated bottom wall. To resolve transport equations, using a finite element formulation based on the weighted residuals Galerkin approach. The results showed that the increase in heat transfer was observed with a flat base wall case in all of the cases studied in comparison with the flat bottom wall case in Grashof number 10^4 and in Re < 400 the flexible bottom wall case was found to have showing significant heat transfer improvements (61.4 %). However, the wavy rectangular profile was increased by heat transfer (maximum: 14.4% in Re = 200) compared to wavy sinusoidal (9.6% in Re = 200) and flexible bottom wall (12.3% in Re = 200).

Fatih Selimefendigil and Oztop, 2014 [19] Numerically[2] investigated the controlling on heat transfer and fluid flow in laminar pulsating flow over a backward -facing step by using of a square obstruction put behind the step. The operating fluid was 0.71 Prandtl Air with a 10 and 200 Reynolds Number. They analyzed at three vertical positions of the square obstruction and various frequencies of the inflow. Using a commercial code based on finite-volume, Navier stocks and energy equation for 2D laminar flow were solved. The duration and intensity of the recirculation zone behind the step was substantially affected by correctly positioning the square obstacle, which can therefore be employed as a passive check element for heat transfer increases. In two different vertical points of the barrier, improvements in maximum values of Nusselt number 228 % and 197% were achieved. On the other hand, two square obstacle sites were efficient in the Reynolds 200 pulsating flow scenario compared to the case without obstacle for heattransfer increase with pulsation.

Fatih Selimefendigil and Öztop 2015 [20] used a backward facing step to accomplish laminar forced convection of nanofluid flow for various magnetic field inclination angles. The channel's bottom wall downstream of the step was isothermally heated, whereas the other sides were believed to be adiabatic. The governing equations were solved using the finite element method. The averaged heat transfer was observed to rise as the Reynolds number increases, and this impact was more pronounced with larger values of the magnetic field's inclination angle. The averaged and local enhancement of heat transmission were seen when the value of the Hartmann number decreased for horizontally oriented magnetic field and the volume percentage of the nanoparticles increased. As the value of Ha grows in the inclined and vertical magnetic fields, the recirculation zone behind the step was suppressed, resulting in increased heat transfer. For a horizontally oriented magnetic field, the total entropy generation ratio increases as Reynolds number, solid volume fraction of nanoparticles, and Hartmann number decrease.

Gallegos and Sharma, 2016 [21] investigated the dynamic behavior of a flexible plate constrained between two parallel walls behind a cylinder. The obstruction effects were studied in this two-dimensional fluid-structure interaction problem for four different cylinder sizes. The effect of cylinder size and blockage ratio (ratio of cylinder diameter to channel width), which ranged from 0.05 to 0.49, on the plate tip oscillation amplitude and frequency was investigated. The combined impacts of obstruction and cylinder size have a significant impact on the plate tip's oscillation amplitude and frequency. The findings imply that altering the blockage and cylinder size can affect the plate's dynamic behavior.

Mehryan et al. 2017 [22] Used finite element method with arbitrary Lagrangian-Eulerian (ALE) technique to analysis the natural convection inside square cavity with equally partitioned. They used a homogeneous magnetic field in various orientations. The obtained data revealed that the by using of a magnetic field well increases the temperature dimensionless for case of high values of the Hartmann numbers ($Ha \geq 50$) and moderate values of the Rayleigh number ($10^6 – 10^7$). The presence of a strong magnetic field, on the other hand, reduces the dimensionless average temperature when the Rayleigh number is high ($Ra = 10^8$).

Fatih Selimefendigil and Öztop, 2017 [23] investigated numerical solution for mixed convection of nanofluid filled lid-driven cavity by adding internal heat generation and a partially flexible wall. The triangle enclosure's bottom wall moves at a steady speed, and the left vertical wall is partially heated. The cavity's sloped wall was chilled and partially flexible. The impacts of the Richardson number (between 0.05 and 50), internal Rayleigh number (between 10^4 and 10^8), partial flexible wall size and elastic modulus, and nanoparticle volume percentage (between 0 and 0.04) on fluid flow and heat transfer were studied computationally. It was discovered that as the Richardson number and internal Rayleigh number increase, the local and averaged heat transfer decreases. Local and average heat transfer improves as the inclined wall's elastic modulus and nanoparticle volume fraction increase. For decreasing values of elastic modulus of the flexible wall, the disparity between the mean Nusselt number increases for different diameters. It was preferable to add nanoparticles to the base fluid when the heat transfer mechanism was effective.

Mahalakshmi et al., 2018 [24] examined MHD mixed convection inside enclosure with central heater. The enclosure's opposing side walls were kept at a constant temperature, while the bottom wall has a constant

heat source. The bottom and top walls were maintained adiabatic for the rest of the time. To solve the governing equations, researchers employed the finite volume approach and the SIMPLE algorithm with a power-law scheme. The effect of relevant parameters such as heater length (Γ= 0.25, 0.50, and 0.75), Richardson number (Ri = 0.01, 1.0, and 100), Hartmann number (Ha = 0, 25, and 50), and solid volume fraction of nanoparticles on the fluid flow and heat transfer performance of the enclosure was investigated in this study. As heater length and Grashof number increase, heat transfer rate increases, however heat transfer decreases as magnetic field effect increases.

Fatih Selimefendigil and Ozotop 2018 [25] investigated nanofluid forced convection flow over backward facing step. The numerical solution by using the finite element method. They study with Re range from 25 to 250 (laminar flow) and elastic modulus from 10^4 to 10^6. Also they used nano fluid with range (0 - 0.035) solid particle volume fraction. The result was shown to increase the local and average heat rate as the value of Re or solid particle volume increases. At the higher Re, for the wall with the lowest elastic module value, the heat transfer rate was higher whereas the situation was reversed for other Re values. Nu_{ave}. reduces the flexible wall with the lowest elastic module by about 9.21% and increases by about 6.1 % compared with a rigid rear wall for 25 and 250, respectively. Increased heat transfer arises from added Nano additives to the base fluid. At the maximum solid particle volume fraction in comparison with nanofluid with a solid volume fraction of 0.01 for case with lowest and highest elastic module, average thermal transfer rates increase by around 35.72 % and 35.32 %

Sabbar et al. 2018 [26] explain the interaction between elastic walls and fluid flow in mixed convection through a cavity-channel. At the bottom of the cavity a discrete heat source was placed while the other walls were

thermally isolated. There was a channel flow on the top of the cavity. Arbitrary Lagrangian–Eulerian (ALE) approach to the interaction between the fluid and elastic walls were determined using a Finite Element method. In comparison with rigid cavity walls, the presence of the elastic wall enhances the heat transfer rate by 17%. Ri = 10 has been pronounced on the role of the elastic wall. With Reynolds and Richardson numbers increasing, the rate of heat transfer increases. When the numbers for Reynolds were risen from 50 to 250 in Ri = 0,1 and 100, respectively, 107% and 171% were increased in the number for Nusselt.

Alsabery et al., 2018 [27] Numerically examined unsteady natural convection with flexible oscillating heat conducting fin installed on the bottom adiabatic wall in a differentially heated oblique cavity. For the wall on the right, a constant temperature was maintained, while the wall on the left with an adiabatic heater, the fin was heated isothermally from the basis. In the central section of the base adiabatic wall was the thermo-conducting elastic wall. This study used governing parameters such as Young's modulus, the dimensionless time, thermal conductivity ratio between the heat conducting fin and working medium, the length of the left wall heater, and the inclination angle of tilted walls (-45 to 45 degrees). It was discovered that the oblique cavity had a major influence on fluid flow and heat transfer when it was implemented using the flexible oscillating heat-conducting fin. When E rises, Nu_f increases. It has the opposite effect, too. At the same time, the dimensionless Young's modulus reduces the Nu on fin wall.

Fatih Selimefendigil & Öztop, 2018 [28] was investigated in a round cylinder under the influence of a uniform magnetic field by means of a finite element technique of forced convection of CuO-water nanofluid. Two by two matrix: four circular cylinders in a channel kept at constant temperature. Effects on fluid flow and convection heat transfer were analyzed with

different appropriate configuration parameters, like the Reynolds number with range of (100 to 1000), Hartmann number (0 to 10), fraction solid volume (0 to 0.04) and a horizontal distance between circular cylinders. The employment of a magnetic field to minimize the wake zone behind the circular cylinder and increase heat transmission has been explored in the presence of nanoparticle inclusion in the base fluid. For moderate and higher Reynolds, the produced secondary peaks in the Nusselt number on the heated surface diminish in quantity with Hartmann and disappear with Hartmann numbers at the highest values.

Fatih Selimefendigil and Öztop 2019 [29] performed a numerical study for the effects of an inner stationary cylinder with an elastic rod such as an expansion on the CNT-water mixed nanofluid convection in a three dimensional ventilated cavity using the finite element technique. Effect of different parameters, such as Reynolds number (100 to 1000), flexible rod elastic module (10^5 and 10^8), elastic rod size (0,05H to 0,3H), circular cylinder size (0.025H to 0,25H), left vertical cavity slant angle (between 0 and 30) and solid volume slanting articles (between 0 and 4%), on the characteristic of convective flow It was found that when the obstacle (cylinder + elastic rod) was installed, geometric and other geometric characteristics (rod elasticity) changed, the varying multiple recircles and isothermals in the three-dimensional ventilated hollow were determined. With increased inclination angle of the cavity's sides the average heat transfer rate for the left vertical surfaces was degraded while the changes in the average heat transfer rate were small for the upper surface. The inclusion of the CNT nanoparticles leads to an average heat transfer improvement of about 60% in the highest solid volume of the nanoparticles and the increase rate was found independent of geometrical obstruction parameters, flexible wall elasticity and cavity angle of inclusion in the side surface.

Ismael 2019 [30] studied the interaction between the fluid-structure (FSI) and the forced heat transferal in the partially heated channel by continuous heat flux. The 2-D benchmarked geometry represented the FSI; a wall of the compliant section. The compliant section was bounded by two alternatives, upstream and downstream, which function as vortex generators. Arbitrary Lagrangian-Eulerian schemes, based on a finite element approach, have articulated the unstable issue. To assess channel performance, the thermal-hydraulic improvement criteria was calculated. Cauchy numbers and distortional lengths regulate the flexibility and strength of the compliant section, while Reynolds number is enforced to measure inertia and viscous forces' competing roles accordingly. The results show that the Nusselt number of a particular compliant confounded channel improves by 94% over a non-flapped channel with Re = 250. The thermal hydraulic study reveals that for Cauchy number 10^7 the greatest performance may be achieved with upstream and downstream baffles of 0.6 and 0.2 times the height of the channel, respectively.

Fatih Selimefendigil and Oztop 2019 [31] studied the Convection of CuO-water nanofluid numerically mixed in cavity, with ports of input and outflow, under the influence of inclined magnetic field and as an elastic corrugated wall. A method of finite elements is used to produce the numerical results of the simulation. For the description of fluid motion with elastic wall in the interaction model fluid-structure, the arbitrary-agrangian–eulerian technique was used. The current study evaluated the multi-step corrugation of the wall, which added further flexibility to regulate convective heat transfer characteristics of the vented cavity. Effects of various pertinent parameters such as the number of Reynolds (from 100 to 500), the number of Hartmann (from 0 to 50), the magnet angle (from 0 to 90°), the module flexible wall (from 5 to 10^4 to 8), the step like fraction of corrugation (from

1 to 8) and the volume of nanopartical (from 3 %) of the flux and thermal transfer features, It was noticed that the local numbers of Nusselt degrade for greater Reynolds, whereas variations in the local Nusselt number for lower numbers of Reynolds deteriorate or increase at different points along the hot wall. Variations in the magnetic fields and the number of steps like corrugation of the wall influence the numerous vortices in the ventilated cavity, but these effects do not affect the magnet angle. When Hartmann numbers rise, the average heat transfer drops to 30 and climbs with Hartmann numbers at their greatest value. With the inclusion of nanoparticles at the maximum volume in the absence and presence of a magnetic field, the average increase in the number of Nusselt is 9-9.5 %. Although the local Nusselt number fluctuates significantly if the number of steps such as corrugation rises,it typically deteriorates the average transmission of heat and the average Nusselt is 5.5% decreased if the number increases from 1 to 8.

Alsabery et al. 2019 [32] Focused on the transitory entropy generation and mixed convection. The effect of several important factors on the properties of the convective heat transfer and entropy production were examined without time dimensions.Application 10-8 $<\tau<$ 3.5. Depending on the non-dimensional elastic modulus of the right flexible wall and cylindrical orientation, several complicated wall deformations were identified. The local and mean numbers of Nusselt were increased with Ra, and for lower values of Ra secondary peaks have been set in the local number of Nusselt. For a chronological rotation of the heated cylinder, the local heat transmission along the thermal cylinder does not change despite a positive wall deformation in the x-direction. In the case of counter-clockwise rotation of the circular cylinder and lower levels of flexible wall deformation, the higher mean thermal transfer and global entropy generation rates were attained.

Fatih Selimefendigil and Öztop 2019 [33] Investigated The effects of the magnetic field in a branching channel with partially elastic walls. Weighed residual finite element technique, the governing equations solved by Galerkin. Effects of different factors like Reynolds Number (100-500), flexible wall elastic modulus (10^6-10^9), Hartmann Number (between 0 and 20), The flexible wall was shown to be efficient in redistributing different zones for the horizontal branching channel by its size and the elastic modulus. With the larger size of the elastic wall, the average Nusselt number decreases and the reduction range was between 8 and 9 %. The magnetic field suppresses the individual flow areas and raises the mean heat transfer rate. Nusselt average improvements in the number were 33.9% and 12.5 %, when the configurations for the absence and presence of magnetic field were compared (at greatest intensity) for lower and upper thermal channel walls.

Fatih Selimefendigil and Öztop 2019 [34] examined The free convection on different portions of the division in a cavity with a corrugated division. The nanotube (CNT)-water-nanofluid carbon with a sloping magnetic field was considered in one of those domains. A conductive corrugated, triangular wave shape has been employed. Galerkin weighted residual finite element technique was used for the numerical simulation. A variety of values for appropriate current thermal configuration parameters like the Rayleigh number (between 10^4 and 10^6), the Hartmann number (between 0 and 50), the magnetic angle of inclination (between 0^o to 90 ^{o}), the fraction in solid particulate volume (between 0 and 0.03), the number of triangular waves (between 1 and 40). Significant increases in the number of Nusselt were reported using CNTs. For larger Hartmann values the average heat transmission reduces but varies slightly when the value of the magnet angle changes.

Fatih Selimefendigil and Öztop, 2019 [35] studied The mixed nanofluid mixed flow in an inclined L-shaped chamber with elastic walls was computationally investigated using finite element methodology with the arbitrary-agrangian-eulerian approach for internal heat production and magnetic field efficiency. Simulations were performed with various values: number of Richardson (between 0.03 and 30), cavity angle inclination (between 0° and 180°), number of Hartmann (between 0 and 50), magnetic field orientation angle (between 0° and 90 °), internal Ra (between 10^4 and 10^6), solid volume of nanoparticles (between 0 and 0.04), flexible modulus of elastic wall (between 10^4 and 10^8) and In comparison with cavity with elastic and rigid cavities, it has been shown that the influence of the elastic wall on the convective heat transfer characteristic was substantial with the lowest value of Richardson numbers and the smallest values of elastics module. For the change of the average Nusselt number, the effect of the magnetic angle was substantial compared to the force of the magnetic field. The angle of inclination in cavity has substantial effects on the change of the average water and nanofluid Nusselt number.

Chamkha et al. 2020 [36] Examined carbon-nanotube/water nanofluid mixed convection in a vented cavity with an internal conductive T-shaped object under pulsing flow circumstances, utilizing finite element procedure in the magnetic field effects. The effects on the tiny convective object of pulsating flow were also examined for various parameter (specifically: number of Richardson between 0.05 and 50), number of Hartmann between 0 and 30; inclination of cavity wall between 0^o and 10^o and dimension (between 0.1H and 0.2H) and orientation (between -90^o and 90^o) and amplitude (between 0.5 and 0.9). It was noted that Nu_{ave} increased magnet field strength, solid nanoparticle volume percentage and pulsing amplitude, whereas greater Ri and cavity wall slanting angles had a contrary

impact. With the presence and adjustments of the T-shaped object's size and orientation, the main flow from the inlet to the outlet and recirculation around the T-shaped object and the thermal cell wall were affected by the magnetic field intensity. Pulsing flow led significant heat transfer improvement in all configurations compared to a continuous flow instance. Because CNT particles were highly conductive in water, substantial increases in the Nusselt average of 97% to 108% were found both in steady-flow and when magnetic field was lacking or present in pulsing instances.

Fatih Selimefendigil, Öztop, and Abu-Hamdeh, 2020 [37] investigated forced convection of nanofluid by employing the internal conductive L-shaped item and magnetic field, in a ventilated chamber with elastic lower wall. A finite element approach was used to conduct simulations. Wall flexibility effects were noted that were significant for a high convection arrangement and the average heat transfer rate for the lower wall was up to a maximum of 11%. Recirculated recirculation was seen with magnetic field in the ventilated cavity and around the L-shaped item. The influence of the magnetic field on the improvement of heat transmission was seen to differ for various portions of the hot wall. When comparison was made between situations with the maximum magnetic field and without the magnetic field. When the magnetic field intensity was raised, the Nusselt number generally decreases somewhat. The position of the L item has a major influence on fluctuation and changes in thermal pattern. When comparing the number of Nusselt with the lowest and maximum values of the horizontal and vertical position of the item, the greatest change in the contribution to the overall heat transfer was evident in the right vertical hot wall section. The L-form object was an effective tool for controlling the heat transfer characteristics of the ventilated cavity.

Fatih Selimefendigil, Öztop, and Sheikholeslami, 2020 [38] Examined the impacts on convective heat transfer of the nanotube (CNT)-water nanofluid U-shaped cavity filled with entropy production by considering inclined magnetic field effects of a partially elastic wall and spinning circular cylinder. ALE using a finite element technique performs numerical simulation (FEM). Impacts on the forced convection of the magnet of the rotating cylinders of several critical factors including Re number, Ha number, magnetic field direction, elastic wall size and modulus as well as angular velocity were examined. The value of Re, the magnet field strength (up to Ha numbers 50) and the angle of orientation increase, while the mean Nu was larger than 0.4H, for higher elastic walls and horizontal positions. When considering the rotating cylindrical effects, up to 60 % increase in the stationary cylinder scenario was achieved at the maximum speed. In terms of the size and modulus of the elastic wall, the average Nu variance was between 9 and 10.45%. Flexible wall impacts on the average number Nu was stronger when the corner speed was higher at the clockwise and at the highest Re number. The increase in the average Nu number at the highest Ha figure was 13%-14 .

Ghalambaz et al., 2020 [39] analyzed a flexible baffling in an L-shaped container flows by free convection. In an arbitrary Lagrangian–Eulerian moving mesh frame are introduced the guiding equations. FEM numerically has been used to solve all governing equations with respect to boundary conditions. To confirm that the findings were accurate, a grid-independent test was done and numerical solver outputs comparable with prior projects. The effect of dimensionless factors such as Rayleigh number, elasticity modulus and flexible disturbance length was analyzed on the flow and transmission of heat. The results show that a rigid blow tends to stand up to the fluid flow and hinders the transmission of convective heat. For a

higher value of Ra, a bigger disturbance leads to greater flux resistance and hinders heat transmission while increasing stress from the disturbance.

Yaseen and Ismael, 2020 [40] studied an open trapezoidal cavity channel, stimulated fluid structure interaction (FSI) and a coupled convective heat exchange takes place. In the laminar zone a non-Newtonian (fluid power law) was investigated. The heat was mimicked by a thermal heat sink behind the wall, while all the remaining solid walls were properly isolated. The upper wall of the channel has a flexible blister and its open end stretches to the open cavity. The position on the top wall of the deformable bubble was different. Together with a numeral of Richardson (Ri = 0.01-100) and power law (n = 0.5-1.5), this position is checked. With the Arbitrary Lagrangian-Eulerian (ALE) approach the problem has been addressed. The findings were compared to the unmounted channel. The analysis reveals that the suggested disturbed canal significantly improves the heat transfer.

Fatih Selimefendigil and Chamkha, 2020 [41] examined the magnetic hydrodynamics using the finite element technique, the Ag–mgO/water hybride nanopartical mixed convective flow of the triangulate cavity with a porous layer. Various effects of relevant parameters Ri (between 0,01 and 100), number Hartmann (between 0 and 60), angle of inclination for magnetic fields (between 0 and 90), number Darcy (between ten to four and five times to ten to two), location of a triangular porous region peak (between 0,2H to 0,8H.) and a hybrid solid volume fraction φ (from 0 to 0.01) of nano were presented in a numerical simulation. It was noted that below the main vortex at the upper wall was a huge vortex at the lowest value Ri. Multi-circulation flow patterns were seen in the right lower corner at the greatest magnetic field strength. Higher levels of porous media permeability,

magnetic field angle inclination, distance of the porous layer top of the hot wall and a solid fraction in the volume of nanoparticles of the hybrid nanofluid were achieved in average heat transfer. For higher Richardson and Hartmann, the influence was reversed.

Fatih Selimefendigil, Okulu, et al., 2020 [42] explain the thermoelectric generator module performance improvement with various nanofluids. In a 3D channel where Thermoelectric Generator Module was attached, CNT–water Nanofluid and Ag/MgO–water hybrid nanofluids were employed. The Galerkin weighted residual Finite-Element technique uses 3D multi-physics simulations. The power output of the module was seen to be improved when nanoparticles were added. Hybrid nanofluid configuration delivers maximum performance. The thermoelectric generator has a power increase of around 5.84% and 9.30% for CNT–water and hybrid nanofluid at Reynolds number 500, raised its solid volume faction from 0.005 to 0.2. At Reynolds number 1500, however, it was possible to use CNT–water nanofluid and the increase will be 6.6 %. With Reynold numbers and solid component volume fractions, the efficiency of the module was increased when the values were low

Jamesahar et al., 2020 [43] examined the influence on the thermal transfer rate and the flow properties within a square enclosure of the nanofluid by two oscillating fin. Both fins were connected to the heated wall, with the same frequencies and amplitudes oscillating. In order to solve the equations describing the interactions and motions of nano-fluids and fins, the finite element approach utilized by the Lagrangian–Eulerian (ALE) arbitrary methodology. Comparisons of our findings with those published in prior research have shown accurate and trustworthy modeling and numerical investigations. The results indicated that the heat transfer rate increased by the fins oscillation. In the same way, when the heat conductivity ratio of the

fins compared to the nanofluid grew, the growing trend in heat transference via the oscillating fins reduced. Improved and weakened the heat transfer rate correspondingly the thermal conductivity and viscosity characteristics.

Table (2- 1) summery of literatures

Ref. No.	**Authors**	**Year of the study**	**Main conclusion and result**
11	Angirasa	2000	At lower values of the Grashof, heat transfer rises in both directions with increasing forced flow. The interaction becomes extremely complicated with larger absolute levels of the Grashof number. The change of the ratio [Gr]/Re2 results in anomalous conduct of the heat transfer.
12	Iwai et al	2000	An aspect ratio of at least AR = 16 was discovered to be necessary to achieve a 2D area near the centerline in Re = 250. For lower Reynolds, this 2D area expanded. Furthermore, it was observed that on the centerline, but not at the two sides, the highest Nusselt number was not always found.
13	Abu-Mulaweh	2003	Detailed overview of the influence on the flow and thermal fields downstream of steps of various factors such as step height, Reynold number, Prandtl angle, expansion relation, temperature differential between the wall and free

Ref. No.	Authors	Year of the study	Main conclusion and result
			stream and booster power (assisted and opposed).
14	Saeidi and Khodadadi,	2006	clockwise CW spinning vortex covering around 75-88 % of the cavity The CW primary vortex decreases in power because the outlet ports on the right wall, while the counter-Clockwise vortex (CCW) which exists near the top right corner rises in size.
15	Abbassi & Ben Nassrallah,	2007	The external magnetic field works to lower the recirculation zone size. Speed profiles demonstrate that the magnetically inducted force dampens the basic flow out of the recirculation zone, whilst the flow is accelerated close to the wall channel.
16	Velazquez et al.	2008	The time-averaged Nusselt number behind the step relies on the two above control parameters and is always greater than that for inlet pressure gradients that prevent reverse inlet flow both upstream and downstream boundary conditions.
17	Khanafer et al.	2008	The structure of fluid flow, heat transfer fields, and skin friction coefficient are all affected by Reynolds number, Richardson number, and dimensionless oscillation frequency.
18	Khalil Khanafer	2014	When compared to a flat bottom wall case, all of the examined cases showed

Ref. No.	Authors	Year of the study	Main conclusion and result
			improved heat transmission. At Grashof number 10^4 and Re 400, a flexible bottom wall case was discovered to have a considerable heat transfer improvement (61.4%) when compared to a flat bottom wall case.
19	Faith selimefendigil and Oztop	2014	The duration and intensity of the recirculation zone behind the step are significantly influenced by the square obstacle, and it may therefore be utilized as a passive control element for heat transfer augmentation.
20	Selimefendigil and Öztop	2015	Heat transfer improves as the Reynolds number rises, and this effect was amplified as the magnetic field's inclination angle increased.
21	Gallegos and Sharma,	2016	Changing the blockage and cylinder size can change the plate's dynamic behavior.
22	Mehryan et al	2017	For moderate levels of the Rayleigh number, the presence of the magnetic field raises the dimensionless average temperature for large Hartmann numbers (10^6 - 10^7). The dimensionless average temperature drops when a strong magnetic field is present.
23	Fatih Selimefendigil and Öztop	2017	As the Richardson number and internal Rayleigh number rise, the local and averaged heat transfer decreases.

Ref. No.	Authors	Year of the study	Main conclusion and result
24	Mahalakshmi et al	2018	The rate of heat transfer increases as the heater length and Grashof number grow, but the rate of heat transfer decreases as the magnetic field effect increases.
25	Selimefendigil and Ozotop	2018	As the value of Re and the volume percentage of solid particles rises, so does the rate of local and average heat transfer. Heat transfer rate was higher for the scenario with the wall having the lowest value of elastic modulus at the greatest value of Re, while the situation was reversed for other values of Re.
26	Selimefendigil and Öztop	2018	The changes of formed multiple re-circulation zones and isotherms with the three dimensional vented cavity are affected by the installation of the obstacle (cylinder + elastic rod) and modifying its geometrical and other characteristics (elasticity of the rod).
27	Sabbar et al	2018	When compared to rigid hollow walls, the presence of elastic wall(s) improves the heat transfer rate by 17%.
28	Alsabery et al.	2018	The flexible oscillating heat-conducting fin has a critical influence on fluid flow and heat transfer inside the oblique cavity.
29	faith selimefendigil and Oztop	2018	For moderate and higher values of Reynolds number, the formed secondary peaks of local Nusselt number along the

Ref. No.	Authors	Year of the study	Main conclusion and result
			hot surface decrease with Hartmann number and vanish at the highest value of Hartmann number.
30	Muneer A. Ismael	2019	At Re = 250, the Nusselt number of a compliant baffled channel increases by 94% compared to a non-baffled channel, while the pressure drop increases by 210%. The optimum performance is obtained at a Cauchy number of 10^7, with the lengths of the upstream and downstream baffles being 0.62 and 0.2 times the channel height.
31	Selimefendigil and Ozotop	2019	The local Nusselt number both deteriorates and improves at various areas along the hot wall for higher Reynolds numbers, but the changes in the local Nusselt number are marginal for lower Reynolds numbers.
32	Alsabery et al	2019	Ra increases the local and verage Nusselt numbers, and secondary peaks in the local Nusselt number have been created for lower Ra values.
33	Selimefendigil and Öztop	2019	The average Nusselt number decreases as the elastic wall becomes larger, and the drop is between 8% and 9%.
34	Selimefendigil and Öztop	2019	CNTs result in substantial increases in the Nusselt number. The average heat transfer reduces as the Hartmann number

Ref. No.	Authors	Year of the study	Main conclusion and result
			increases, although it fluctuates slightly as the magnetic inclination angle changes.
35	F. Selimefendigil and Öztop	2019	When comparing cavities with elastic and rigid walls, the impact of the elastic wall on convective heat transfer characteristics are substantial at the lowest values of Richardson number and lowest values of elastic modulus, while there is an 11% disparity in the average Nusselt number.
36	Chamkha et al	2020	Nu_{ave} increased when the magnetic field intensity, solid nanoparticle volume proportion, and pulsation amplitude increased, but the effect was reversed for larger Ri numbers and cavity wall inclination angles.
37	Fatih Selimefendigil, Öztop, and Abu-Hamdeh	2020	As the rotating cylinder effects are taken into account, at the maximum speed, an increase of up to 60% is observed when compared to the stationary cylinder scenario.
38	Fatih Selimefendigil, Öztop, and Sheikholeslami,	2020	When the Re number, magnetic field intensity (up to Ha number 50), and orientation angle are raised, the average Nu value rises; however, when the elastic wall size and horizontal position of the cylinder exceed 0.4H, the influence is contrary.

Ref. No.	Authors	Year of the study	Main conclusion and result
39	Ghalambaz et al.,	2020	The fluid flow is resisted by a stiffer baffle, which hinders convective heat transmission. A bigger baffle results in more resistance to the flow and hinders heat transmission for a higher Ra value, while also increasing the stress over the baffle.
40	Yaseen and Ismael	2020	The suggested baffled channel significantly improves heat transfer.
41	Fatih Selimefendigil and Chamkha,	2020	For the lowest value Ri number, a large vortex forms below the main vortex towards the top wall. In the right bottom corner, at the maximum magnetic field intensity, a multi-recirculation flow pattern can be seen.
42	faith selimefendigil , okulu, et al	2020	With the addition of nanoparticles, the module's power output increases. The hybrid nanofluid configuration produces the maximum output power. .
43	Jamesahar et al	2020	The oscillation of the fins caused an increase in the heat transfer rate. Furthermore, when the ratio of the thermal conductivity of the fins compared to the nanofluid rose, the growing trend in the heat transfer rate due to the oscillating fins reduced..

2.3 Concluding Remarks

"From the studies that were reviewed" before, it "could conclude the following".

1. Experimental works are rarely found, this because of the difficulty in control on the movement of the elastic element experimentally.
2. Most studies have considered the simple flow conditions, that is, unsteady, incompressible, laminar and Newtonian flow.
3. Most studies have considered the air or water as working fluid.
4. Most studies without the effect of entropy generations.
5. Most studies did not use step elastic-step type corrugation effects.
6. Most previous studies utilized the Arbitrary Lagrangian Eulerian (ALE) finite element method to solve the governing equations.
7. Most previous studies did not used flow around bodes with FSI.

"The present studies is similar" and different "from the published work by the following":

1. This study is not use experimental study because the difficulty in control on the movement of the elastic element experimentally according to previous studies.
2. Using CNT Nanofluid as working fluid in this study.
3. Entropy generations and bejan number "are studied in this work.
4. Using step elastic-step type corrugation effects from (1-8) and study the effect it on mixed convection.
5. Using flow around hexagonal solid with different location.
6. Utilized the Arbitrary Lagrangian Eulerian (ALE) finite element method to solve the governing equations by Comsol.

CHAPTER THREE

Numerical Analysis

Chapter Three: Numerical Analysis

3.1 Introduction

The numerical simulation results are obtained with the Finite Element method by responding numerically to the two-dimensional FSI interaction (flow-structure) problem of CNT-water nanofluid mixtures in cavity with inlet and outlet ports in the form of incline-magnet-field effects, as well as steps such as corrugated elastic walls. The entropy generation was also calculated. For the description of fluid motion with the elastic wall in the fluid structure interaction model, the Arbitrary-Lagrangian-Eulerian approach is used. In this study, several steps such as corrugation are taken into account, making it elastic and adding extra flexibility to manage the convective heat transfer functions of the ventilated cavity. Two-dimensional calculation The numerical problem for Navier Stocks equations is clearly two principal causes; the first is their non-linearity, and the second is the unknown numerical value. The equation system grows complicated when other equations, such as elastic structural mechanical equations, are introduced to these equations. Some simplifications, particularly if computer resources are restricted, are therefore necessary. To tackle the coupling of an FSI problem, the Arbitrary Lagrangian-Eulerian technique software package COMSOl 5.5 Multi-physics (ALE).

In this steady, some simplifications were assumed with maintaining acceptable accuracy and reliability.

1. The fluid flow considered as two dimensional,
2. laminar flow (no disruption between the layers),
3. incompressible (constant density)

4. Newtonian (linear relationship between shear stress and shear strain rate).
5. wall material does not affect by temperature change (the properties of the baffle material maintain constant), dissipation rate neglected (the amount of energy lost by the viscous forces neglect).
6. Effects of thermal radiation are neglected.

3.2 Determinants

1. Theoretical study only.
2. Fluid-structure interaction (FSI).
3. Mixed convection.
4. Vented square cavity with inlet and outflow ports.
5. Flexible wall elastic modulus (between 104 and 108).
6. Magnetic inclination angle (between 0° and 90°).
7. Hexagonal solid inside the cavity at different locations.
8. Unsteady state, laminar, two dimensional, Newtonian, incompressible flow.
9. CNT-water nanofluid.
10. Reynolds number (between 100 and 500).
11. Hartmann number (between 0 and 60).
12. nanofluid concentration (0 to 6%).
13. Richardson was 105.

3.3 Mathematical model description

The geometry of the problem in this study is a two-dimensional vented square cavity with two apertures for input and outflow located on the vertical walls, as well as an elastic step. The fluid enters the square cavity with length H and temperature T_c, while both ports have sizes of 0.25H and the wall below the inlet port, with size 0.25 H, is stiff, and other wall assumed to be elastic. The elastic walls are maintained at a constant temperature of $T_h > T_c$. For the side elastic walls, a corrugation in the form of steps is employed, with N steps for the heated region of the wall. In the hollow filled with CNT–water nanofluid, an angled magnetic field is applied in a uniform way. The magnetic field intersects the horizontal axis at an angle of γ. A Hexagonal solid inside the cavity has length of a, angle is 120^o, and height 1 as shown in figure 3-1and 3-2. Table 3-1 shows the thermophysical of water and CNT at the reference temperature.

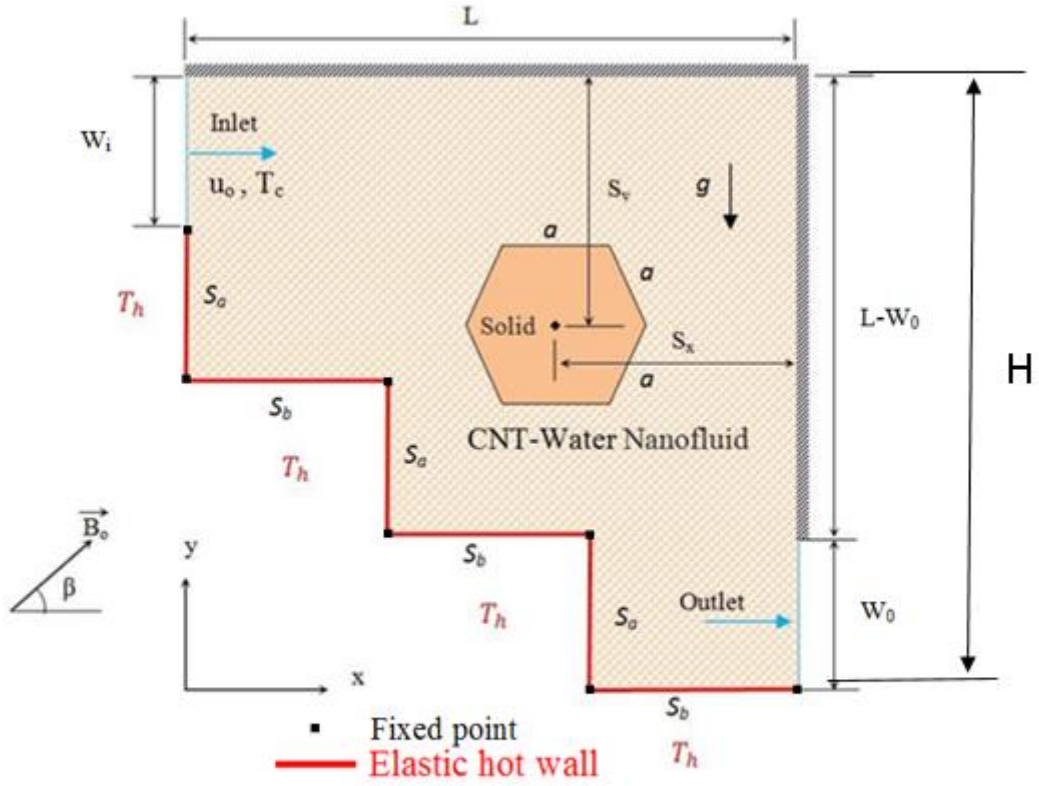

Figure (3- 1) Schematic diagram and coordinates arrangements

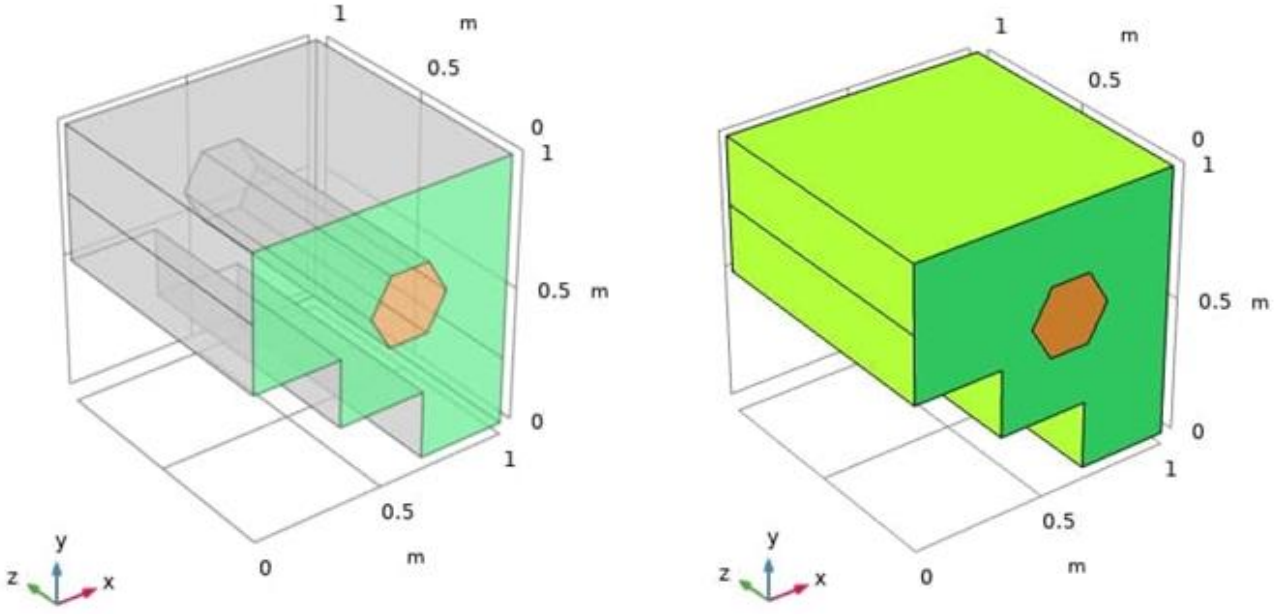

Figure (3- 2) (3D)Schematic diagram and coordinates arrangements

3.4 Effective Thermal Properties of Nanofluid

The use of nanofluid flow leads to the definition of effective properties which is empirically for the effect of nanofluid. Nanofluids' transport properties, such as heat capacity, density, thermal conductivity, viscosity, and specific heat, are the most important factors in convective heat transfer. The physical properties of the nanofluid that are taken as function of the volume concentrations, are defined as follows:

1. Thermal Conductivity of nanofluid.

Bayat and Nikseresht [44] proposed an alternate formula for estimating thermal conductivity, which is written as:

$$\frac{k_{nf}}{k_{bf}} = \frac{k_p + 2\,k_{bf} + 2\,(k_{pf} - k_p)\varphi}{k_p + 2\,k_{bf} - (k_{bf} - k_p)\varphi} \qquad (3.1)$$

2. Specific Heat of nanofluid.

Based on the heat capacity concept, **Xuan and Roetzel [45]** suggested the following equation for estimating the specific heat of nanofluids:

$$c_{p_{nf}} = \varphi\,(c_p)_P + (1-\varphi)\left(c_p\right)_{bf} \qquad (3.2)$$

3.Effective Viscosity of nanofluid.

Drew and Passman [46] demonstrated the viscosity of the nanofluid. For estimating viscosity, they proposed using Einstein's equation. They used spherical particles shape with volume fractions less than 5 % volume percent, and is defined as follows:

$$\mu_{nf} = \mu_{bf}(1 + 2.5\varphi) \qquad (3.3)$$

4. Effective density of nanofluid.

According to **Pak and Cho [47]**, the effective density of nanofluids containing suspended particles may be calculated as follows:

$$\rho_{nf} = (1-\varphi)\rho_{bf} + \varphi\rho_P \qquad (3.4)$$

5. Effective thermal diffusivity.

The effective thermal diffusivity of nanofluid can be calculated as **Xuan and Roetzel [45]**:

$$\alpha_{nf} = \frac{k_{nf}}{(1-\varphi)(\rho\, c_p)_{bf} + \varphi(\rho\, c_p)_p} \qquad (3.5)$$

Table (3-1). properties for CNT, water nanoparticle and base fluid. Ref. [34].

	ρ (kg/m^3)	C_p (J/kg k)	k (W/m. k)	μ (N.s/m^2)
CNT	2600	425	6600	-
Pure water	983.3	4179	0.595	0.000899

3.5 Dimensional governing equations

The unsteady fluid and elasto-dynamic structure governing equations are stated in dimensions' vector form as: **[48, 49]**

For fluid layer:

Continuity Eq.

$$\nabla \cdot u^* = 0 \qquad (3.6)$$

Momentum Eq.

$$\frac{\partial u^*}{\partial t^*} + (u^* - w^*) \cdot \nabla u^* = -\frac{1}{\rho_f}\nabla p^* + \upsilon_f \nabla^2 u + \beta g_y (T^* - T_c^*) \qquad (3.7)$$

Thermal energy:

$$\frac{\partial T^*}{\partial t^*} + (u^* - w^*) \cdot \nabla T^* = \alpha_f \nabla^2 T^* \qquad (3.8)$$

Thermal energy in solid layer:

$$\frac{\partial T^*}{\partial t^*} = \alpha_f \nabla^2 T^* \qquad (3.9)$$

For elastic structure domain:

The nonlinear elastic displacement equations and the wall's energy may be expressed as:

$$\rho_s \frac{d^2 ds^*}{dt^{*2}} + \nabla\sigma^* = F\upsilon^* \qquad (3.10)$$

$$\frac{\mathrm{dT}^*}{\mathrm{dt}^*} = \alpha_s \nabla^2 \mathrm{T}^* \qquad (3.11)$$

Fv* in Eq. (10) is representing the gravitational forces per unit volume and written as:

$$\mathrm{Fv}^* = \rho_s \, g_y \qquad (3.12)$$

When an elastic wall is subjected to a stress tensor as a result of fluid flow pressure and nonlinear geometry fluctuation, the following equations can be used to explain the stress:

$$\sigma^* = \mathrm{J}^{-1}\mathrm{FSF}^{\mathrm{T}} \qquad (13)$$

Where $F = (I + \nabla d_s^*)$, (I: unity matrix), J=det.(F) and S is the second piola-kirchhoff stress tensor that relevant to the strains in the elastic wall **[9]** as:

$$\mathrm{S}=\mathrm{C} : \mathrm{\mathcal{E}} \;,\; \mathrm{\mathcal{E}} = \frac{1}{2}\left(\nabla d_s^* + \nabla d_s^{*T} + \nabla d_s^{*T} \nabla d_s^*\right) \qquad (3.14)$$

Where C is a function of dimensional modulus of elasticity and possin's ratio as shown below and the colon ":" is the double-dot tensor product.

$$\mathrm{C} = \mathrm{C}(\mathrm{C} \,.\, \upsilon) \qquad (3.15)$$

Where E is the modulus of elasticity of the wall and v is the Poisson's ratio.

3.6 Dimensional boundary conditions

(1) The boundary conditions on the elastic wall are dynamic movement continuity and kinematic forces. When the fluid boundary conditions at the solid-fluid contact are evaluated with no-slip, the result is;

$$\frac{\partial d_s^*}{\partial t^*} = u^* \qquad (3.16)$$

$$\sigma^* \cdot n = -p^* + M_f \nabla u^* \qquad (3.17)$$

(2) The energy balance at the interface between the fluid and the solid may be stated as:

$$k_f \frac{\partial T^*}{\partial n}\Big|_f = k_s \frac{\partial T^*}{\partial n}\Big|_s \qquad (3.18)$$

(3) The elastic wall in the present work with different positions and free displacement fixed with $\frac{\partial d_s^*}{\partial t^*} = 0$ at all corner this mean end and starting of piece of elastic line. The condition of the pressure constraint is applied at the exit hole at the right wall, i.e. $p^* = 0$.

(4) The fluid inlet velocity is $u^* = u_{in}$

(5) $T^* = T_h$ at $x = 0$. $b < y \leq H$

(6) $T^* = T_c$ at $x = H$. $0 < y \leq H - b$

(7) $\frac{\partial T^*}{\partial y^*} = 0$ at $y = 0$. $y = H$

The following non-dimensional parameter definitions were used to non-dimensionless the governing equations:

$$(X.Y.W_0, W_i.S_a, S_b) = \frac{(x^*.y^*.w_0.w_i.s_a, s_b)}{H} \; . \; u = \frac{u^*}{u_{in}} .$$

$$p = \frac{p^*}{\rho_f u_{in}^2} , \qquad t = \frac{t^* u_{in}}{H} , \qquad \theta = \frac{T^* - T_c}{T_h - T_c} , \qquad d_s = \frac{d_s^*}{L} ,$$

$$\sigma = \frac{\sigma^*}{E}\ , \quad pr = \frac{v_f}{\alpha_f}, \quad Re = \frac{u_{in}}{v_f}, \quad Gr = \frac{gB_f\Delta\theta H^3}{v_f^2},$$

$$\mathrm{Ri} = \frac{\mathrm{Gr}}{\mathrm{Re}^2}\ , \quad Gr = \frac{g\beta L^3(T_w - T_\infty)}{\upsilon^2}\ , \quad \mathrm{Re} = \frac{\rho \mathrm{vD}}{\mu}, \quad \mathrm{Ha} = \mathrm{B_0 L}\sqrt{\frac{\sigma}{\mu}}\ ,$$

$$\mathrm{Pr} = \frac{\mu\ \mathrm{Cp}}{\mathrm{k}}, \ \mathrm{Nu} = \frac{\mathrm{h\ D}}{\mathrm{k}}, \ Be = \frac{S_{gen,T}^{'}}{S_{gen}}$$

The dimensional governing equations (6) to (11) may be expressed in non-dimensional form after applying the prior non-dimensional parameters as:

For the fluid
Continuity Eq.

$$\nabla \cdot u = 0 \tag{3.19}$$

Momentum Eq.

$$\frac{\partial u}{\partial t} + (u - w)\cdot\nabla u = -\frac{\rho_f}{\rho_{nf}}\nabla p + 2\frac{w}{H}\frac{1}{Re}\frac{\mu_{eff}}{v_f.\rho_{nf}}\ \nabla^2 u + F\ \theta \tag{3.20}$$

Where:

$$\mathrm{F = Fx = (Ha^2/Re)*((v*\sin(\gamma)\ \cos(\gamma))-(u\sin^2(\gamma))} \tag{3.21}$$

$$F = Fy = 4\left(\frac{w^2}{H^2}\right)\frac{(\varphi\rho_p\beta_p + (1-\varphi)\rho_f\beta_f}{\rho_{nf}\beta_f}\frac{Gr}{Re^2}\theta + \left(\frac{Ha^2}{Re}\right) * ((u * \sin(\gamma)\cos(\gamma)) - (vcos^2(\gamma)) \tag{3.22}$$

$$F = 4\frac{w^2}{H^2}\frac{\emptyset\rho_p\beta_p + (1-\emptyset)\rho_f\beta_f}{\rho_{nf}\beta_f}\frac{Gr}{Re^2}\theta$$

Energy Eq.

$$\frac{\partial\theta}{\partial t} + (u - w)\cdot\nabla\theta = 2\frac{w}{H}\frac{\alpha_{nf}}{\alpha_f}\ \frac{1}{Pr.Re}\nabla^2\theta \tag{3.23}$$

For the elastic wall

$$\frac{C_a}{P_r}\frac{d^2 d_s}{dt^2} - \nabla\sigma = 0 \qquad (3.24)$$

$$\frac{\partial\theta}{\partial t} = \alpha_r \nabla^2\theta \qquad (3.25)$$

For the hexagonal solid

$$\frac{\partial\theta}{\partial t} = ks\,\nabla^2\theta \qquad (3.26)$$

By using the dimensionless numbers, the above equations converted to the non-dimensional system

Where:

To make the problem easier, the value of the body force was set to zero($F_\upsilon = 0$)

k_s=10 k_{nf}

3.7 Dimensionless boundary conditions

The preceding boundary conditions for the fluid and solid may now be rewritten as follows in dimensionless form:

1) $\theta = 1 \quad at \quad X = 0 \ .0.5L < Y \leq 0.75L$

2) $\theta = 0 \quad at \quad X = 1 \ .l - Wo < Y \leq 1$

3) $\frac{\partial\theta}{\partial Y} = 0 \quad at \quad 0 \leq X \leq L = 0 \ .Y = 1$

4) $\frac{\partial\theta_f}{\partial n} = k_r \frac{\partial\theta_s}{\partial n}$, Where $k_r = \frac{k_s}{k_f}$ is the thermal conductivity ratio.

5) $\theta = 1 \quad at$, Lower wall

The fluid-structure interaction boundary conditions are alternatively expressed as follows:

$$u = \frac{\partial d_s}{\partial t} \tag{3.27}$$

$$\frac{1}{C_a}\sigma \cdot n = -p + \frac{1}{R_e}\nabla u \tag{3.28}$$

In the dimensionless version, the entrance velocity becomes U = 1, and the starting temperatures of the wall and the fluid inside the cavity become zero. Furthermore, u in=0 is the dimensionless inlet velocity. The dimensionless pressure (P = 0) is equivalent to zero.

The Nusselt number is the most important parameter in this investigation. It determines the rate at which heat is transferred along a specific wall. In a given boundary, it is the ratio of convection to conduction heat transfer. The heated wall, on the other hand, was used to compute the local Nusselt number, as illustrated below.

$$Nu_L = \frac{h \cdot L}{K_f} \text{ at (x=0)} \tag{3.29}$$

The heat transfer along the heated wall is accomplished by conduction at the wall-fluid contact, which may be described as:

$$q_{cond.} = k_f \frac{\partial T^*}{\partial x^*} = h(T_h^* - T^*) \tag{3.30}$$

The preceding Eq. yields when dimensionless definitions are used.:

$$Nu_t = -\frac{k_{nf}}{k_f}\frac{\partial \theta}{\partial n}\,|_{wall} \tag{3.31}$$

$$\overline{Nu_l}(\tau) = -\frac{1}{l_i}\int_0^{L_i}\frac{k_{nf}}{k_f}\,\frac{\partial \theta}{\partial n}\,|_{wall} ds. \tag{3.32}$$

At the point where the wall and the fluid meet, Furthermore, the average Nusselt number is immediately determined by integrating the instantaneous local temperature gradient (Eq. 30) over the distance of interest at the cavity's hot left wall as:

Where $Nu(t)_{av}$. is the average Nusselt number, *Li* is the length of hot wall.

The formula above is averaged over a cyclic time period (τ) to give the time averaged Nusselt number:

$$Nu_{av} = \frac{1}{\tau}\int_0^{\tau} Nu(t)_{av}dt \tag{3.33}$$

3.8 Entropy generation

There are two separate sources of heat flow and viscous dissipation for local entropy in this study. The rate of entropy may be expressed as local, [49]:

$$S_{gen} = \frac{K_{nf}}{T_0^2}\left[\left(\frac{\partial T}{\partial X}\right)^2 + \left(\frac{\partial T}{\partial y}\right)^2\right] + \frac{\mu_{nf}}{kT_0}\left[S_2(u^2+v^2) + k\left(2\left(\frac{\partial u}{\partial x}\right)^2 + 2\left(\frac{\partial v}{\partial y}\right)^2 + \left(\frac{\partial u}{\partial y} + \frac{\partial v}{\partial x}\right)^2\right)\right] \tag{3.34}$$

The local entropy production can be represented in dimensionless form:

$$S_{gen} = S_{gen,T} + S_{gen,\mu} \tag{3.35}$$

$$S_{gen,T} = \frac{S_\circ}{K_F}\left[\left(\frac{\partial \theta}{\partial X}\right)^2 + \left(\frac{\partial \theta}{\partial Y}\right)^2\right] \tag{3.36}$$

$$S_{\text{gen},\,\mu} = s_1\left[s_2(U^2+V^2) + S_3\left\{2\left(\frac{\partial U}{\partial X}\right)^2 + 2\left(\frac{\partial V}{\partial Y}\right)^2 + \left(\frac{\partial U}{\partial Y} + \frac{\partial V}{\partial X}\right)^2\right\}\right] \tag{3.37}$$

Where the dimensionless local entropy generation:

$$S_{gen}\frac{T_\circ^2 L_c^2}{k_f \Delta T^2}$$

The constants that mentioned in eqs (3.34) and (3.35) are follows

$$S_{gen}^{\cdot} = \int S_{gen}\,dA \tag{3.38}$$

The rule of Simpson is used to assess the development of local entropy over a unit area. The Bejan number is an alternative parameter for defining irreversibility.:

$$B_e = \frac{\dot{S_{gen,T}}}{S_{gen}} \tag{3.39}$$

3.9 Mesh independence, solver and code verification

The Delaunay Triangular method will be used to discretize the computational domain into unstructured triangles in this numerical procedure. The Delaunay triangulation is a geometric structure that has been widely used in mesh production from the early days of mesh creation. The Delaunay triangulation of a vertex set maximizes the least angle between all feasible triangulations of that vertex set in two dimensions. The mesh mode for the current numerical computation is shown in Figure (3-3). The mesh generating process has been thoroughly carried out.

The finite element approach was used to solve the equations (24). Using a weak formulation method, the Galerkin technique is employed to solve the governing equations of the finite element methods. The cells are divided into non-structural mesh distribution components, as shown in Figure (3-3). Interpolation algorithms are used to discretize the non-overlapping districts throughout the computational domain. For velocity, pressure, and temperature variables, Lagrange triangular finite elements of various orders are utilized throughout the computing domain. The governing equations are approximated in order to derive the residuals conservation equations. To make the nonlinear momentum equations easier to solve, the Newton-Raphson technique was applied. Solution convergence is predicted if the following prerequisites are met.

$$\left|\frac{\xi^{m+1}-\xi^{m}}{\xi^{m+1}}\right| \leq 10^{-6}$$

Any independent variables, where m denotes the number of iterations (velocity, temperature or pressure). To validate the correctness of the calculated findings, a grid-independent test is now required. Five grid resolutions were used to accomplish this, as shown in Table (3-2). The average Nusselt number on the heated surface at E=1e^4, Re=300, φ=0.02, ɣ=45, Ha=30, Ra=1e^5 was studied during this test. As shown in table 3.2, the grid size of (57453) with boundary elements of 2875 was efficient enough to be incorporated in the numerical solution with a percentage error of roughly 0.001 percent on surface 1 to 0.008 percent on surface 5. On the other hand, the numerical findings must be confirmed. Figure (3-4) shows Grid independent test average Nusselt number on hot surface1 at E=1e4, Re=300,φ=0.02,γ=45,Ha=30,Ra=1e5).

Table (3-2) Grid independent test average Nusselt number on hot surface1 at E=1e4,Re=300,φ=0.02,γ=45,Ha=30,Ra=1e5)

				Hot surface1		Hot surface2		Hot surface3	
grid	domain elements	bounday elemens	Time hours	Nu_{ave}	$\|Error\|$ %	Nu_{ave}	$\|Error\|$ %	Nu_{ave}	$\|Error\|$ %
G1	19532	2599	9+16min	8.8423	-	16.357	-	11.420	-
G2	19629	2607	9+66min	10.621	16.74	17.094	4.31	12.652	9.73
G3	23028	2634	10+30min	11.241	5.51	18.663	8.40	13.976	9.47
G4	29156	2706	11+34min	11.361	1.05	19.100	2.28	14.709	4.98
G5	57453	2875	12+44min	11.359	0.01	19.2	0.05	14.700	0.061

	Hot surface 4		Hot surface 5		Hot surface 6	
	Nu_{ave}	$\|Error\|$%	Nu_{ave}	$\|Error\|$%	Nu_{ave}	$\|Error\|$%
G1	15.685	-	6.8895	-	18.800	
G2	17.334	9.5	7.021	1.87	20.531	8.431
G3	18.931	8.48	7.221	2.72	21.456	4.31

G4	19.935	5.03	7.4118	2.5	22.679	4.40
G5	19.932	0.015	7.412	0.002	22.681	0.008

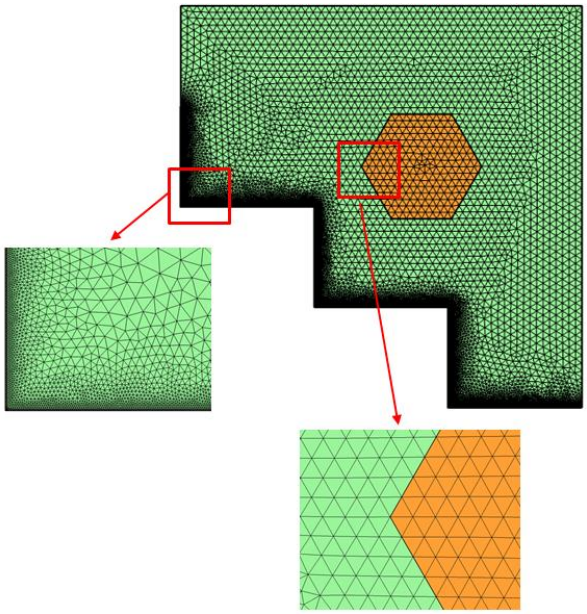

Figure (3- 3) The mesh mode for the present numerical computation

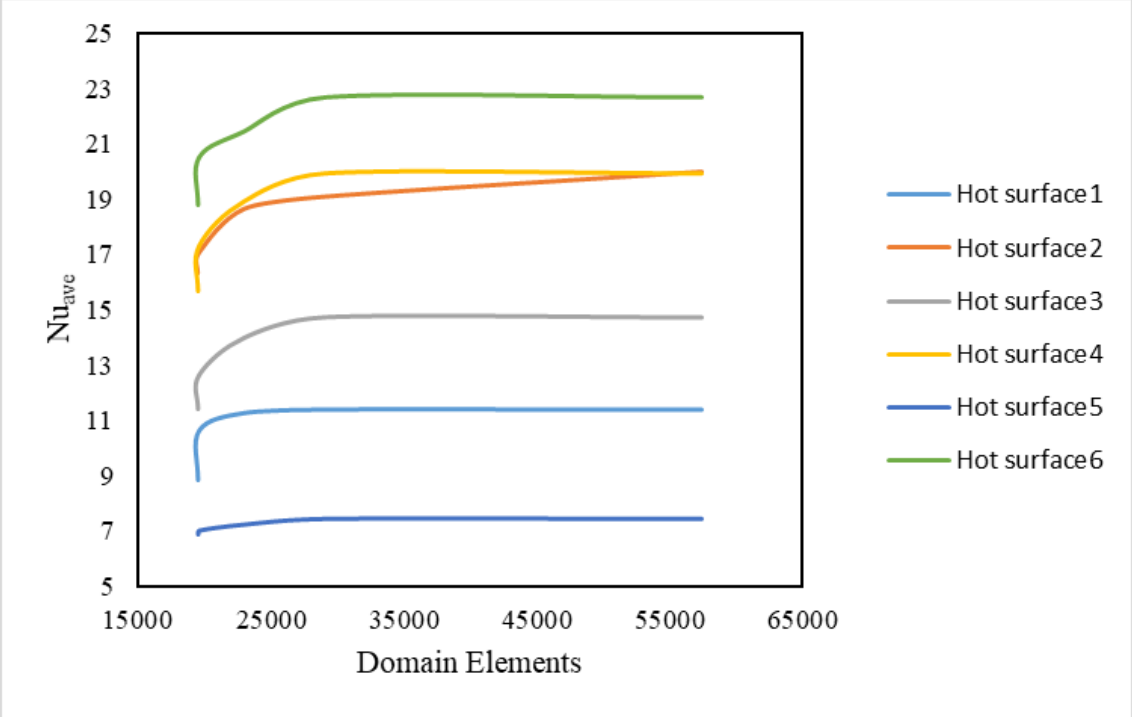

Figure (3- 4) Grid independent test average Nusselt number on hot surface1 at E=1e4,Re=300,φ=0.02,γ=45,Ha=30,Ra=1e5)

3.10 Solution method

one of the important numerical methods that deal with the phenomenon of interaction between the flowing fluid and the flexible structure is the Galerkin finite element method implementation in arbitrary Eulerian-Lagrangian technique. Description of this method is as shown below:

3.10.1 Finite element analysis and its general steps

i. Discretization the entire structure into tiny elements

ii. Selection of the displacement (or velocities of fluid) function

iii. Formulation of the element stiffness matrix.

iv. Assembly the stiffness matrices

v. solution the equations system

vi. Calculate parameters

3.10.2 The principle of the Lagragian-Eulerian Arbitrary method (ALE)

The ALE technique characterizes the structure field with a Lagrangian lattice (mesh) and the stream field with a Eulerian lattice (mesh) **[50]**.

While using this strategy, it's crucial to keep in mind how to keep the fluid domain's mesh quality (Eulerian mesh) when it's deformed by the flexible wall's movement. Large automated operations in the fluid domain (Eulerian mesh) must be taken in the case of severe distortions in order to retain the shape and type of excellent mesh in order to continue the computation. If this step is not done, the mesh quality will be poor, resulting in system instability and failure of the calculating process. This approach is

a hybrid of CFD (computational fluid dynamics) and FEA (finite element analysis) software. As a result, this is one of the method's benefits. One of the downsides of this strategy is that it causes unpredictability in the mesh interaction zone as a result of the process of upgrading a faulty mesh type. Data can be transferred via a monolithic or partitioned system in the Arbitrary Lagrangian-Eulerian approach.

3.10.3 Data transfer techniques in ALE method

The transfer of information between the different domains requires a description of the frequency and route of the shared data. Defined by kind of link, monolithic method, or partitioned approach, the frequency at which the needed data are transmitted. While the method of data transfer is one or two (one way or two ways).

Monolithic coupling involves the resolution of a coupled system of equations, which simultaneously describes the fluid-structured interaction, as shown in figure 3-5. The monolithic transmission of information often employs secret computer codes and requires processors with huge potential compared with other coupling processes.

On the other hand, partitioned techniques including strong and low coupling are used to solve two distinct solvers separately, but under common boundary conditions, the fluid and structural system equations **[48]**. In commercial simulation systems like as ANSYS, COMSOL Multiphysics, both strong and weak coupling techniques are offered. Where and how to transmit data from one domain to another for each solution step is the key distinction between the strong and the weak connecting processes. Each field is computed once and the data is replaced between areas as seen in figure 3-3 when the field is strongly connected. Then the same step is computed using up-dated boundary conditions for the obtained data from the second domain. This exchange method is repetited until a convergent solution is

found in both fields, the next solution step is taken and the fresh data is again shared.

For a weak link the data will at most be exchanged once across the multiple domains before starting the next step, such that there is no verification, as stated in Figure 3-5, to guarantee convergent data flow. Moreover, data might be less frequently transferred, which leads to very weak interconnection and eventually one-way interconnection.

Depending on the type of connection each approach has its pros and downsides. Low coupling usually yields more quick results, however the system is usually unstable and calculated results are less exact, particularly if significant distortions occur within the domain.

Some of those problems can be solved by strong connections, but with time of implementation more than weak connectivity and the difficulties of instability cannot be entirely eliminated by mass effects. A monolithic process allows an estimate of extremely unstable systems, but at the price of the time necessary to solve the problem compared to a partitioned process.

In these approaches, data transmission between various domains may be one-way or two-way. Temperatures, displacements, heat transfer, distortion and other data may be sent. The one-way link transfers data on a single path, which means the system transfers data either from the solid to the fluid domain or the other way round. One-way coupling is a helpful tool for reducing the time required to implement the model. This sort of connection may only be utilized, however, if calculated results of one domain influence other domain substantially.

This method uses a double-way connection to transmit data from solid to fluid and fluid to solid on a regular basis in both directions. In cases where there are substantial distortions, such as blood circulation inside the artery,

the peristaltic pump and excessive heat expansion issues, this kind of transport is extremely essential, such that the findings of each model have effects and effects directly on the boundary conditions.

3.10.4 COMSOL Multiphysics software

COMSOL Multiphysics was the software platform for studying and simulating the phenomena of interaction of the fluid structure. It is an integrated simulation platform for many disciplines and in numerous academic, medical and other sectors of engineering. Because of its great capacity and the aim of this research, this software was chosen. Commercial software tools are utilized to analyze and perform the fluid flow simulation and heat transfer in a square enclosure using the finite element approach having two input and output fluid holes as well as a flexible cartridge.

In COMSOL Multiphysics program, each simulation has the ability to link or interaction with others. This harsh condition actually reflects what actually take place in actual-world. COMSOL Multiphysics tool has distinctive abilities for resolving the microfluidic and fluid flow simulations phenomena for actual world problems **[54]**.

COMSOL software is adaptive tool. If the simulation needs any modification regarding to the geometry or changing any of the input variables, it can be easily modified. It produces an easy way for electing the necessary module from the library of the program, which comprises of many modules describe various engineering, natural and industrial applications.

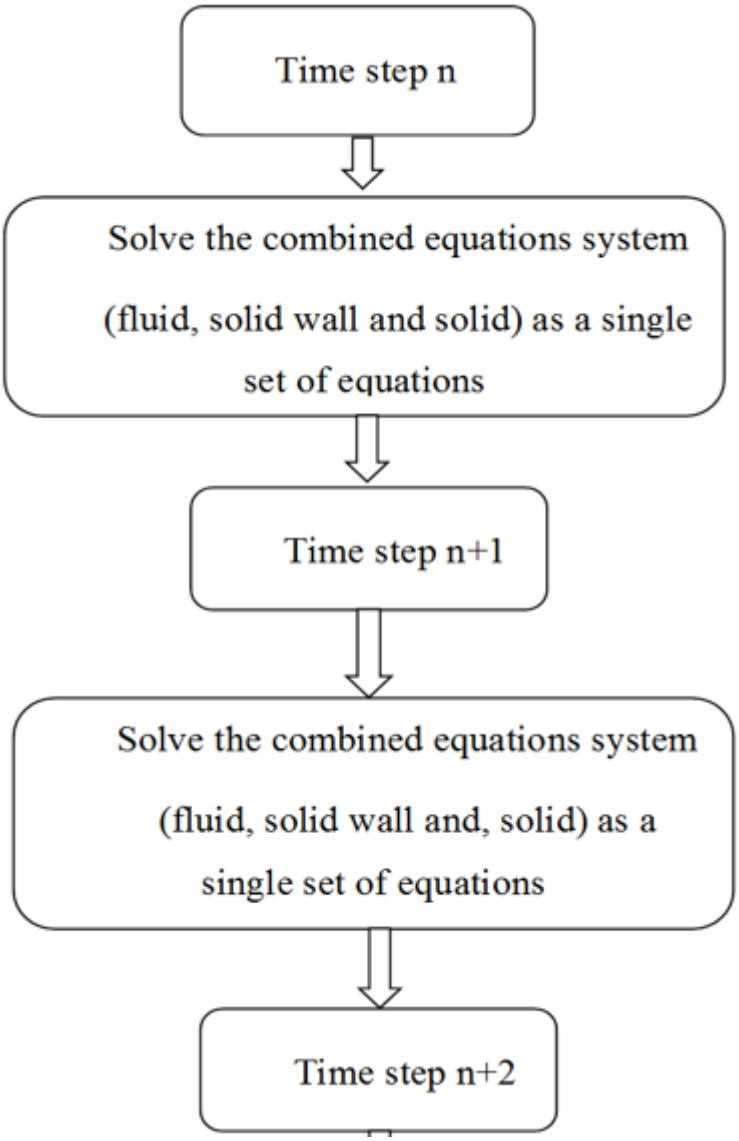

Figure (3- 5) Two-way monolithic method in FSI simulation

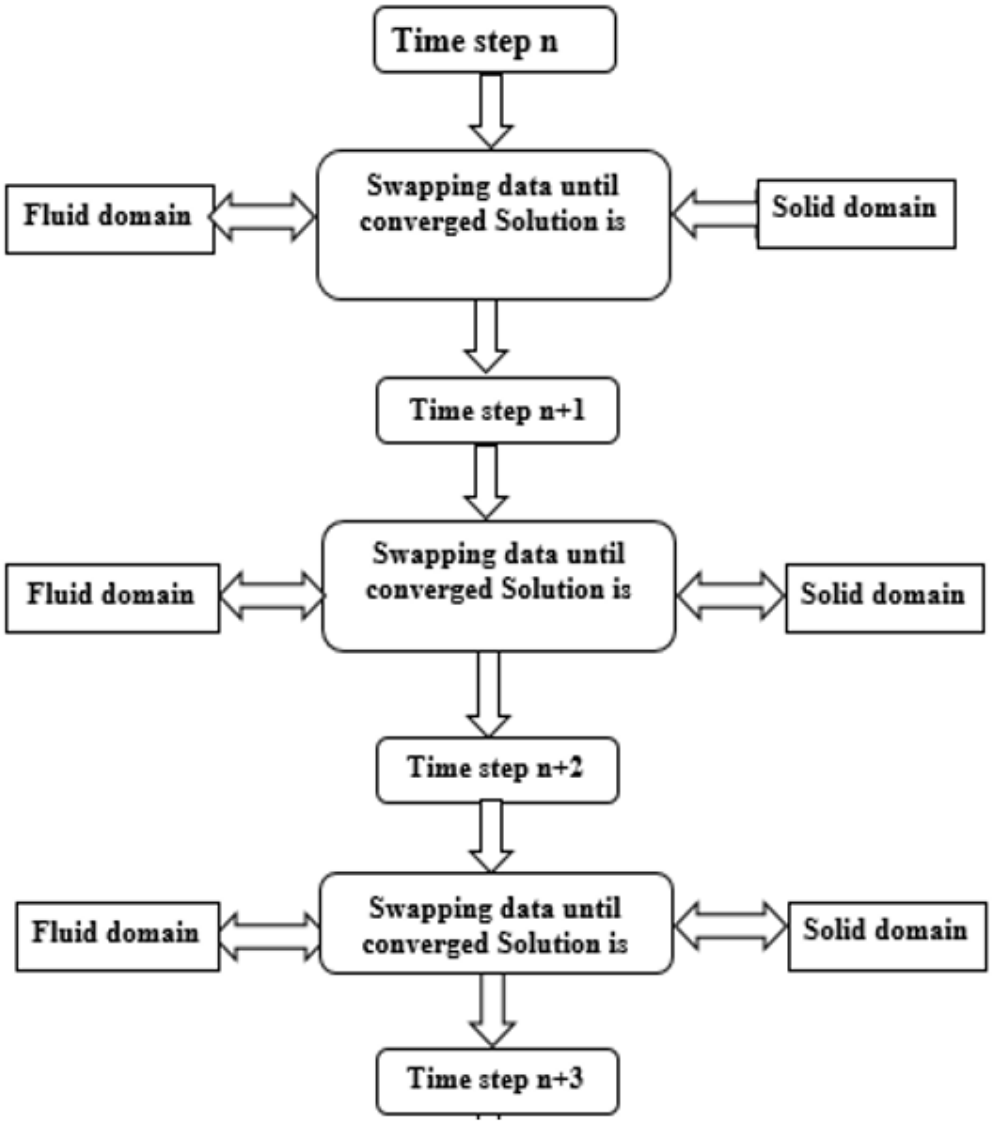

Figure (3- 6) Two-way strong coupling algorithms

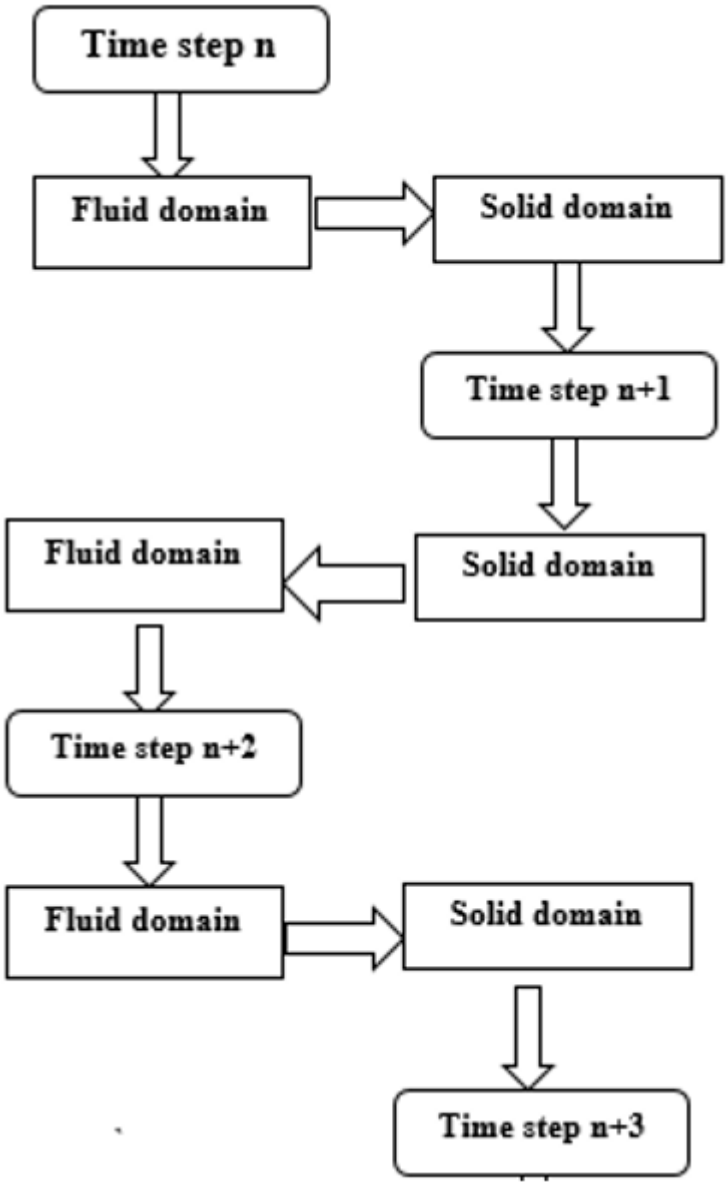

Figure (3- 7) Two-way weak coupling algorithms

CHAPTER FOUR

Results And Discussion

Chapter Four: Results and Discussion

4.1 Introduction

The numerical results of the influence of hexagonal location and steps number, elastic modules of the flexible wall (E), Reynold (Re) Hartman number, began number, on the unsteady mixed convection inside a square cavity including a hexagonal solid, the hot wall is flexible and it was heated differentially are presented in this chapter. The present study focused upon on fluid flow as well as thermal distribution regions. As a result, the elastic hot wall stress study was ignored and delayed to future research. However, the main pertinent parameters for this research are: Rayleigh number (Ri = 10^5), elastic modulus of the flexible wall (E = 10^8, 10^5, 10^4), Reynolds number (Re= 100, 300, 500), hexagonal location (X=0.5, Y=0.7), (X=0.6, Y=0.6), (X=0.6, Y=0.7), (X =0.7, Y=0.5). Magnetic inclination angle (between 0° and 90°), Hartmann number (between 0 and 60). The effects of the number of step-like corrugations (between 1 and 8) and the nanoparticle volume fraction (between 0 and 6%) on fluid flow and heat transfer are numerically investigated. The Nanofluid in the current thesis was taken to be CNT/water Nanofluid, of Prandtl number (Pr = 6.9). The density ratio is ($\rho_r = 1.1$) . the diffusivity ratio is (α_r) $= 1$. The fluid enters the cavity at an opening on the top of the vertical left wall, leaving the cavity through another opening on the bottom right vertical wall. High thermal conductivity is seen as being hexagonal solid to nanofluid, 10 times the amount of water. The results are shown as streamlines and isotherms as well as the Nusselt average. COMSOL Multiphysics ver.5.5 commercial software program was utilized to achieve numerical findings in present research.

4.2 Validation

To ensure that the numerical findings of current work are accurate, which is achieved using COMSOL Multiphysics software, the outcomes of the present code were compared with the results of other researchers. The validation was with researcher as follow.

1- The numerical solution was validated with the published work of **Ismael and jasim [49].** With the published work of Ismael and Jasim **[49]**, the numerical solution with the specified grid size was validated The numeric code was adjusted to recalculate the results shown in **[49]**, a mixing convection in a square shape with a flexible fin on the bottom heated wall. The comparison of the flux and the is thermal lines as illustrated in Figure 4 to 1, Evolution of streamlining and finishing with the Ri time, =100, Re =50, Ca =10^{-4}, and Xf = 0,2 as shown in Figure (4-1) and (4-2), was made in the case Re =150, Ca = 10^{4} and Xf = 0,2 respectively. There was a pretty excellent agreement between the present and outcomes **[49]**. The proposed numerical solution is therefore confirmed to be able to produce results of high confidence.

2- With the published work of **Selimefendigil et al. [37]**the numerical solution was validated . A mixed convection inside a square envelope of a solid L-shaped, was used to recalculate results. The comparison was done with the fluctuations of the current and those obtained by **Selimefendigil et al. [37]**and for the Re = 500, E = 10^{6}, d1 = 0,3H, y_c= 0,5H , xc = 0,5H), φ = 0,02) and the changes in stream and isothermal lines as shown at figure (4-3). The existing numerical solutions can thus be determined to provide a high degree of confidence. Variations Average number against number of Reynolds for hot walls were also studied (Ha=25, E = 106, d 1 = 0.30 H, = 45, xc = 0.5H, and = 0.5H, yc = 0.02), as seen in figure (4-4). The picture

was now presented as the figures. **Selimefendigil et al. [37]**had really nice findings today and those achieved..

3- With published work **Selimefendigil and Oztop [31]** , the numerical solution has been validated. A number analysis of the convection mixed of CuO-water nanofluid is carried out under the influence of the sloping magnetic field and steps like corrugated elastic walls in a hollow with entrance and exit ports. The comparison was done with the changes of Re = 100, E = 102, α = 45º, τ = 0.03,Ha=30) and the current findings and those of **Selimefendigil and Oztop [31]**, as shown in Figure (4-5) was very good.

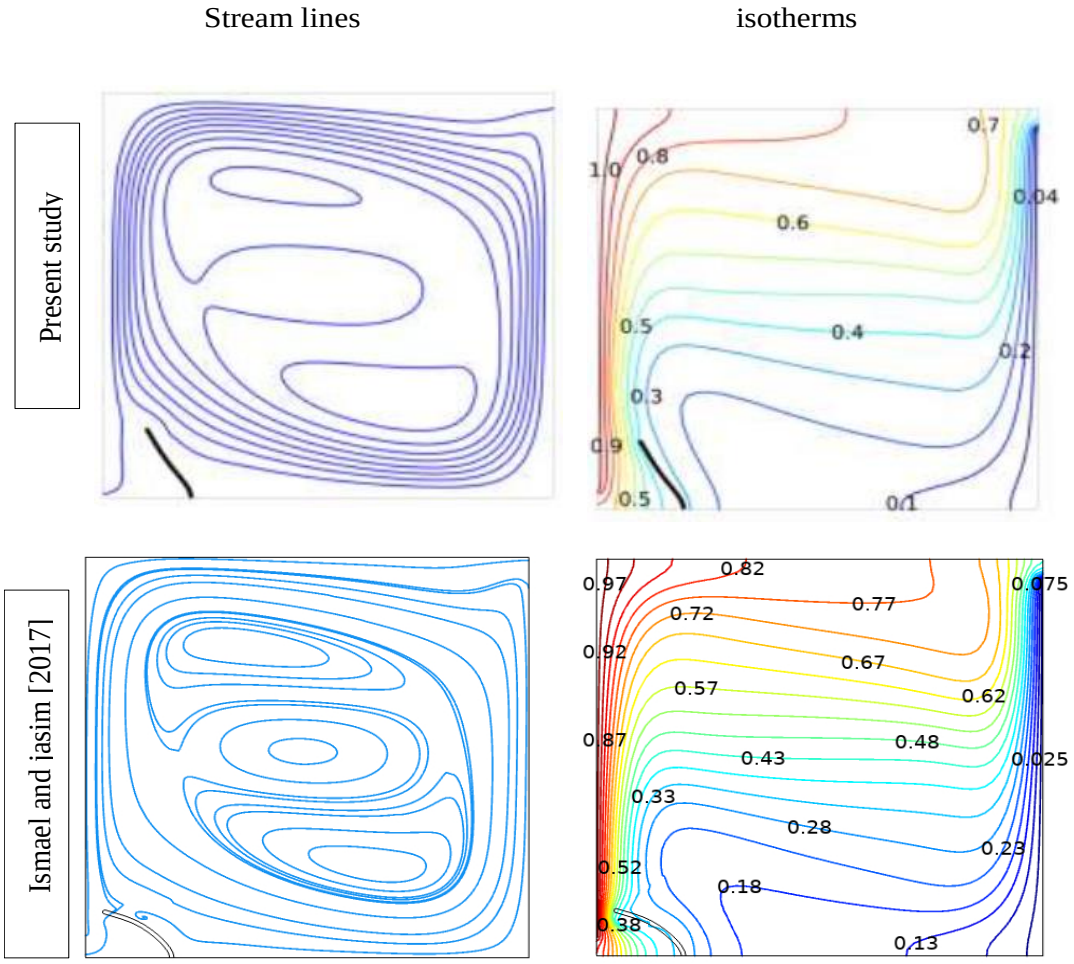

Figure (4- 1) Comparison between the current study software results and the study Ismael and jasim [2017] [49]at Re =150, Ca = 10^{-4}, and Xf= 0.2.

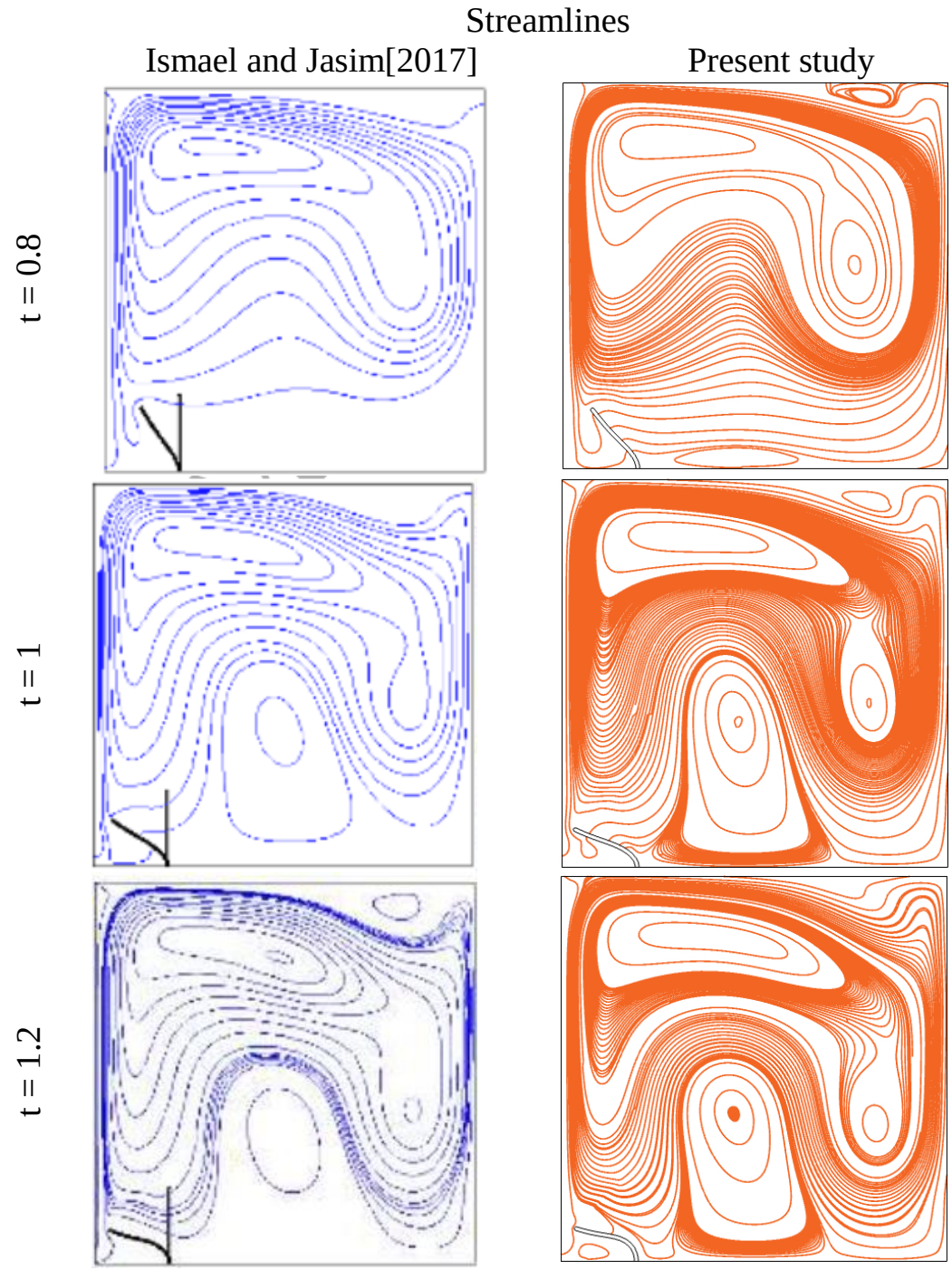

Figure (4- 2) Streamline Evolution withtime at Re= 250, Ca =10^{-4}, Xf = 0.2, andRi = 100.

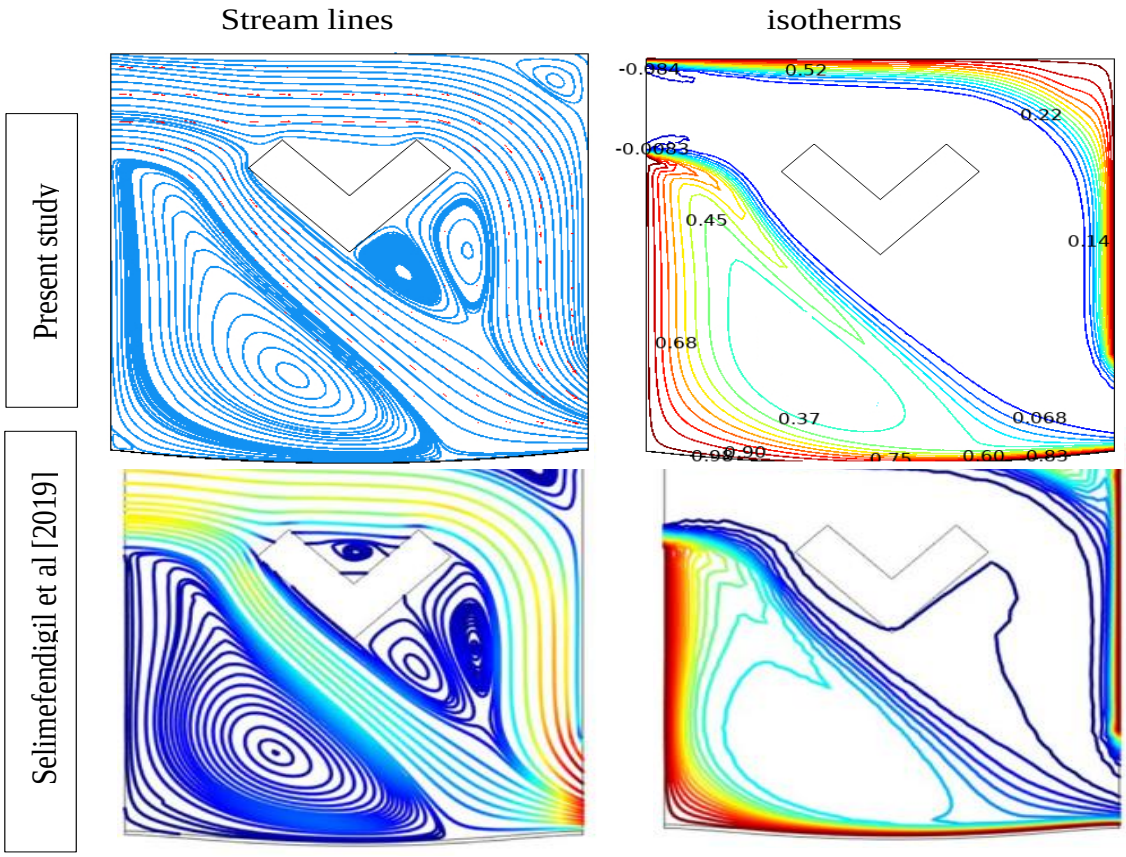

Figure (4- 3) Comparison between present study program and Selimefendigil et al. [37] results at. (Re =500, E = 10^6, d_1 = 0.3H, Ω = 45, x_c = 0.5H, y_c = 0.5H, φ =0.02, Ha=0)

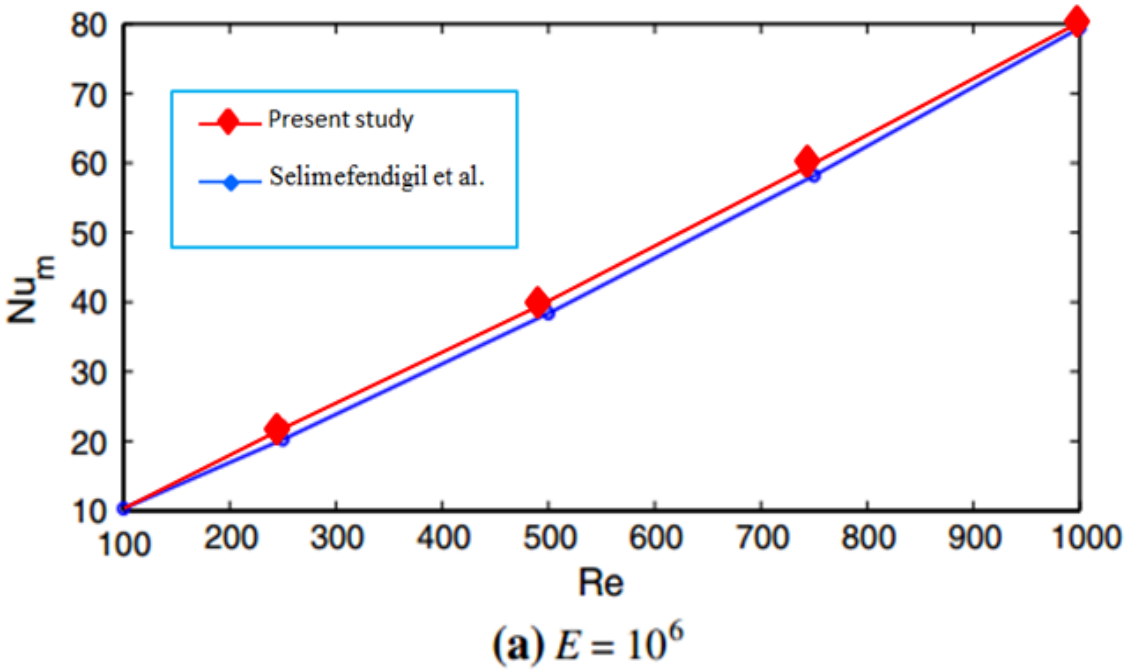

Figure (4- 4) Average number of Nussult against Reynolds for all heated walls (Ha=25, E = 10^6, Ω= 45, d_1 = 0.3H , φ = 0.02, x_c = 0.5H, y_c = 0.5H).

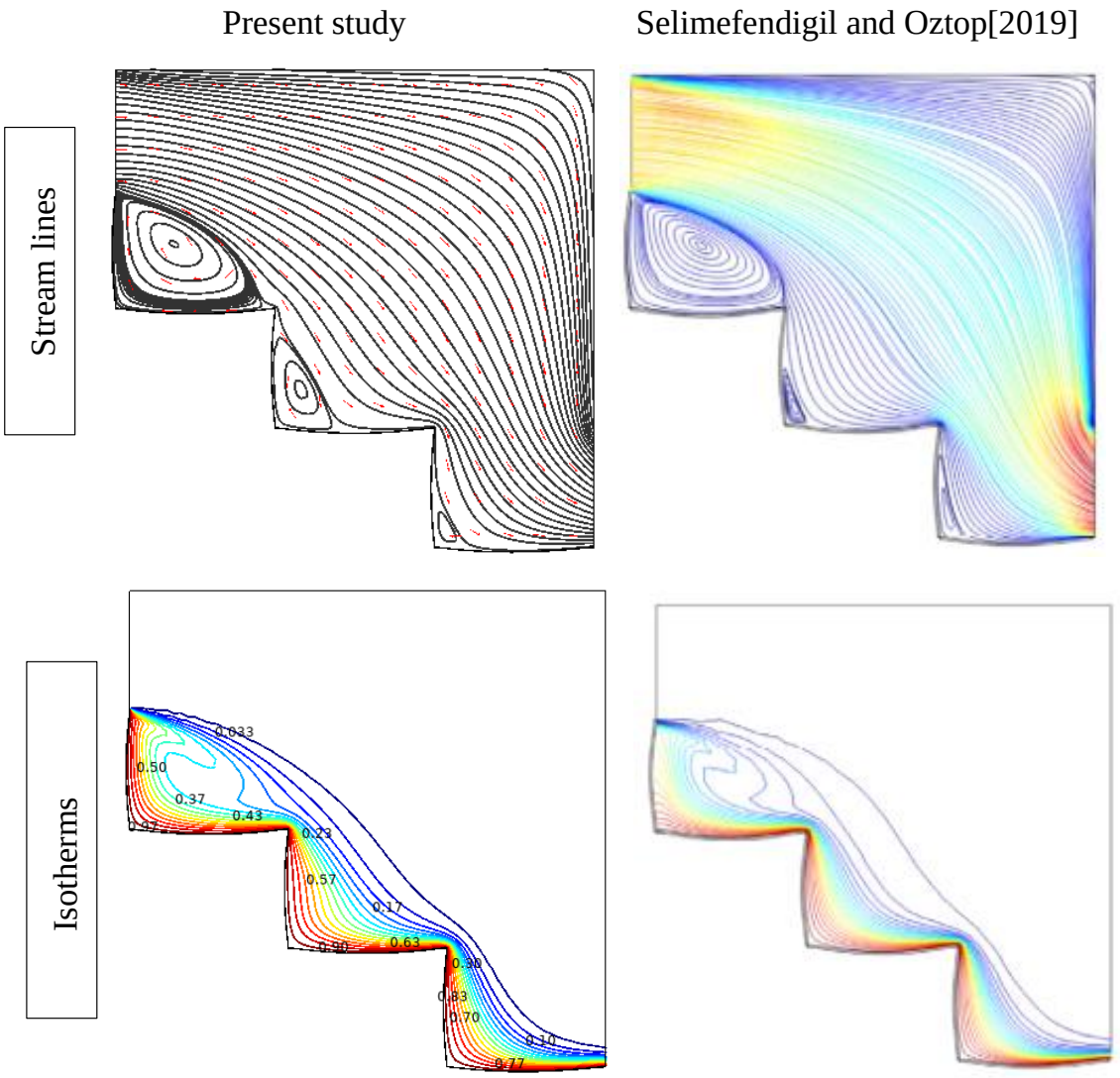

Figure (4- 5) Comparison with natural convection in a square enclosure with a flexible wall with Selimefendigil and Oztop [31]. (Re = 100, E = 105,φ = 0.03,Ha=20,γ=45º)

4.3 Thesis results

They are included in the following sub-sections to understand the results.

4.3.1 Evolution of the fluid and thermal fields

As the current problem is unsteady, it is important to identify the evolution of the fluid and thermal fields transient behaviors to quantify whether the flexible hot wall is stable or cyclically oscillates over time. Several calculations have led to see that a time step of 0.01 can provide the

average Nusselt number a minimal difference. This time the whole calculation has been completed. The development of the instantaneous Nusselt numbers is seen in Figure 4-6 (a). For, $E = 10^4$ and various numerical values. The flexible hot wall is predicted to suffer a high deformation rate under these conditions. The Nusselt number must attain the constant stable state values beyond t = 4 except in case of Re = 100. This cyclical activity has likewise reached its constant regular status, as seen in Figure 4-6. (a). However, it was determined via a number of other parameter implementation that there is no regular Nusselt number status as shown in Figure 4-6. (b). There are also no lower E value wall deformations. This is not enough to distort the steep wall because of the fluid circulation. The evolution of the fluid field was, on the other hand, investigated for specified time periods by the stream lines and wall form. Figure 4-5 depicts the progress of streamlines in the initial and three additional cycles based on Figure 4-6(a). Because of the wall temperature differential in the convective heat transfer and the liquid entering the cavity, a major vortex from the clockwise occurs within the cavity. The size of the outlet hole is inadequate to discharge all the entry fluid, which forms a circular vortex. The flowing fluid strikes the right hand side of the hexagonal wall and then the lower hot wall of the hydrogen, the fluid entering the cavity works as a hexagonal jet and force the hot wall into the original position. This increases the size over time, over and above the hexagonal solid producing a two circular vortex.

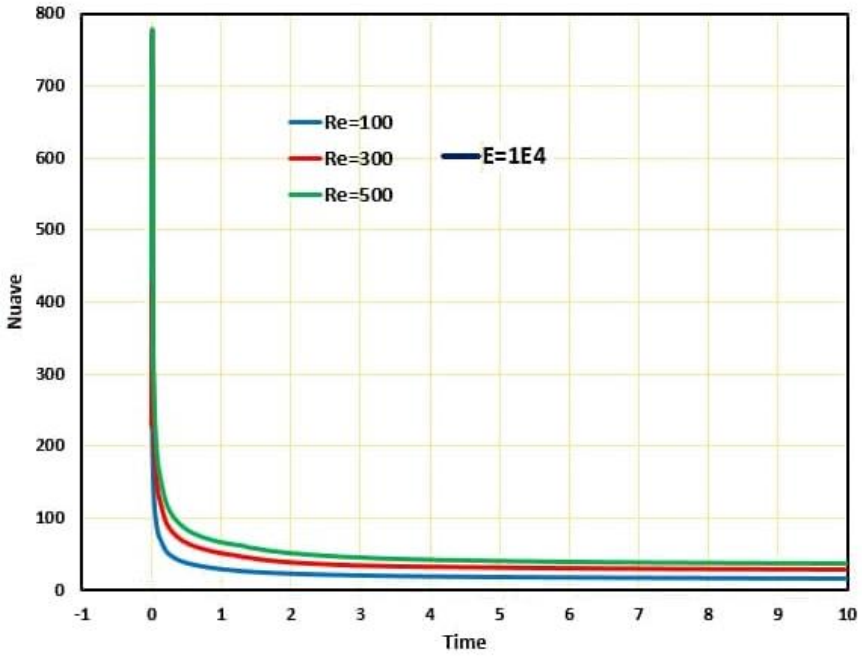

(a)

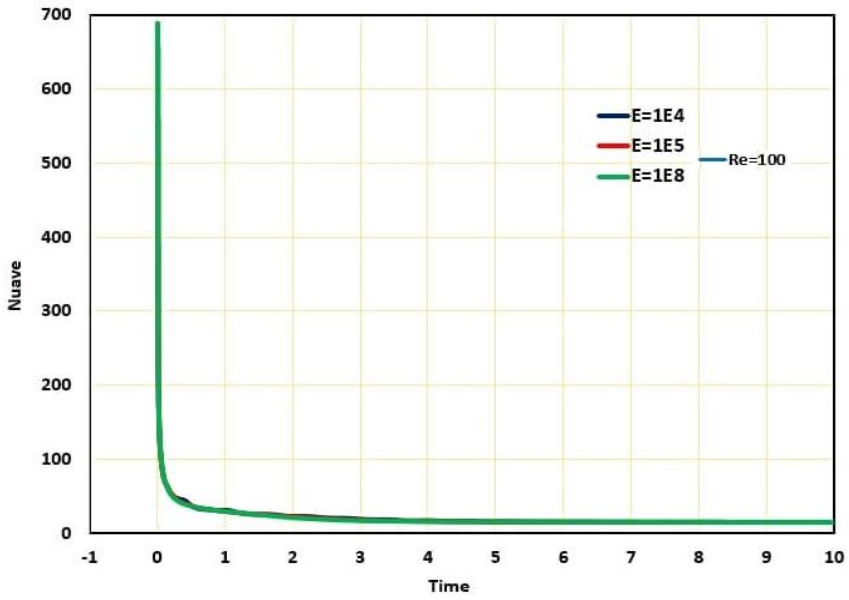

(b)

Figure (4- 6) average Nusselt number variation with time for φ = 0.03,Ha=20,γ=45o (a) different Re number and (b) different E

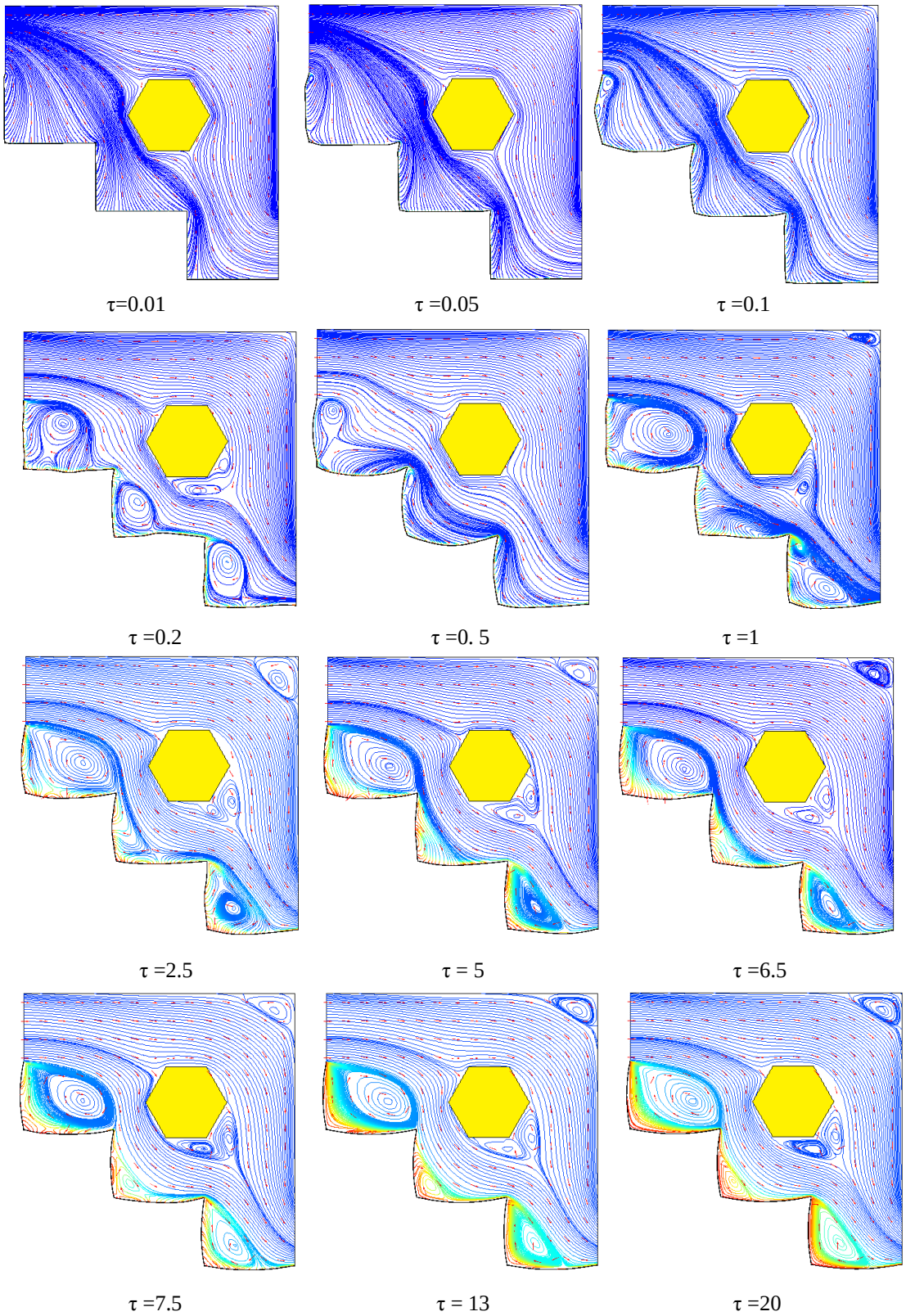

Figure (4- 7) streamlines and the flexible wall shape for Ha=25 , E=1e5 , Re=500 , ϕ=0.02 , γ=45

4.3.2 Effect of Reynolds number and elastic modulus of the step corrugation.

4.3.2.1 Streamlines and isotherms

Hereafter, unless stated, the instantaneous maps of the streamlines, isotherms and velocity vector are presented at $\tau = 20$. In order to demonstrate the impact of Re on both fluid flow (streamlines) and thermal (isotherms) fields inside the square cavity with hexagonal solid at different locations, several cases were studied, including changing some parameters and fixing others, as indicated by figures 4-8 to 4-13.

Figure 4-8 and 4-9 shows the stream and isothermal lines respectively for different Reynolds values at Ha = 25, $\gamma = 45^{\circ}$, $\phi = 0.03$. At Reynolds numbers values (Re = 100 ,300, and 500), and $E=10^4,10^5,10^8$ the fluid circulates inside the cavity and strike the hexagonal solid and then leaves it. For the first step directly below the port entrance, flow is separated at the end of the step like a corrugation, and for lower Reynolds numbers. Founding vortices close to the top right corner and building the two vortex centers under the main flow, from intake to outlet, resulting in a further increase of the Reynolds number. In the first step below the port of input at Reynolds number 500, an extra vortex is achieved while the scope of the upper right corner is increasing. Because of the greater velocity, the distortion of the flexible hot wall increases in the case of higher Reynolds and gives more room in step like corrugation for the formed vortices. For the first horizontal hot wall, steep temperatures are seen for the lower Reynolds number values due of the smaller deformation of the first step, and for the others with higher Reynolds number values the development is opposite. Also The recirculation of Reynolds is greater behind the hexagonal.

At Re = 100, the flow and thermal models for the various elastic modulus values vary marginally, but at a higher Reynolds value, discrepancies become obvious. A flexible wall with a lower elastic module

value at Re = 500 produces greater distortion and space for the fluid under the input port. With a rise in the value of the elastic module, the extent of the vortex near the heated horizontal wall near the port of entry decreases, and a decreasing size decreases the separated flow zone near the port of entry on the side of the step. Due to the resize of the distinct flow zones on the edges of the steps, at Re = 500, the location at Re = 100 is the sharpest gradient, although in the thermal patterns at Re = 100 there have been very little changes in the changes in temperature under the entry port.

4.3.2.2 Average and local Nusselt number.

Figure 4-10 and 4-13 represent the relation between Nusselt number for different values of Reynolds numbers. Figure 4-10 represent the relation between Average Nusselt number for different values of Reynolds numbers and elastic modulus on step of flexible hot wall location at (Ha = 25, γ= 45 ◦, ϕ= 0.03). The value of Average Nusselt number in step 1 increase and in step 6 decrease with increasing Reynolds numbers and elastic modulus. This is due to the step 6 is closer to exit port.

The relationship between Average Nusselt numbers and elastic modules for various Reynolds levels is shown in Figure 4-11. Increasing the number of Reynolds and reduced with elastic modulus, the value of the average Nusselt number increase. At Re=500 the Average Nusselt value fell from 30 at E=1e4 to 26 at E=1e8, whereas at Re=100 the value fell from 10 in E=1e4 to 6 in E=1e8.

Figure 4-12 illustrates Local Nusselt number variation for different Reynolds number values. Higher values of Reynolds number are locally increased except at the position of the first step below the intake, which is due to a less deformed value of Reynolds. The ultimate consequence is to increase Nusselt numbers to higher Reynolds and to increase nanofluid value because of improved thermal transport of nanoparticles.

The variation of the average Nusselt number for the different Reynolds numbers values is shown in Fig. 4-13. The variance in local Nusselt Number was reduced from 16% in E=1e4 to 13 percent for E =1e8 for various Reynolds and elastic modulus (Ha = 25, ɣ = 45 in the Re=100).

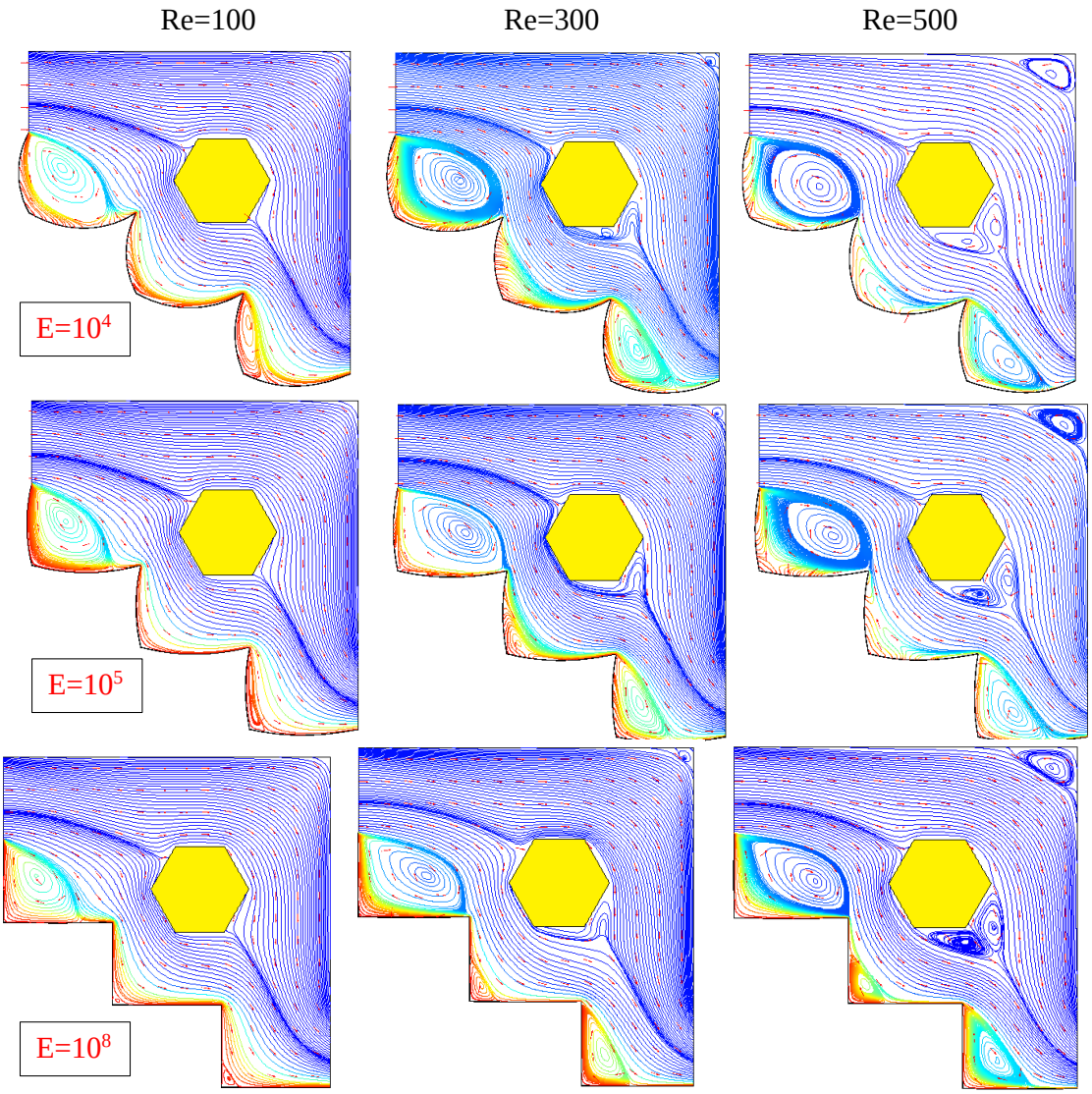

Figure (4- 8) effect of Reynold number and elastic modulus on the variation of streamlines (Ha = 25, γ= 45 ◦, ϕ= 0.03).

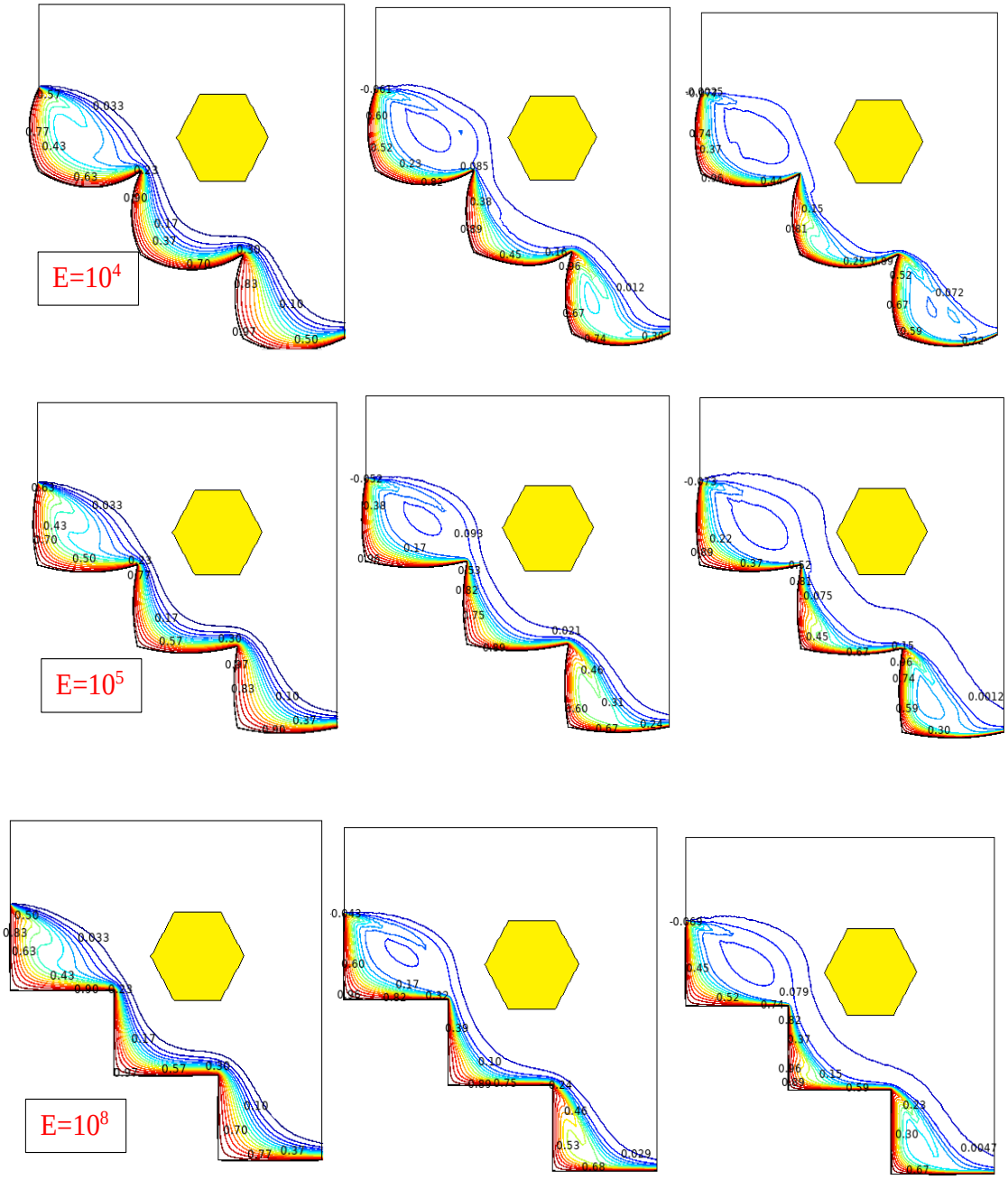

Figure (4- 9) effect of Reynolds number and elastic modulus on the variation of isotherms (Ha = 20, γ= 45 ◦, ϕ= 0 .03).

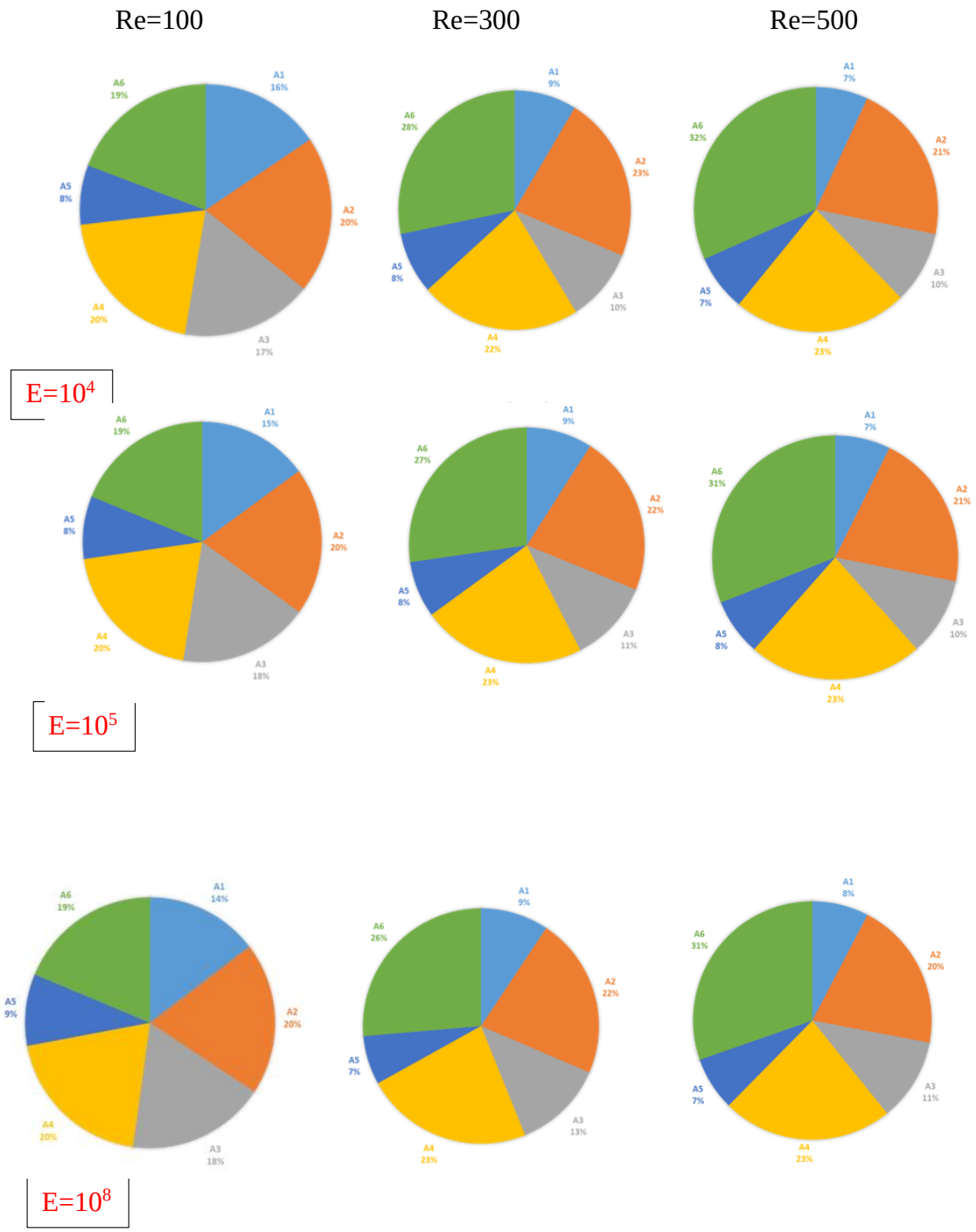

Figure (4- 10) Average Nusselt number for steps hot walls variation for different Reynolds numbers and elastic modulus at (Ha = 25, γ= 45 ◦, ϕ= 0.03).

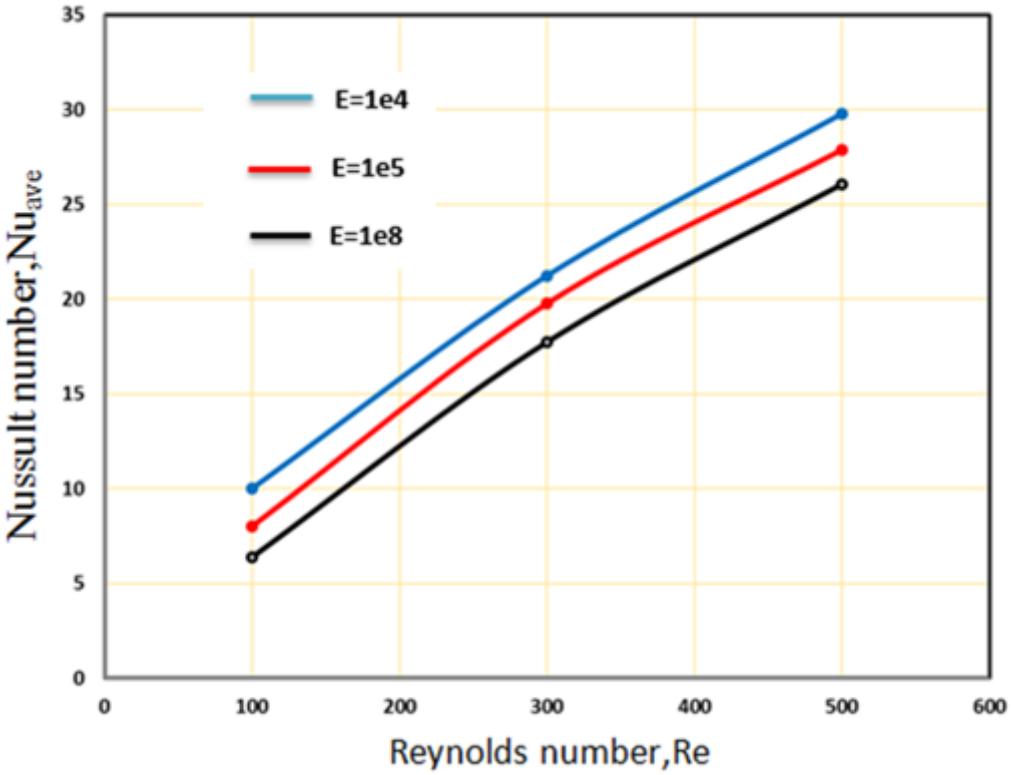

Figure (4- 11) relation between Reynolds numbers and Average Nusselt number for different and elastic modulus (Ha = 20,γ= 45°,ϕ= 0.03)

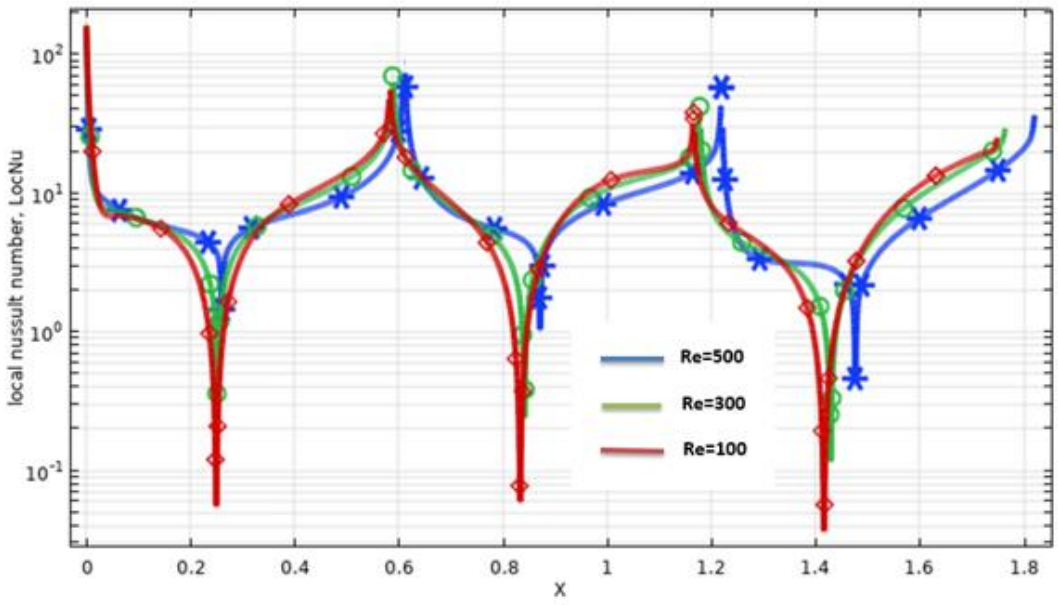

Figure (4- 12) Variation of local Nusselt numbers for various Reynolds and elastic module numbers (Ha = 25, γ= 45 ◦, ϕ= 0 .03).

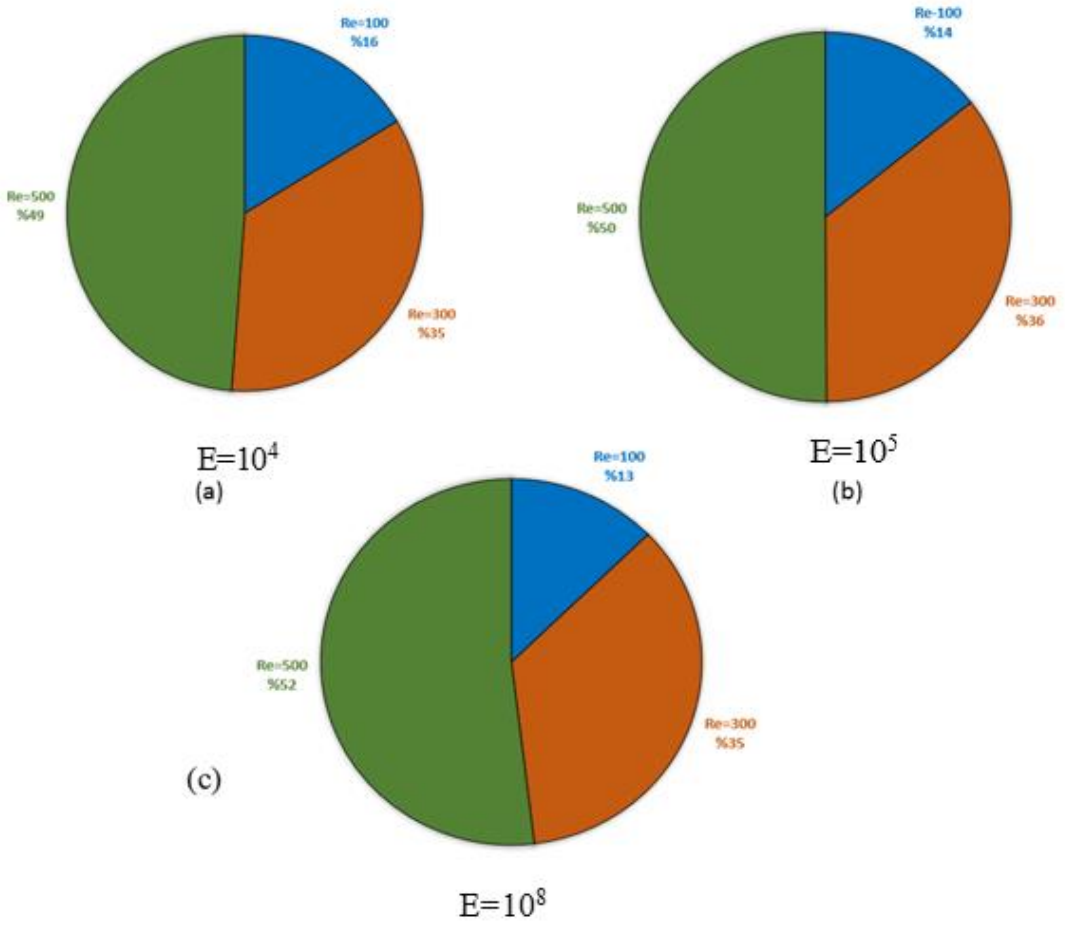

Figure (4- 13) Nusselt number average for all hot wall steps variation for different Reynolds numbers and elastic modulus at (Ha = 25, γ= 45 ◦, ϕ= 0 . 02). (a) $E=10^4$,(b) $E=10^5$,(c) $E=10^8$

4.3.3 Effect of Hartman number

4.3.3.1 Streamlines and isotherms

The influences of Hartmann on variations in the streamlines and isotherms in the vented cavity are shown in the figs 4-14 and 4-15 (N=3, Re=500, β=45 kin, ±=0 0-0.02). Without magnetic field, along the vertical wall underneath the input port is produced one vortex, and at the border of second stage a small recirculation zone is seen. In the top right wall of the ventilated chamber a vortex is revealed to be Ha=0 and its extent is decreased to Ha=30 and eventually vanishes to Ha=60. Behind its hexagonal solid, it was detected two vortices in Ha=0 and its spread for Ha=30 is reduced and ultimately Ha=60 evaporates. Increasing the number of Hartmanns will

reduce the number of zones within the vented cavity. Magnetic field strength also affects the clustering of isothermals close to the heat barriers. If the number of Hartmann increases, temperature gradients step down the heated horizontal wall underneath the entrance port due to the magnetic field removal of the tourbillons and local heat transfer in this area.

4.3.3.2 Average and local Nusselt number.

Figure 4-16 represent the relation between average Nusselt number variation and Harman number ($E=10^4$, $\gamma=45^\circ$, $\phi=0.03$). The value of Nussult number decrease at H=30 and then increase with increasing of Hartman for the same previous reasons.

Figure 4-17 represent the relation between average Nusselt number variation for different Harman numbers and elastic modulus (Re = 300, $\gamma= 45^\circ$, $\phi= 0.03$). the value of $E=10^4$ gives higher Nussult number.

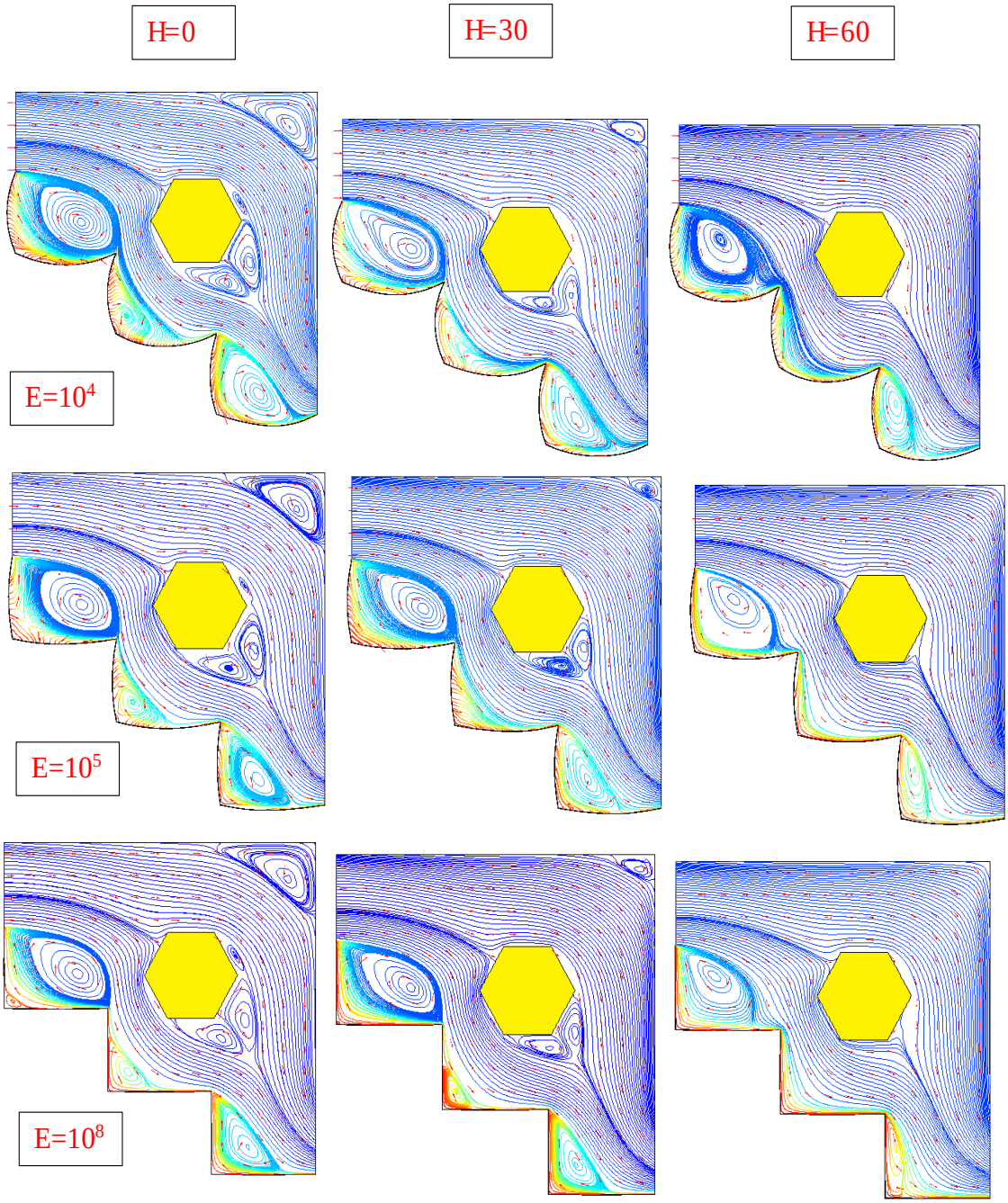

Figure (4- 14) Influence of Hartman number and elastic modulus on the variation of streamlines (Re = 500, γ= 45 ◦, ϕ= 0 .02).

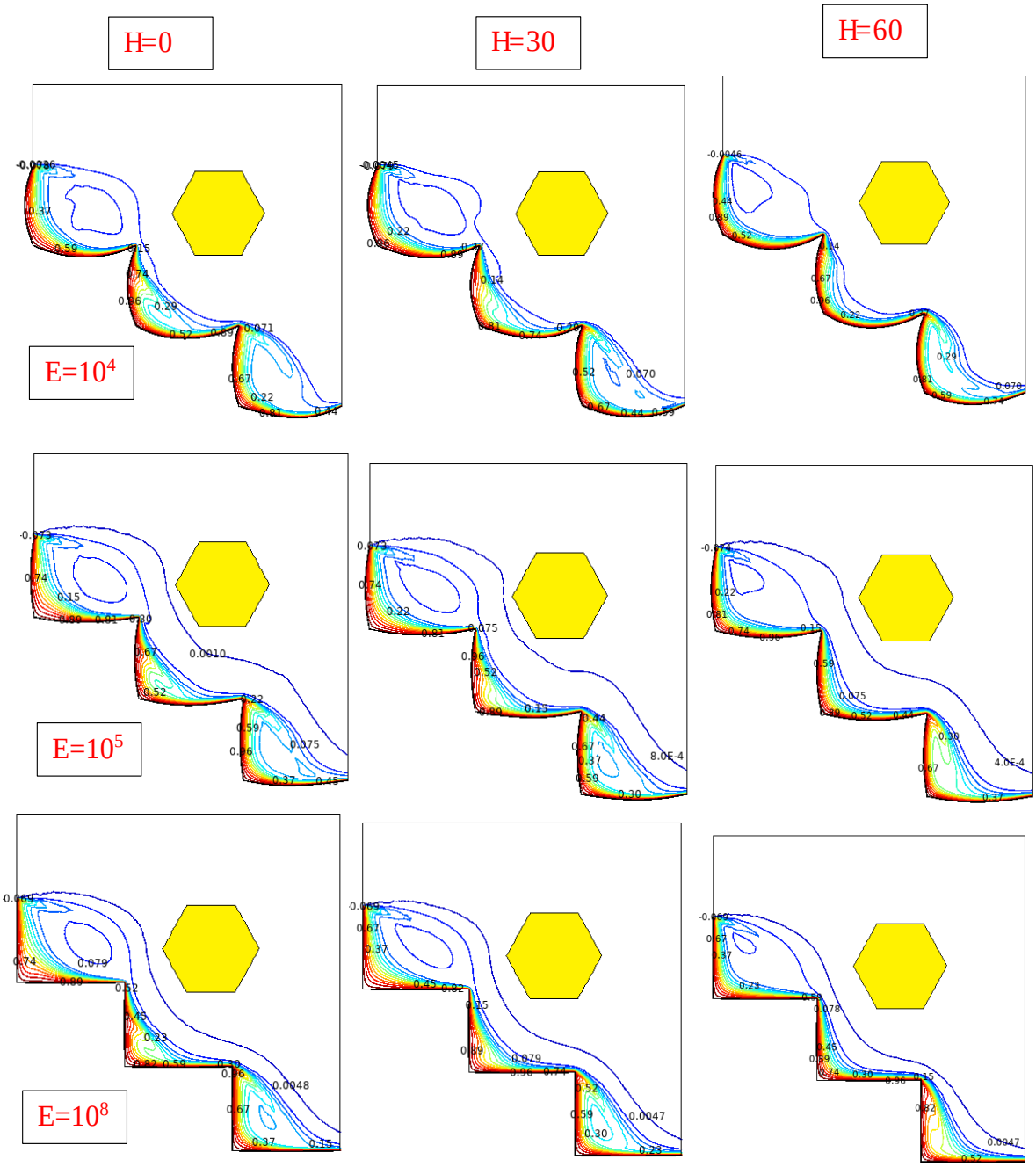

Figure (4- 15) Influence of Hartman number and elastic modulus on the variation of isotherms (Re = 500, γ= 45 ◦, ϕ= 0 .02).

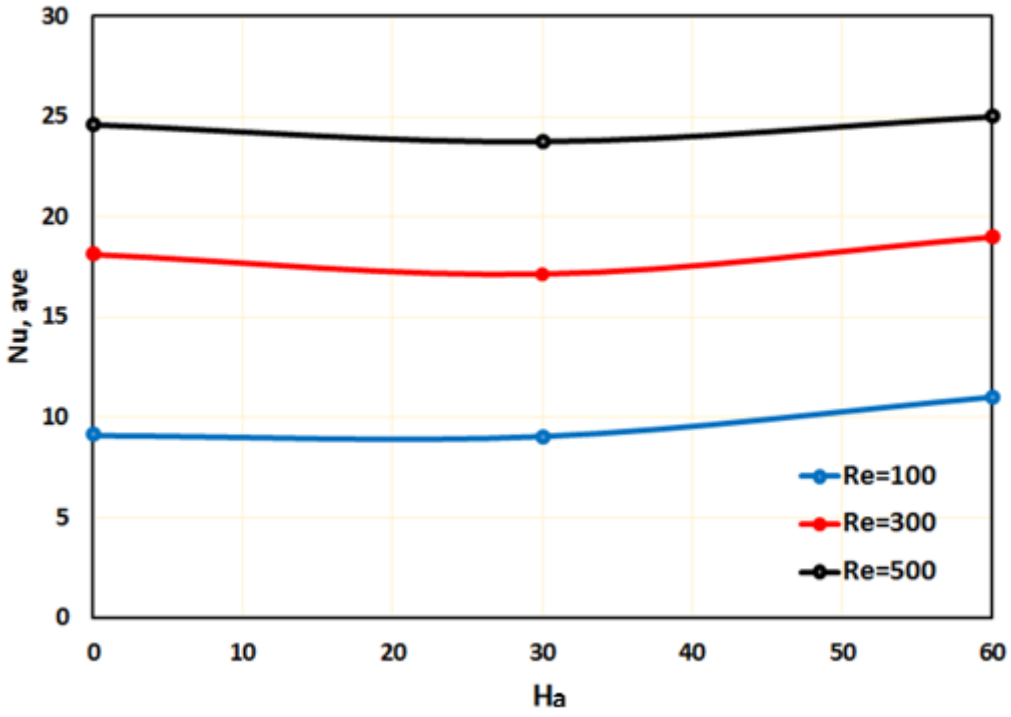

Figure (4- 16) Average Nusselt number variation for different Reynolds numbers and Harman number ($E = 10^4, \gamma = 45^\circ, \phi = 0.03$)

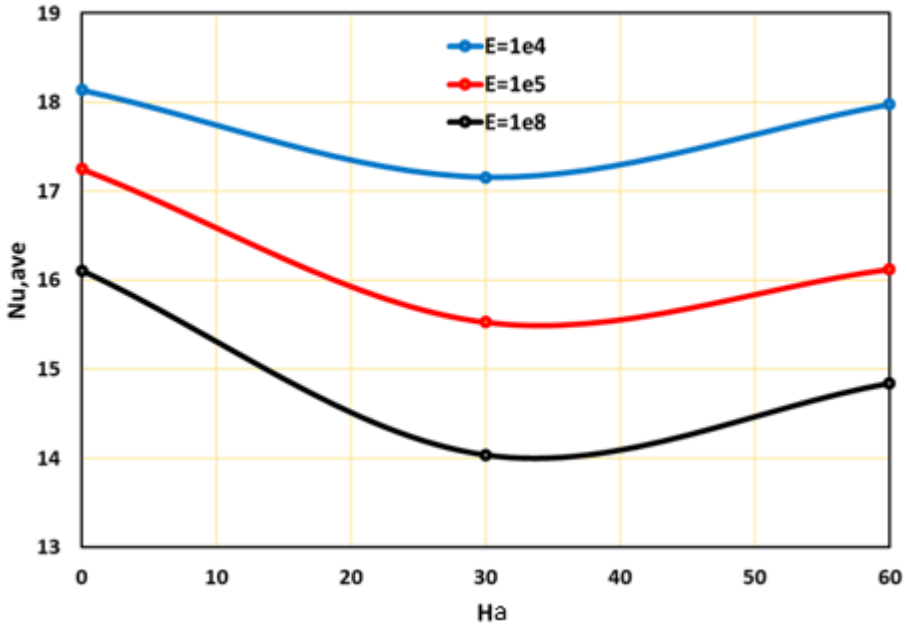

Figure (4- 17) Average Nusselt number variation for different Harman numbers and elastic modulus ($Re = 300, \gamma = 45^\circ, \phi = 0.03$)

4.3.4 Effect of magnetic inclination angles

4.3.4.1 Streamlines and isotherms

The angle of inclination of the magnetic field significantly influences flow variations and temperature patterns in the cavity, notably in the early stages below the input port for γ=0 and γ=45. Isotherms are clustered for this site when the value of γ rises.

Fig. 4-20 illustrates an average number fluctuation of Nusselt with numbers of Reynold and for various angles of magnetic inclination ($E = 10^4$, $Ha=25$,$\phi= 0.03$). This figure appears on the hot elastic wall step as circles at Nussult value. The magnetic field works in order to increase the local heat transfer rate, particularly at places near the entrance and the outlet ports, but in situations near the intake port there are very minor changes between γ=45, and γ=90 In the magnetic inclination movement

Fig. 4-21 and 4-22 represent average Nusselt number variation with Reynolds numbers and for different magnetic inclination angles at ($E = 10^4$,$Ha=25$,$\phi= 0.03$). As γ increase the Nussult number decrease. this due to as the angle of inclination toward the flow this lead to smashing the vortices.

Fig. 4-23. Shows average Nusselt number variation with magnetic inclination angles for different Re ($E = 10^5$,Ha=25 , $\phi= 0.03$), it shows as Re increase the average Nussult numbers increase.

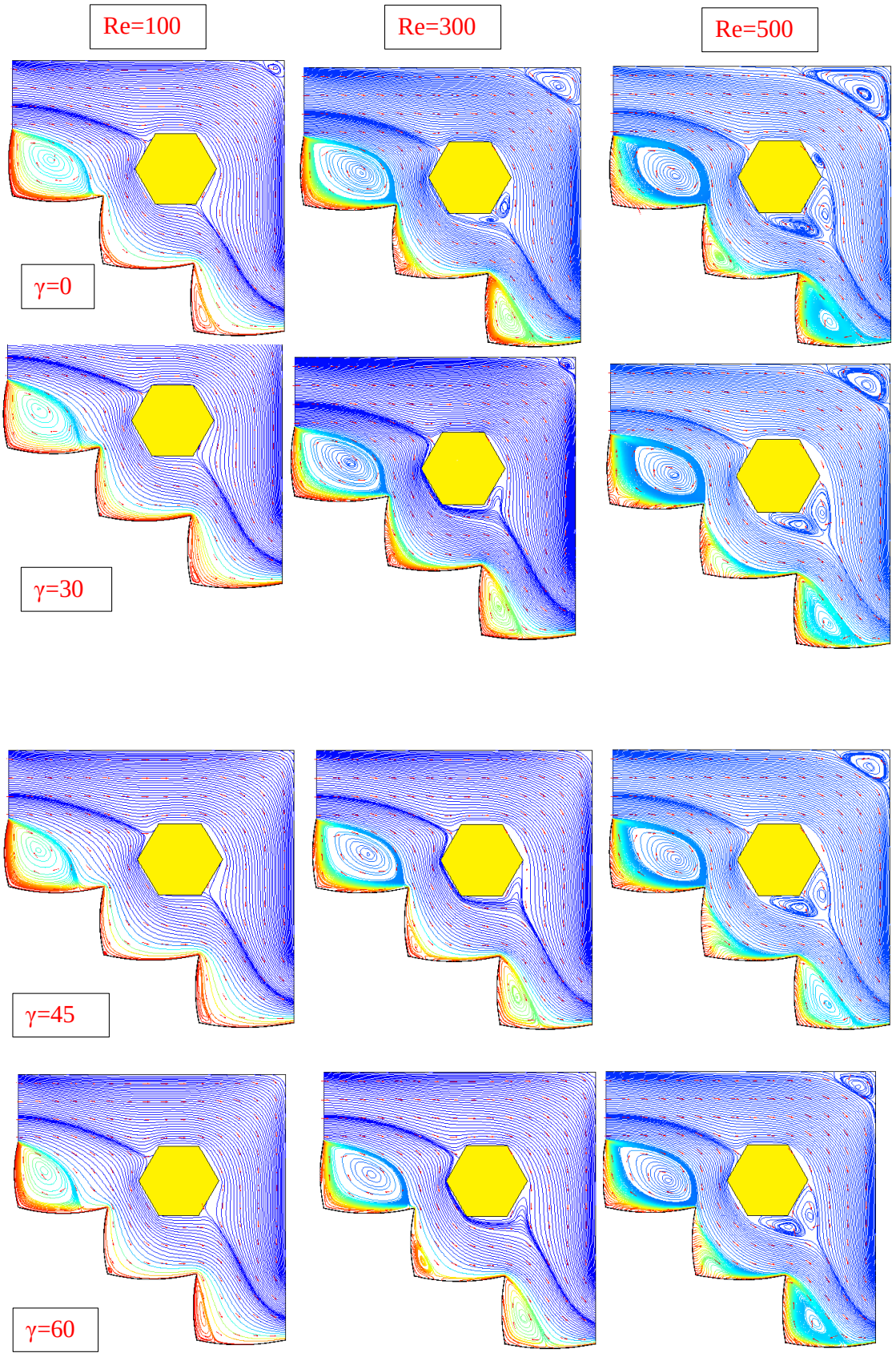
Re=100
Re=300
Re=500
γ=0
γ=30
γ=45
γ=60

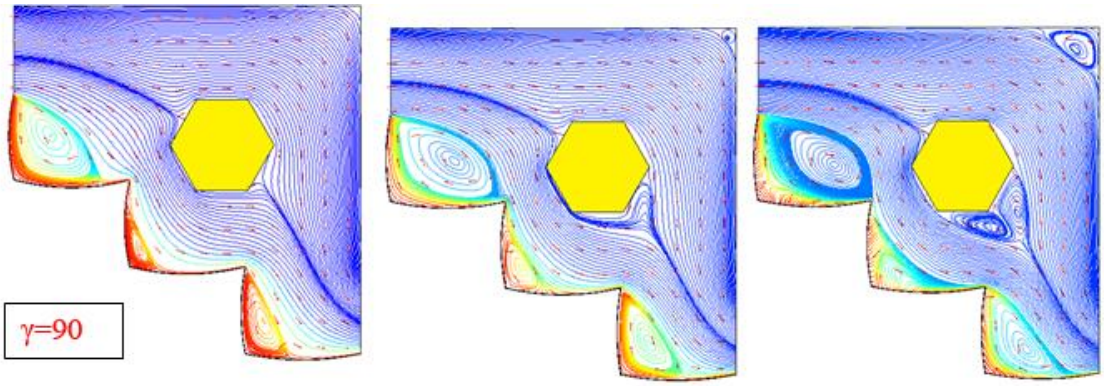

Figure (4- 18) Distribution of streamlines for various Reynolds number and magnetic inclination angles (E = 10^5 , Ha = 30, ϕ= 0 .02)

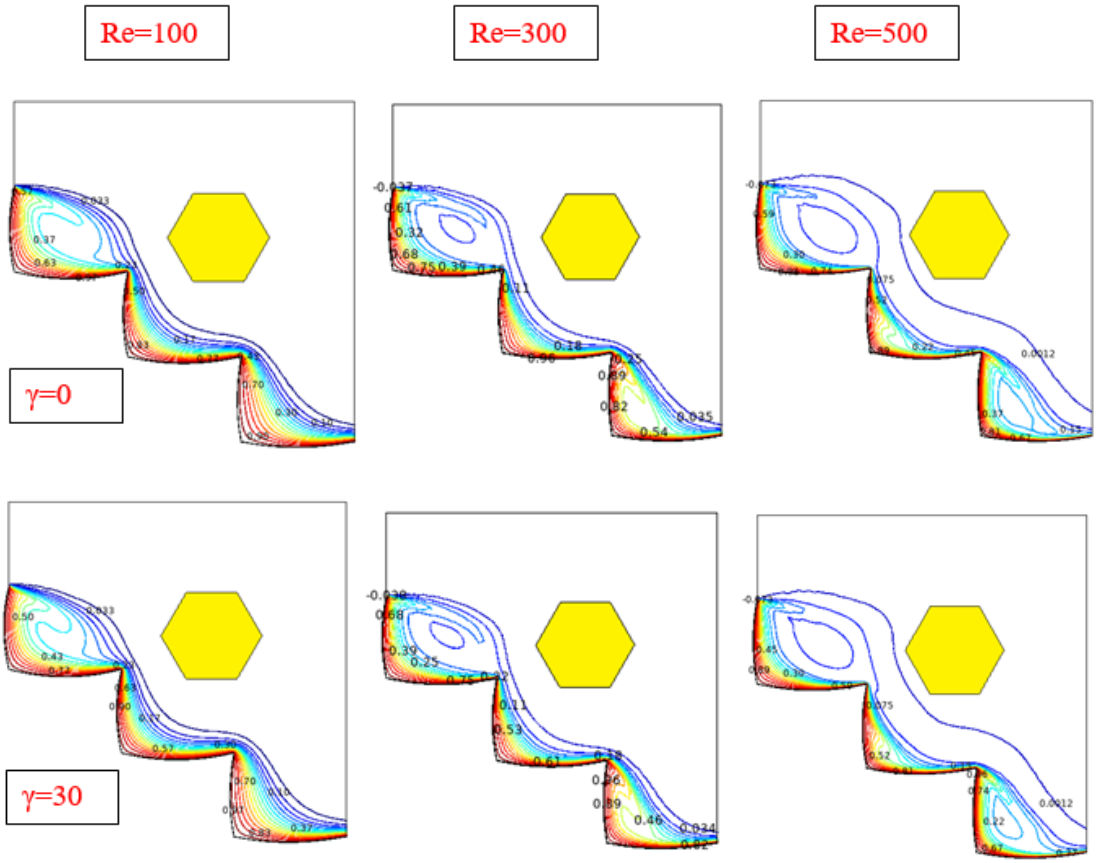

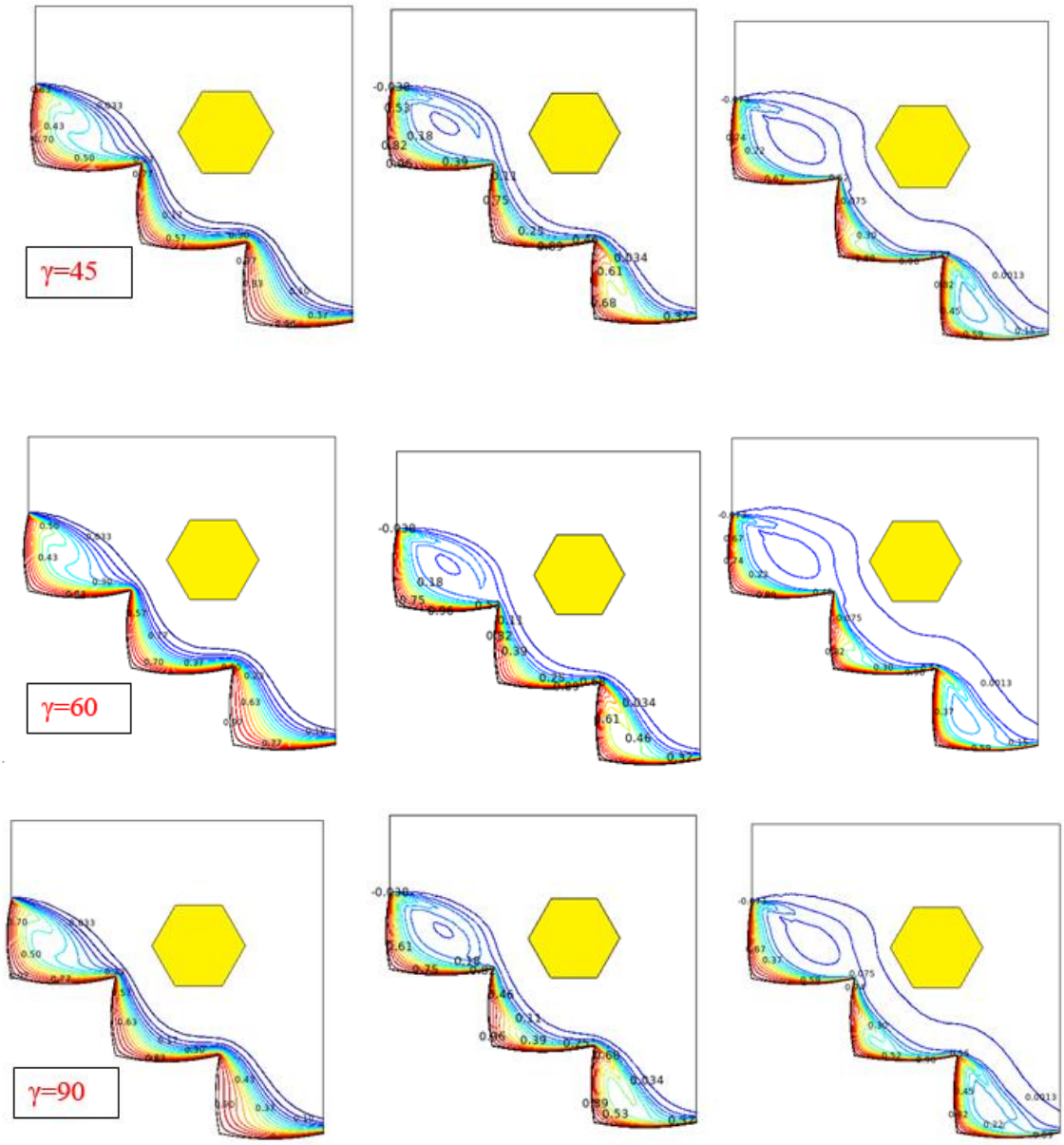

Figure (4- 19) Distribution of isotherms for various Reynolds number and magnetic inclination angles (E = 10^5 , Ha = 30, ϕ= 0 .02)

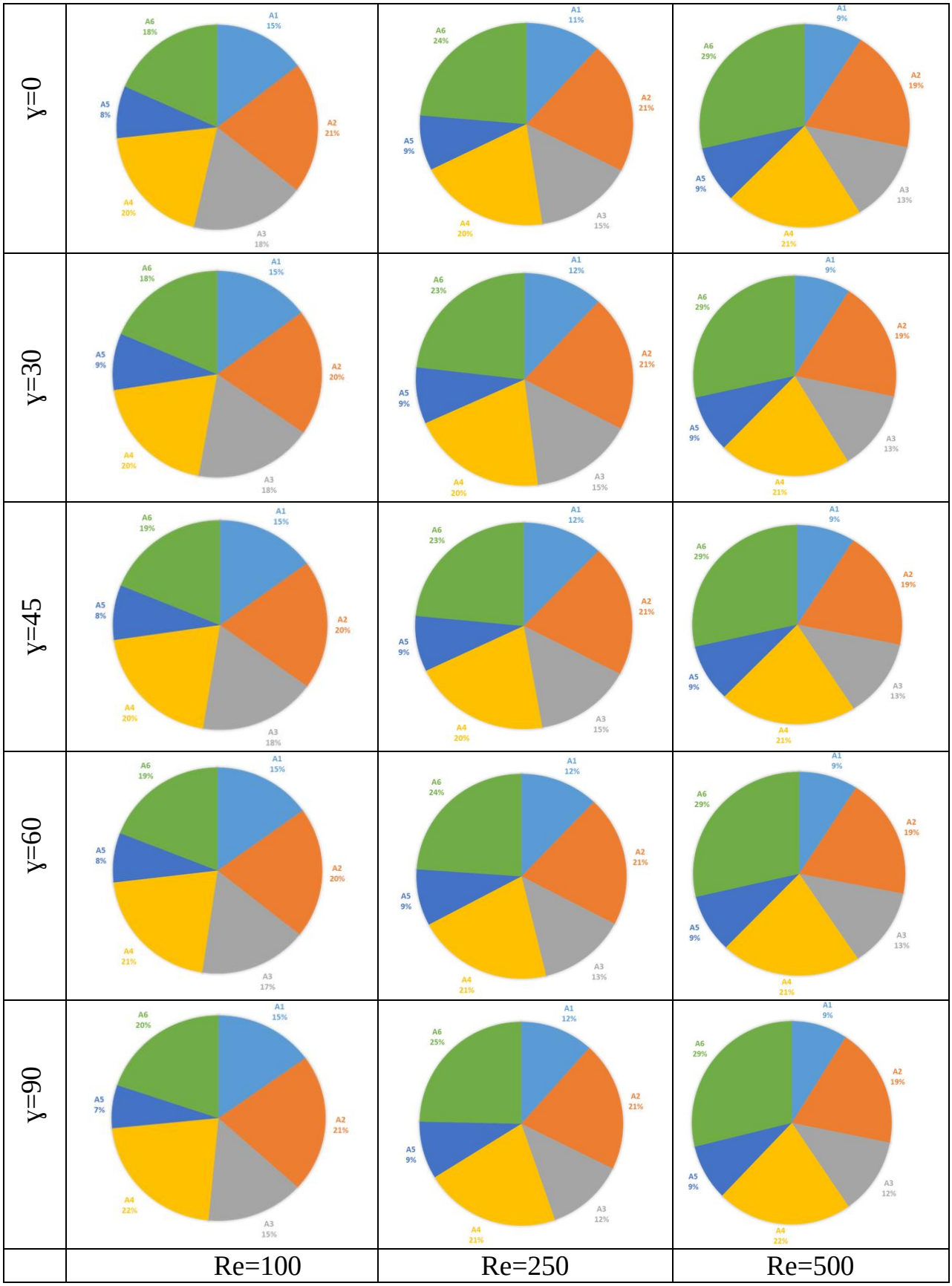

Figure (4- 20) Average Nusselt number variation with Reynolds numbers and for different magnetic inclination angles ($E = 10^4, Ha = 25, \phi = 0.03$)

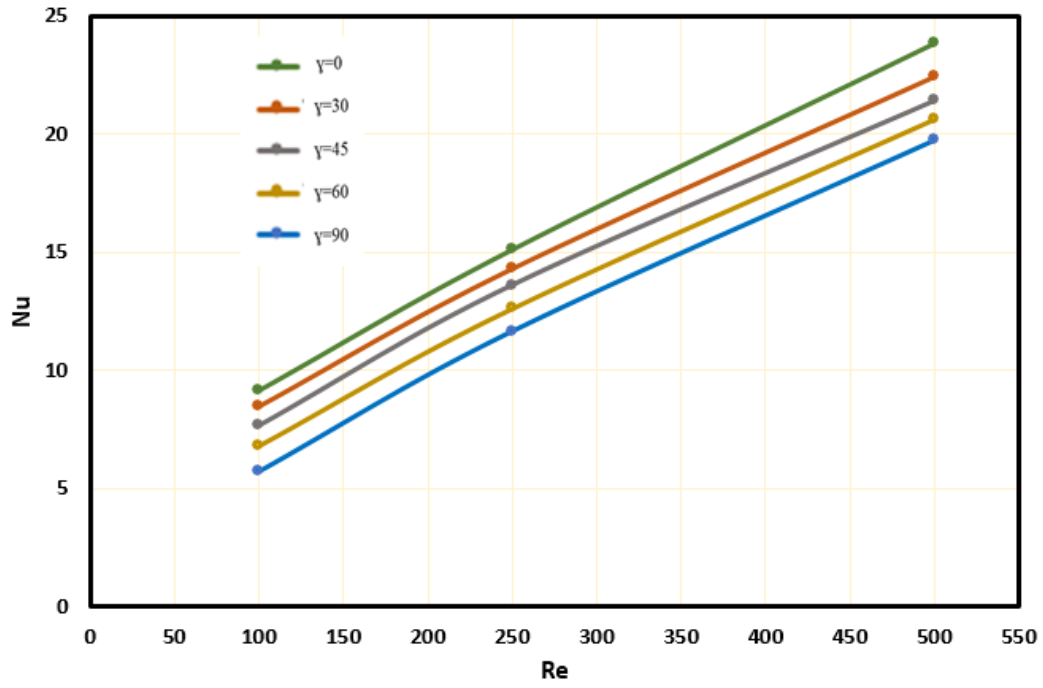

Figure (4- 21) Average Nusselt number variation with Reynolds numbers and for different magnetic inclination angles at ($E = 10^4, Ha=25, \phi= 0.03$) .

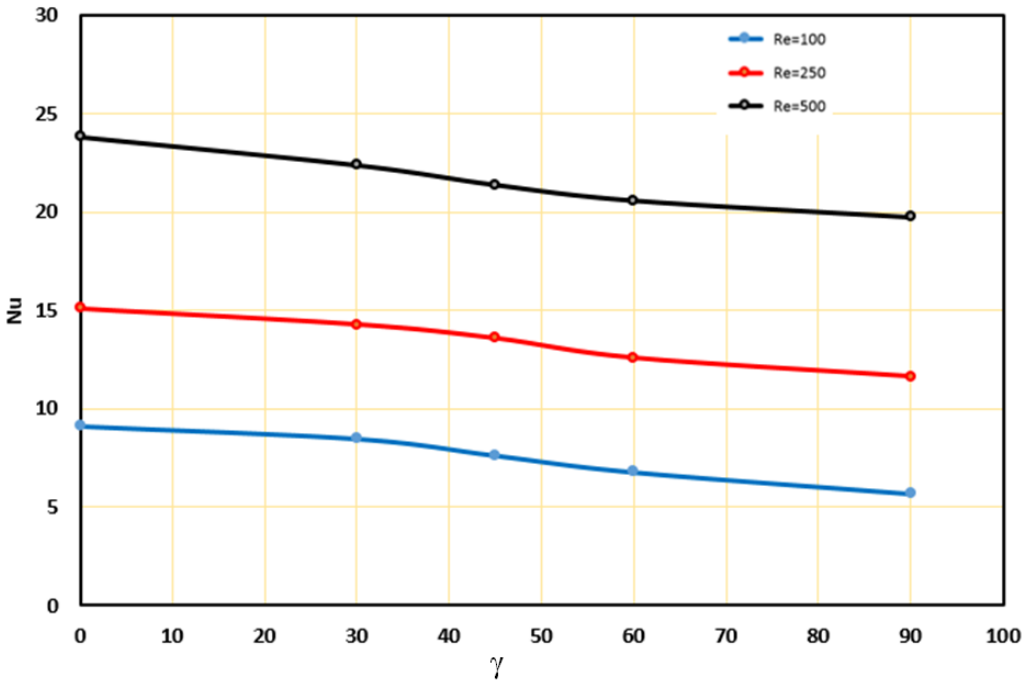

Figure (4- 22) Average Nusselt number variation with magnetic inclination angles for different Reynolds numbers ($E = 10^4$, $Ha=25$, $\phi= 0.03$)

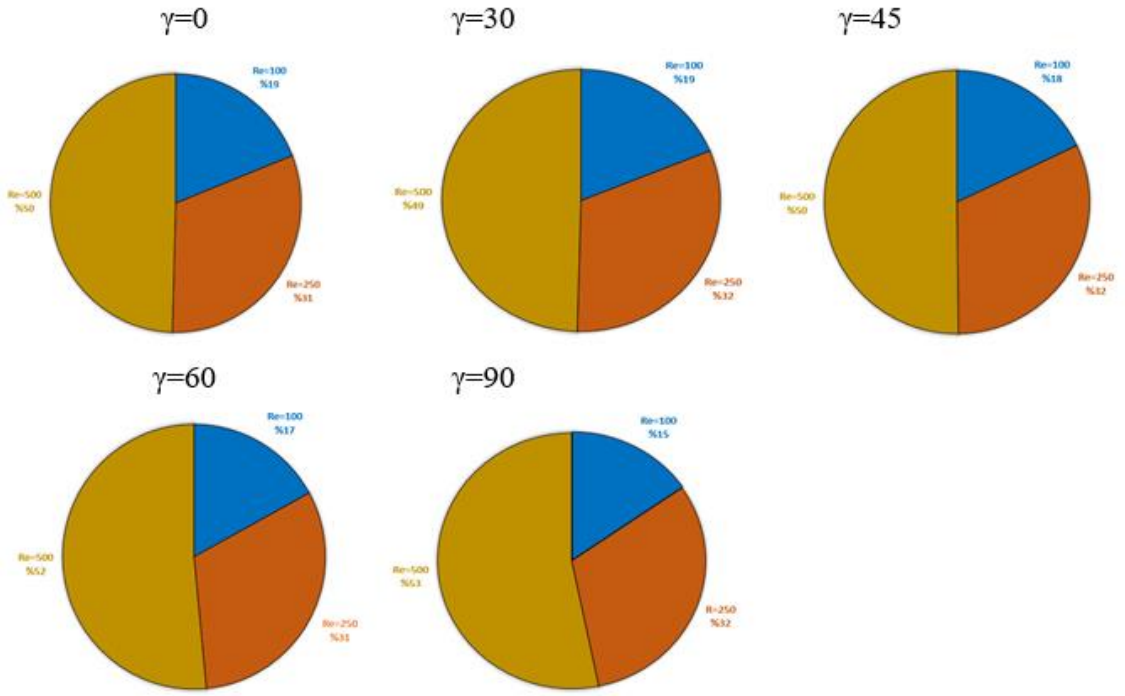

Figure (4- 23) Average Nusselt number variation with magnetic inclination angles for different Reynolds numbers (E = 10^5, Ha=25 ,ϕ= 0.03)

4.3.5 Effect of nanofluid concentration (φ)

4.3.5.1 Streamlines and isotherms

The graphs in Figures 4-24 and 4-25 illustrate the variation in streamlines and isotherms as a function of the volume fraction (φ) for the vented cavity (N= 3, E =10^4, Ha = 10, γ = 45°). As Reynolds number values vary. Overall heat transfer increases as Reynolds number increases, except in the location of the first step, which occurs at the inlet because of reduced deformation. In the A vortex that's found near the hot wall of the vented cavity for φ= 0, the vortex's magnitude is reduced when φ=0.06 is substituted in. Also the two vortex behind the hexagonal is reduced in size with increasing the volume fraction this due to cracking the boundary layers near the wall.

4.3.5.2 Average and local Nusselt number.

Fig. 4-26 shows how increasing the Reynolds number can increase the average Nusselt number and the results show that with nanoparticle fluid, the Nusselt number is higher. for Reynolds number of 150 and 500, the average

heat transfer rate of water is 8% below that of nanofluid, as shown in fig.4-27.

Local Nusselt number variation as well as Reynolds number variation is illustrated in Fig. 4-28. This figure shows that the local Nussult number is always the lower value.

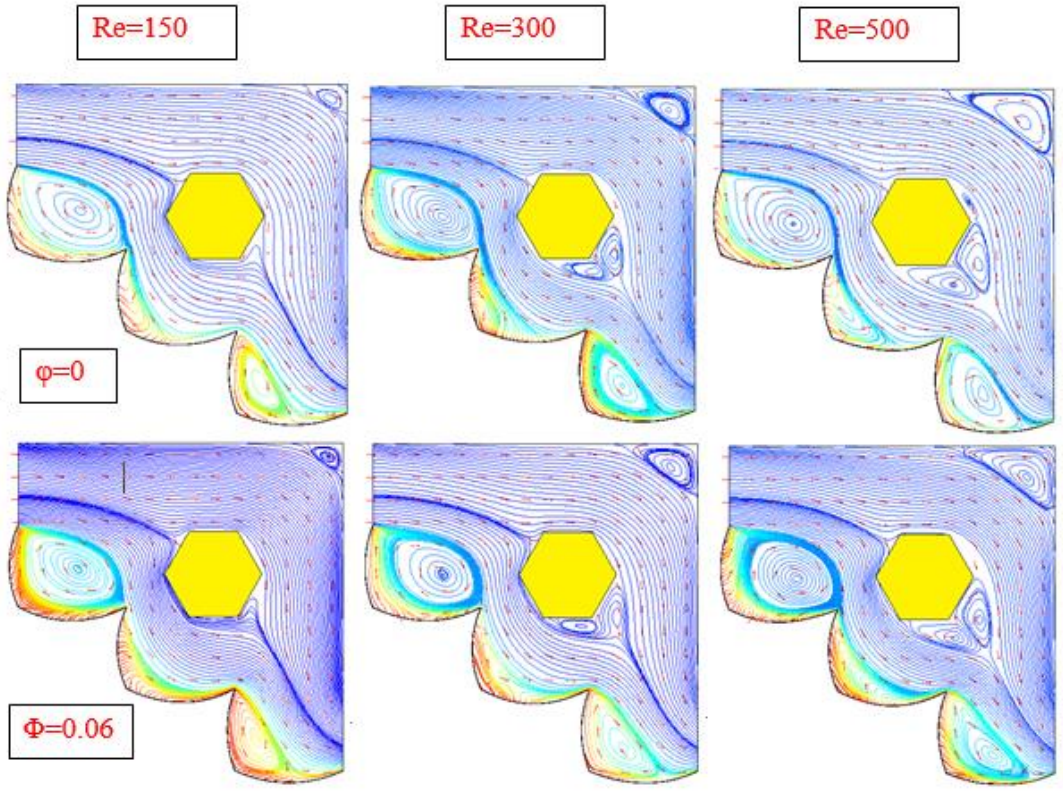

Figure (4- 24) Distribution of streamlines for various Reynolds number and volume fraction (N=3, E = 10^4, Ha = 10, γ=45)

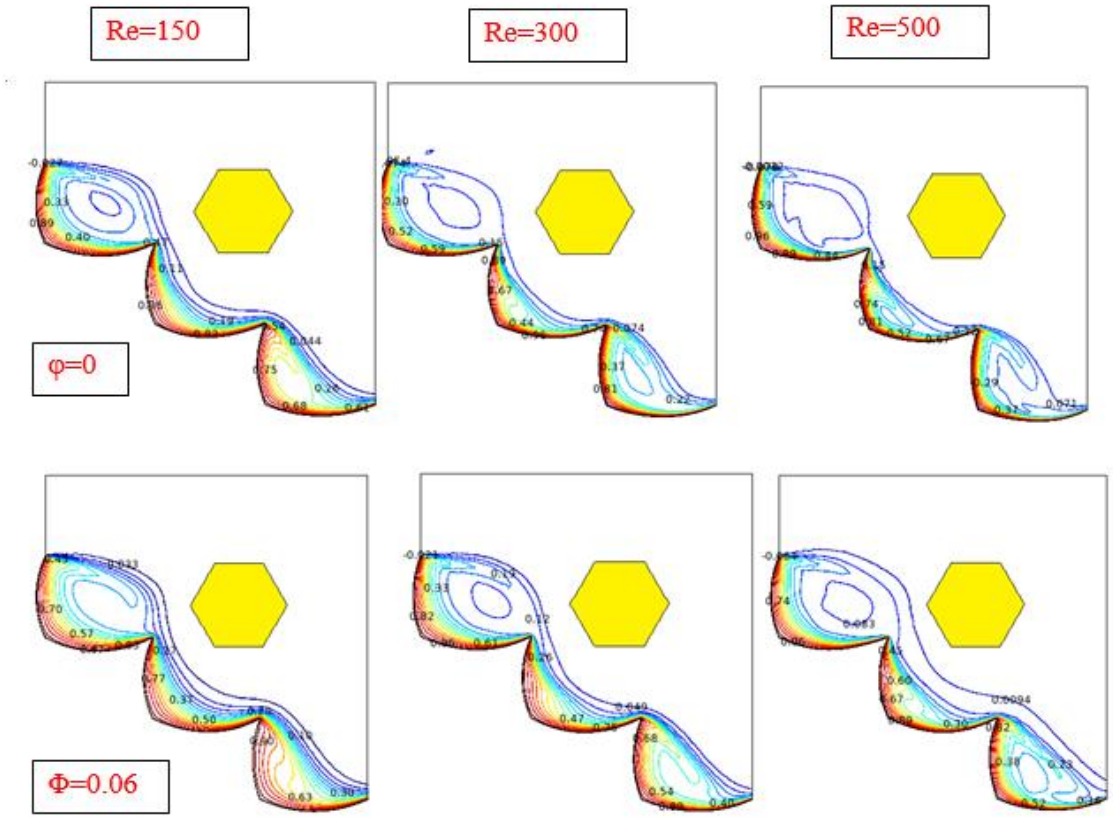

Figure (4- 25) Distribution of isotherms for various Reynolds number and volume fraction ($E = 10^4$, $Ha = 10$, $\gamma=45$)

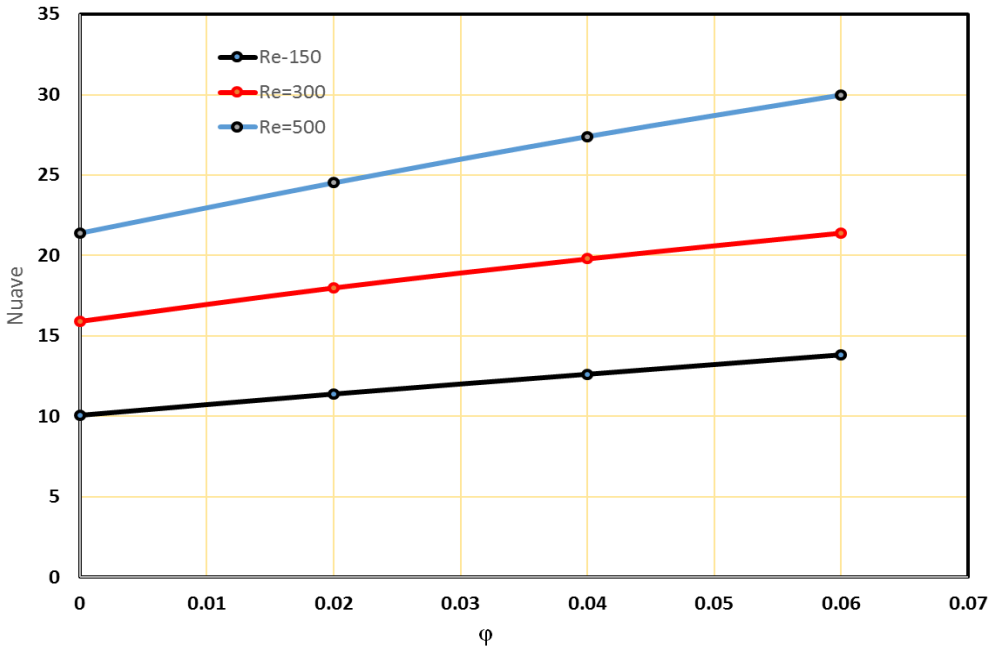

Figure (4- 26) Average Nusselt number variation with volume fraction for different Reynolds numbers ($E = 10^4$, $Ha = 10$, $\gamma=45$)

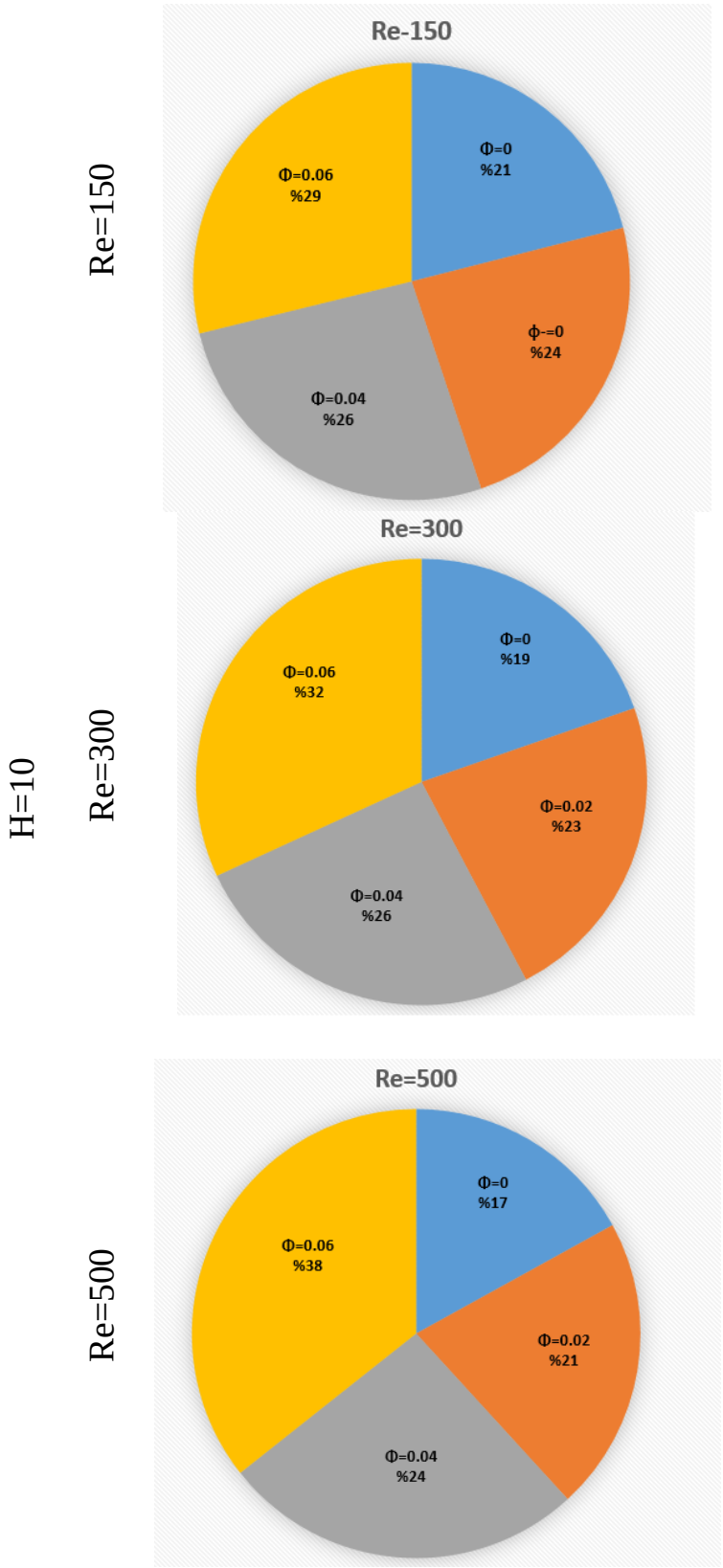

Figure (4- 27) Average Nusselt number ratio variation with volume fraction for different Reynolds numbers ($E = 10^4$, $Ha = 10$, $\gamma = 45$)

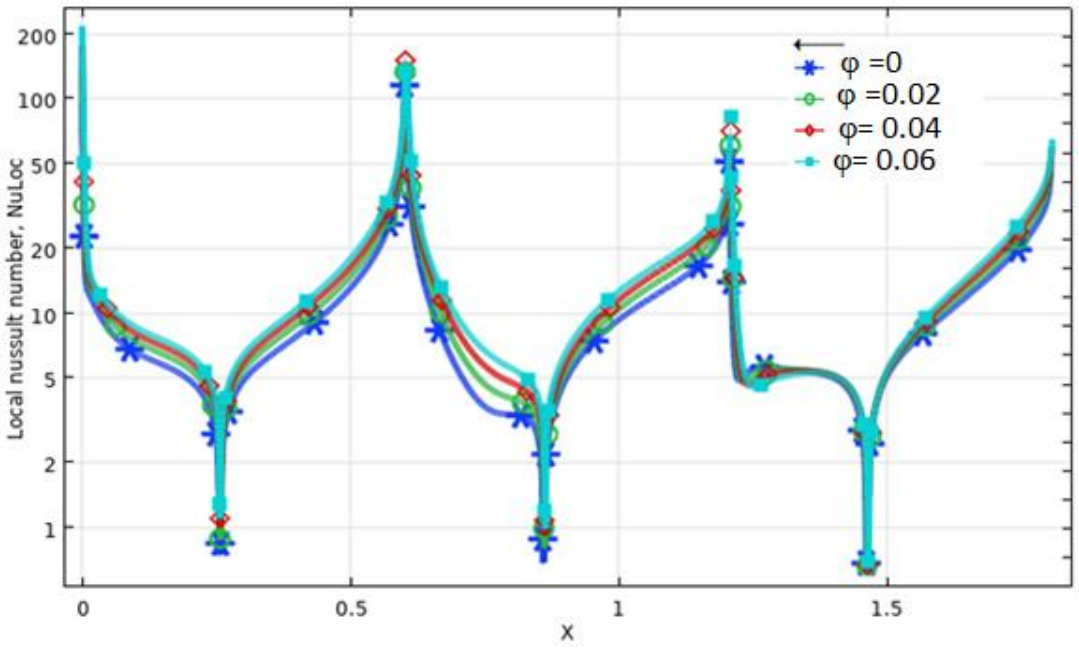

Figure (4- 28) Local Nusselt number variation with volume fraction for different Reynolds numbers (E = 10^4, Ha = 10, γ = 45)

4.3.6 Effect of number of steps

4.3.6.1 Streamlines, isotherms and Nusselt number.

Figures 4-29 and 4-30 compare the results of streamlines and isotherms with changes in the number of step-like corrugations of the hot wall at condition of (Re=400, Ha=25, ɣ=45^0, E=104, φ=0.02). There are small two vortices behind the hexagonal solid when N = 1, but large three vortices in the vented cavity when N = 2. In the first step, one vortex is created for N=5 and N=7, and smaller vortices are created for N=8 and N=9..

With each additional step, the recirculation zone below the main flow stream becomes bigger, while the separated flow along the edges becomes smaller. As the number of steps increases, so do the vortices behind the hexagonal solid. With a higher number of steps, temperature gradients become steeper toward the ends of the horizontal walls, while isotherm clustering becomes more intense toward the outlet. According to Figure 4-30, the local Nusselt number peaks at the outlet port and the local

enhancement of the heat transfer is toward the outlet port with more steps. It is generally true that the average Nusselt number decreases with increasing N values , but there is a slight increase at N = 4. When N is increased from 1 to 8, the average Nusselt number decreases by about 4% as shown in figure (4-31).

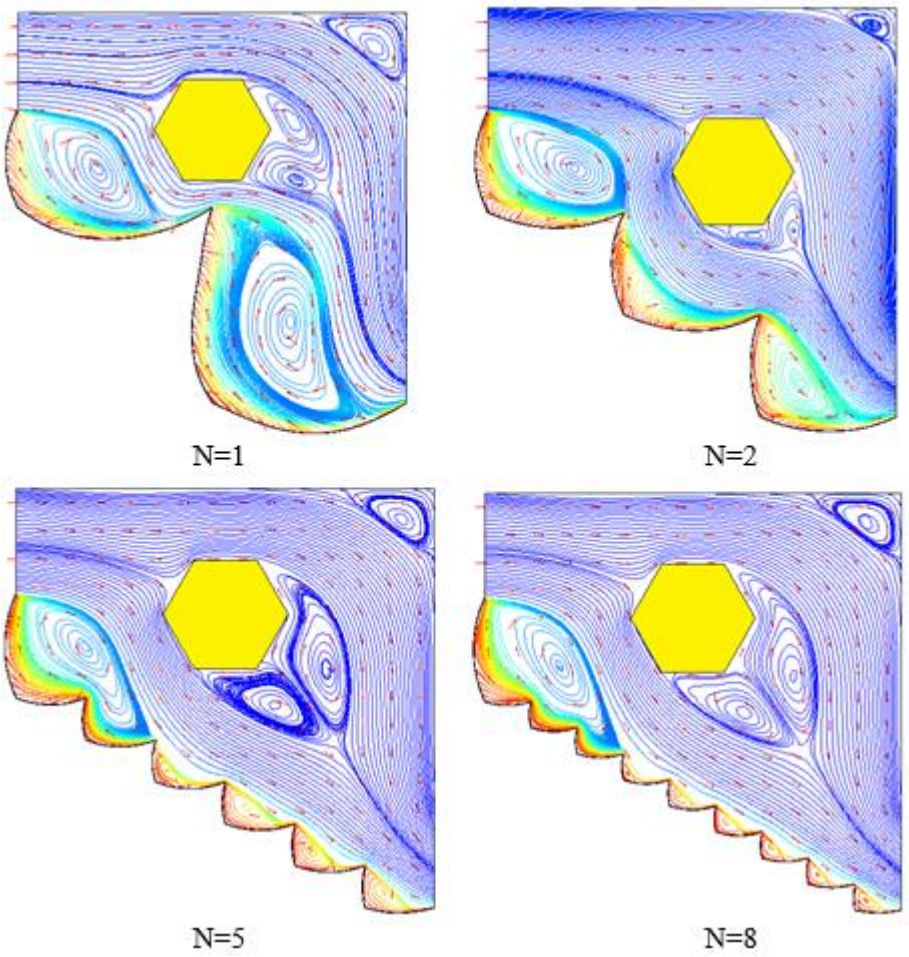

Figure (4- 29) Streamlines distributions for different number of steps corrugations (Re=400, Ha = 25, $\gamma = 45^0$, $E=1e^4$, $\varphi=0.02$)

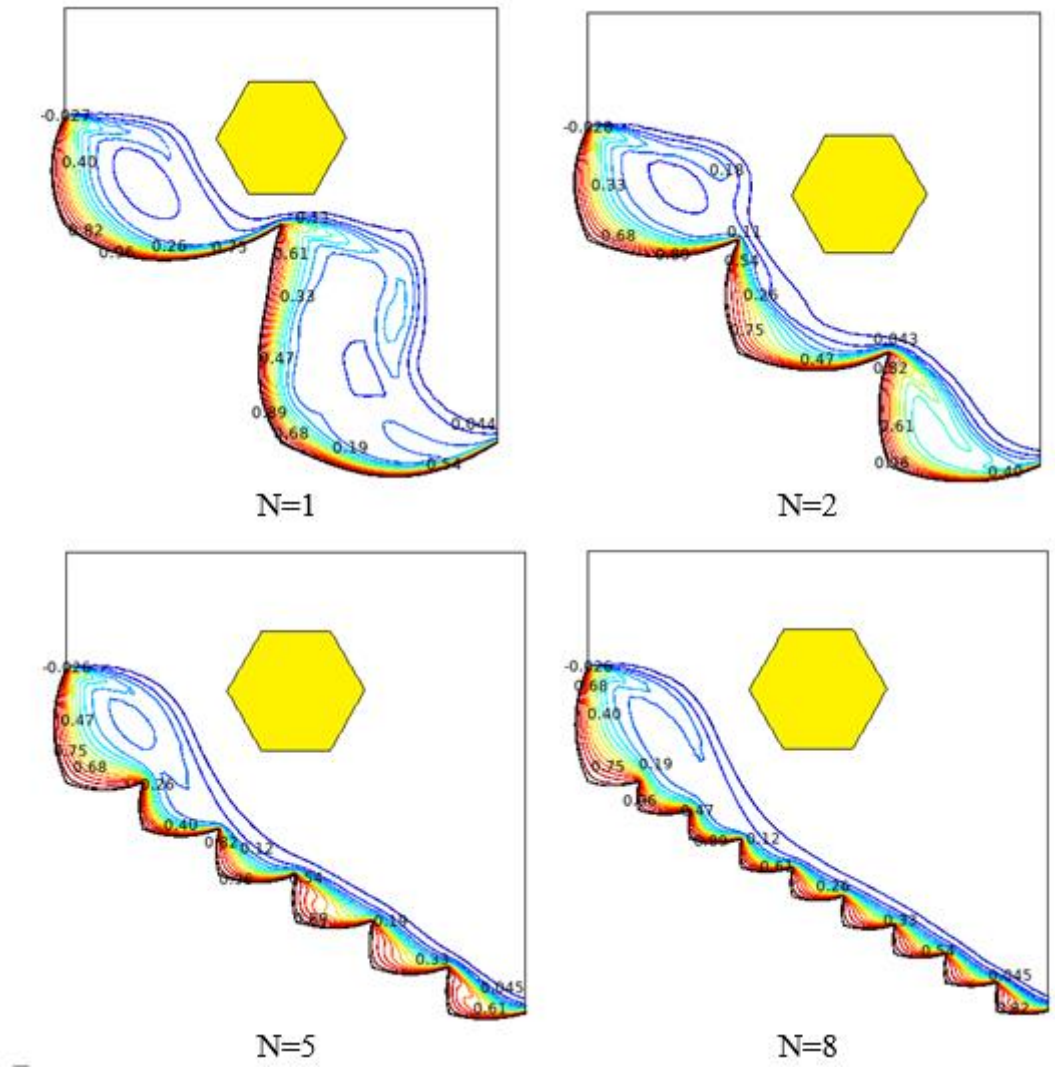

Figure (4- 30) Isotherm distributions for different number of steps corrugations (Re=400, Ha = 25, γ= 450, E=1e4, φ=0.02)

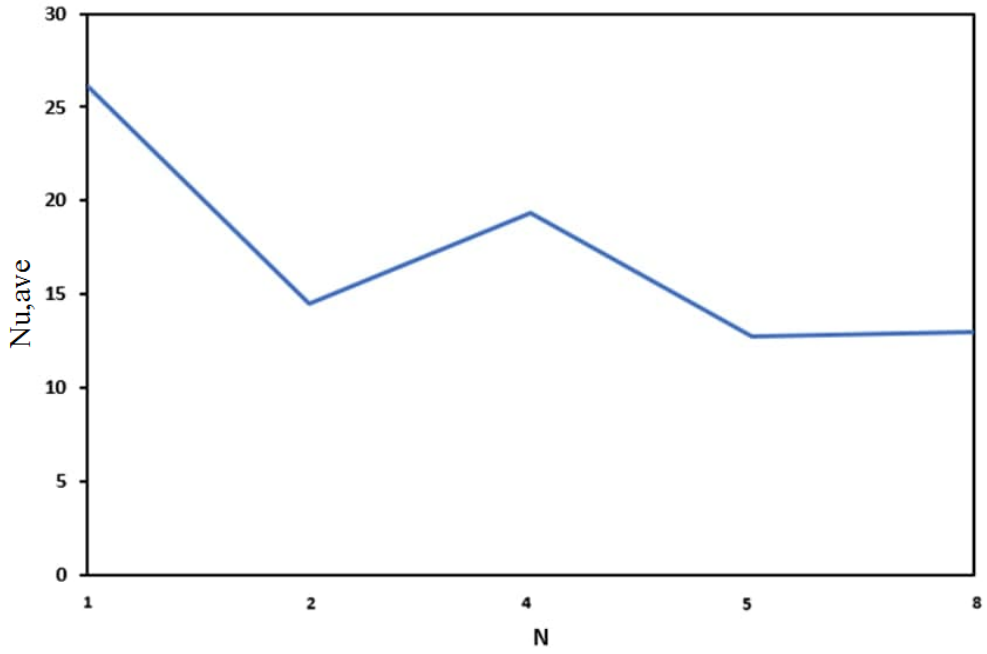

Figure (4- 31) Average Nussult number for different number of steps corrugations (Re=400, Ha = 25, γ= 45^0, E=1e^4, φ=0.02)

4.3.7 Effect of location of hexagonal solid

4.3.7.1 Streamlines, isotherms and Nussult number.

Figures 4-32 and 4-33 compare streamlines and isotherms in relation to changes in hexagonal solid location. at (Re=300, Ha = 25, γ= 45^0 , φ=0.02). left Column at E=1e4 and right Column at E=1e8. At x =0.5 and y=0.7 represent more value of Nussult number duo to large vortices behind the hexagonal solid and has three vortices near hot walls.

In regions with hexagonal solids, temperature gradients become higher toward the ends of horizontal walls, while isotherm clustering becomes more intense toward the outlets.

Figure (4-34). show Average Nusselt number ratio variation with different location of hexagonal solid and steps of wall at (Re=300, Ha = 25, γ= 45 ◦, ϕ= 0.02). A1 has more value of Nussult number at x=0.5, y=0.7.

Figure (4-35) and figure(4-36) show at x =0.5 and y=0.7 has more value of Nussult number was 5% more the without hexagonal due to large vortices behind the hexagonal solid and has three vortices near hot walls. Also the amount of flowed flow under the hexagonal is higher from others.

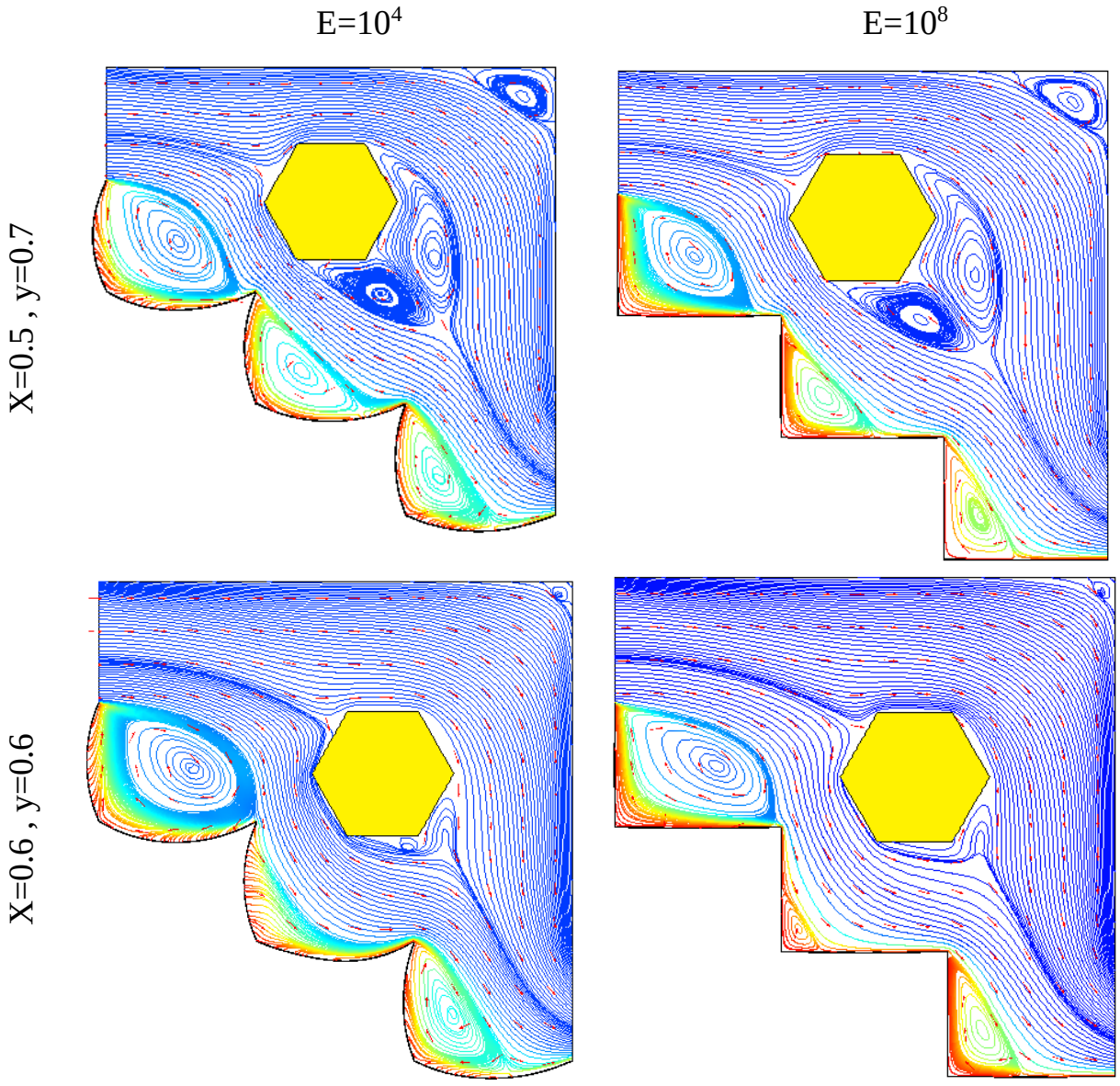

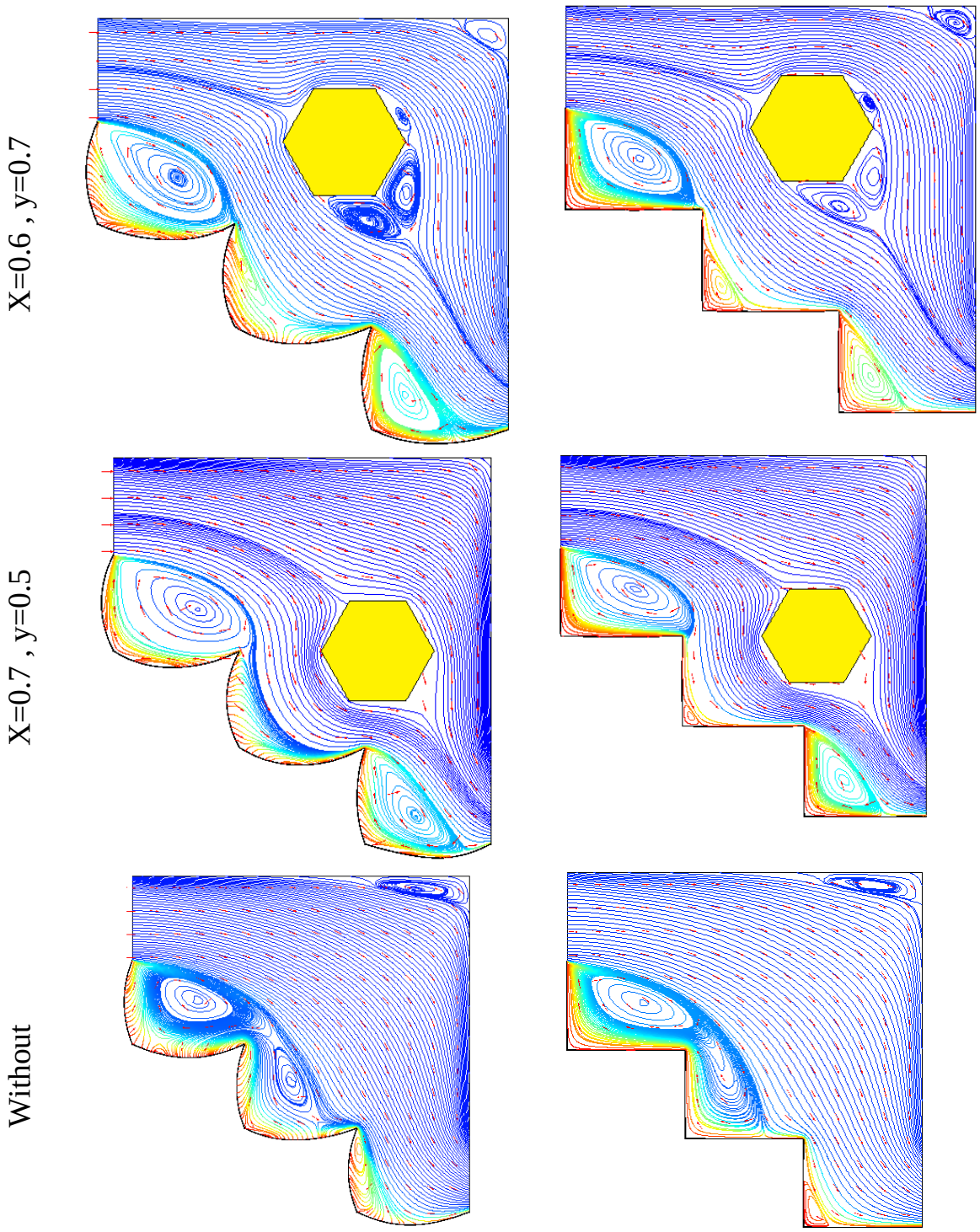

Figure (4- 32). Streamlines distributions for different location of hexagonal solid and without at (Re=300, Ha = 25, γ= 45 ◦, ϕ= 0. 02).

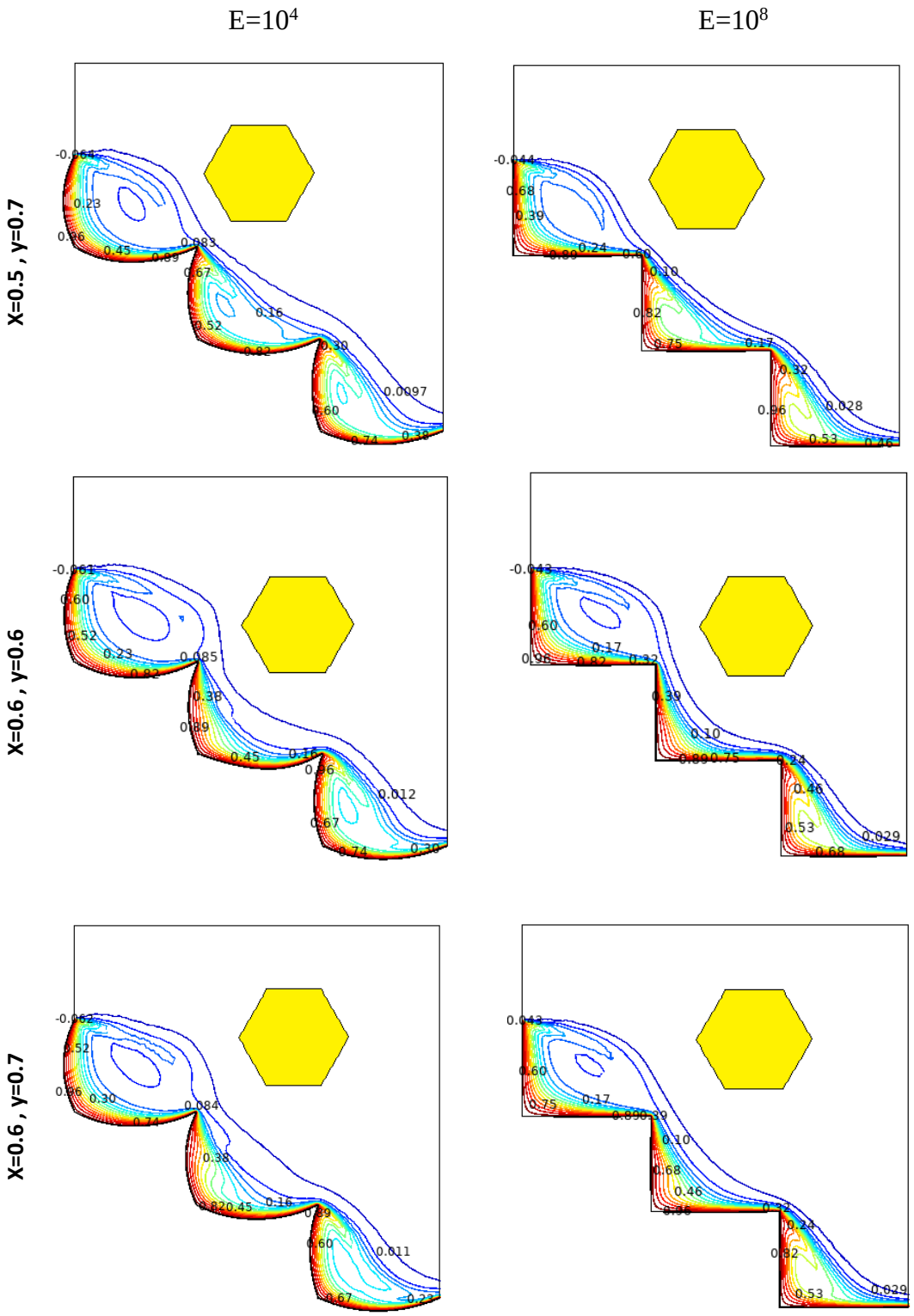
E=10^4
E=10^8
X=0.5 , y=0.7
X=0.6 , y=0.6
X=0.6 , y=0.7

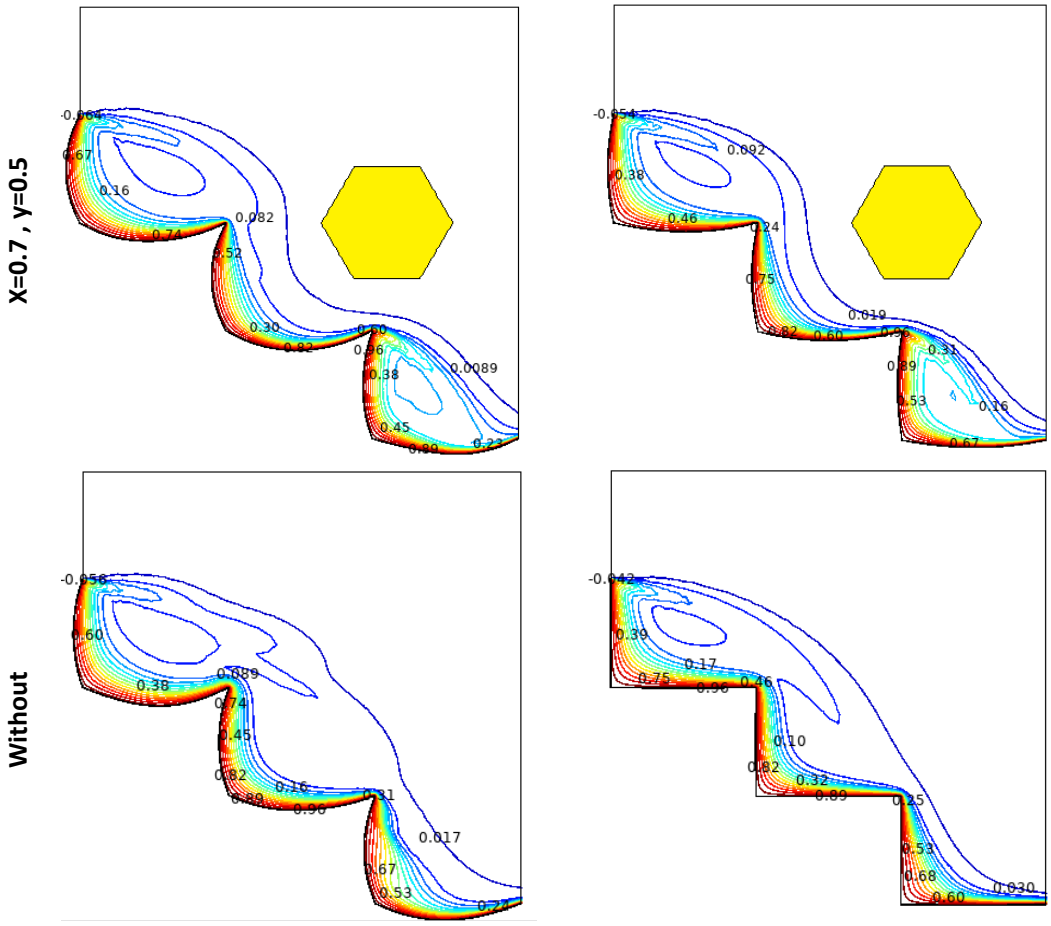

Figure (4- 33) Isotherm distributions for different location of hexagonal solid at (Re=300 , Ha = 25, γ= 45 ◦, ϕ= 0 . 02).

	$E=10^4$	$E=10^8$
X=0.5, y=0.7	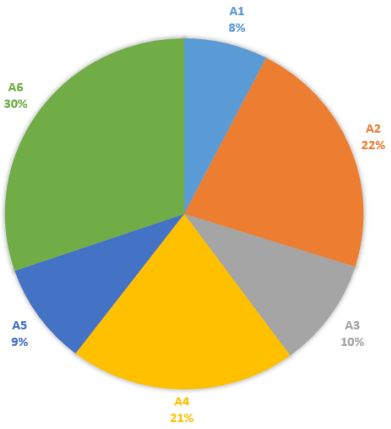	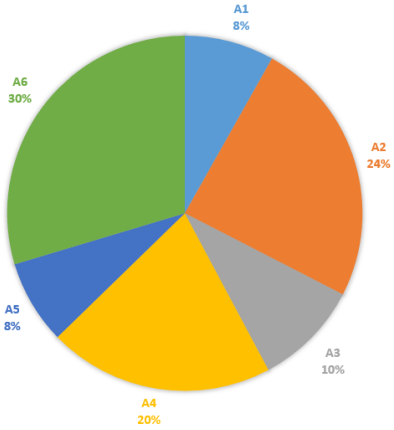
X=0.7,y=0.5	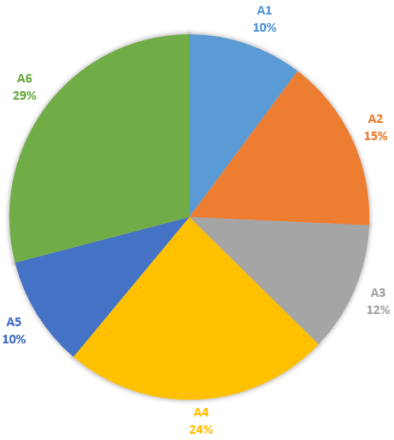	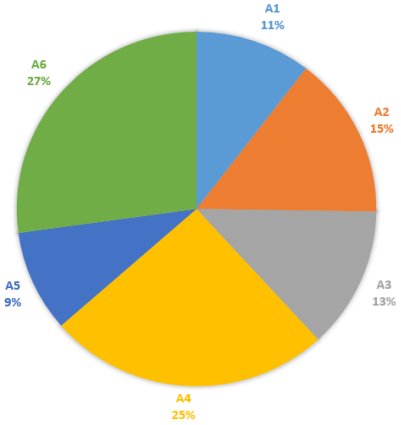
X=0.6, y=0.7	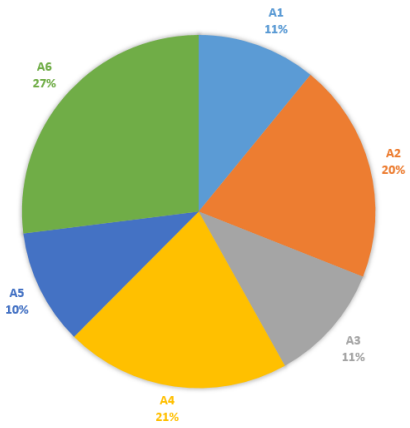	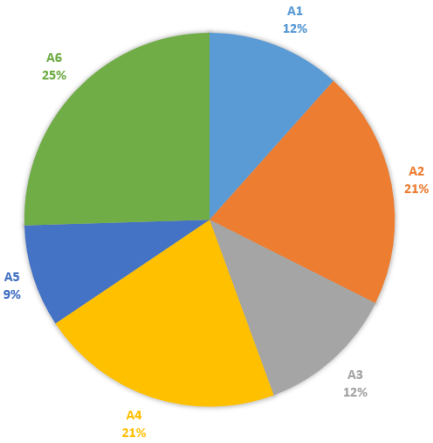

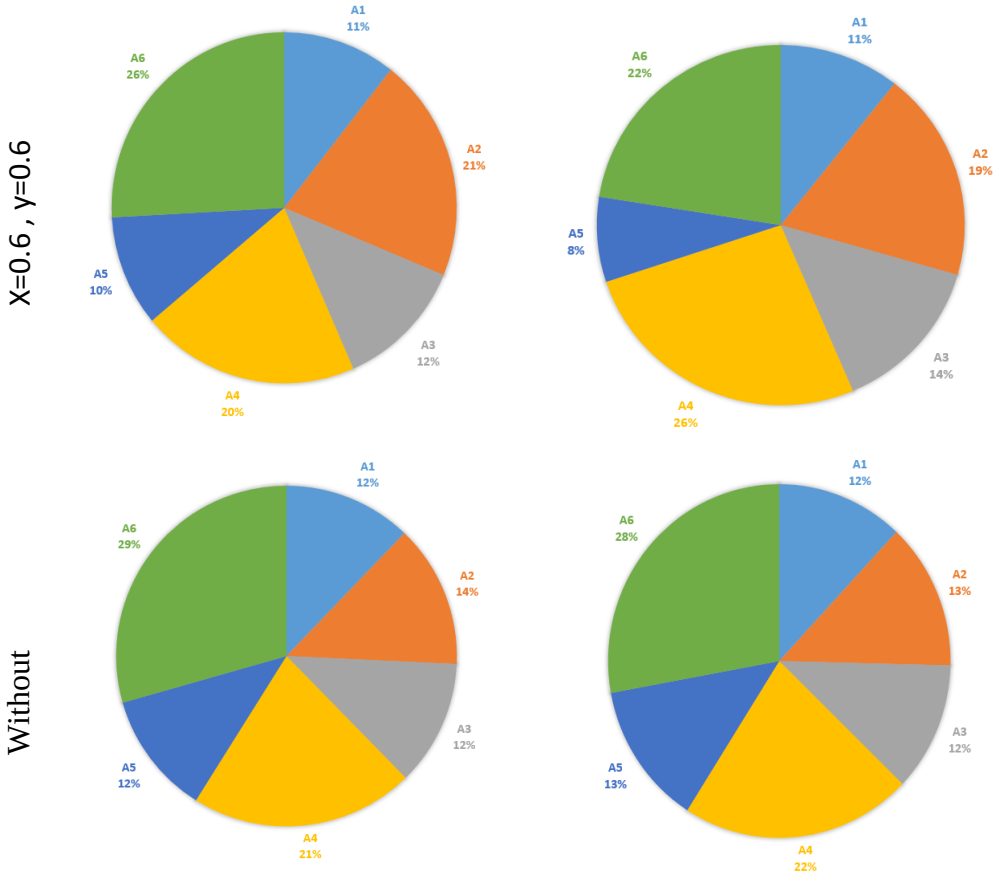

Figure (4- 34) Average Nusselt number ratio variation with for different location of hexagonal solid and steps of wall at (Re=300 , Ha = 25, γ= 45 ◦, ϕ= 0 . 02).

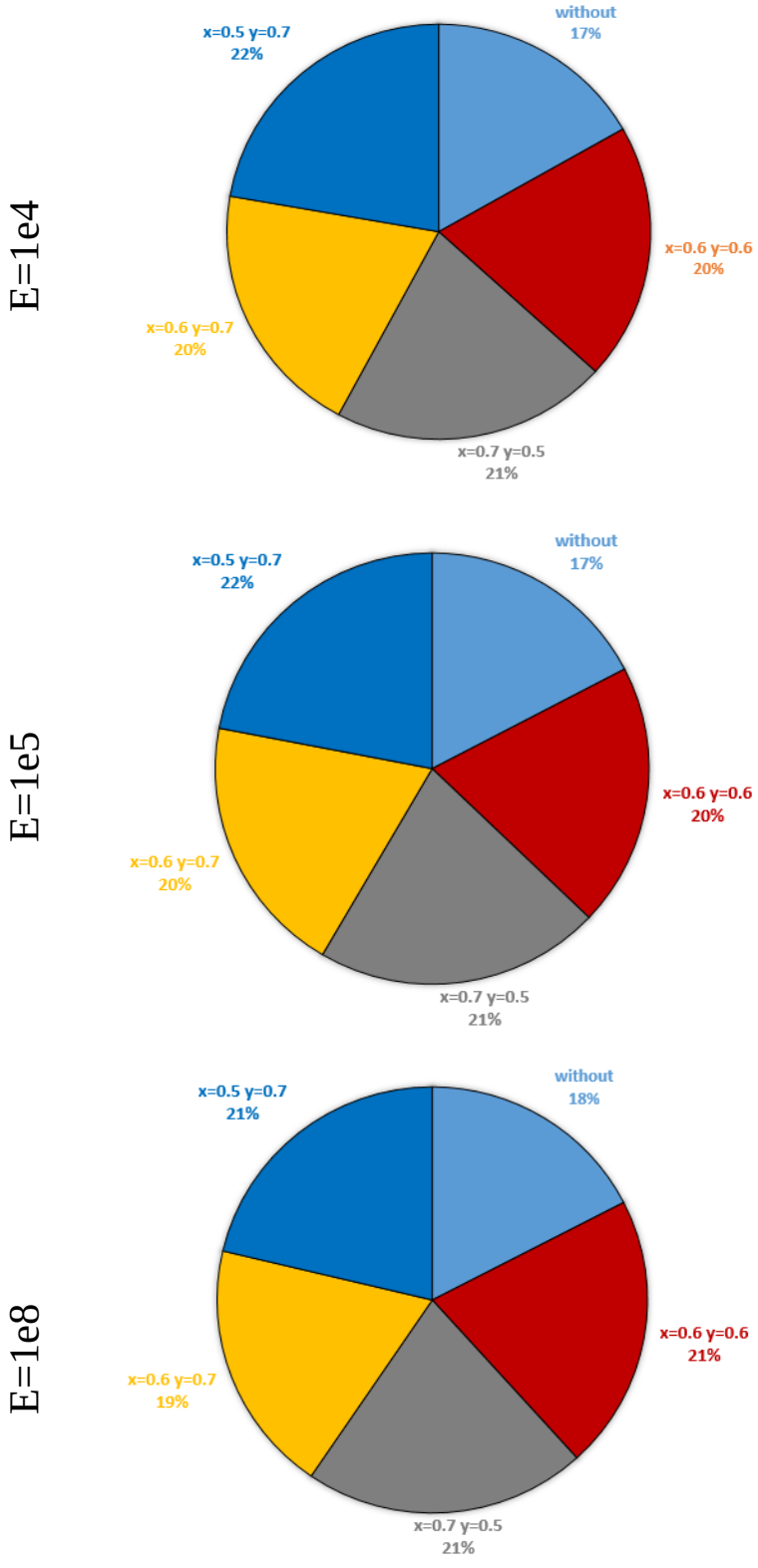

Figure (4- 35). Average Nusselt number ratio variation with for different location of hexagonal solid and E at (Re=300 , Ha = 25, γ= 45 ◦, ϕ= 0 . 02).

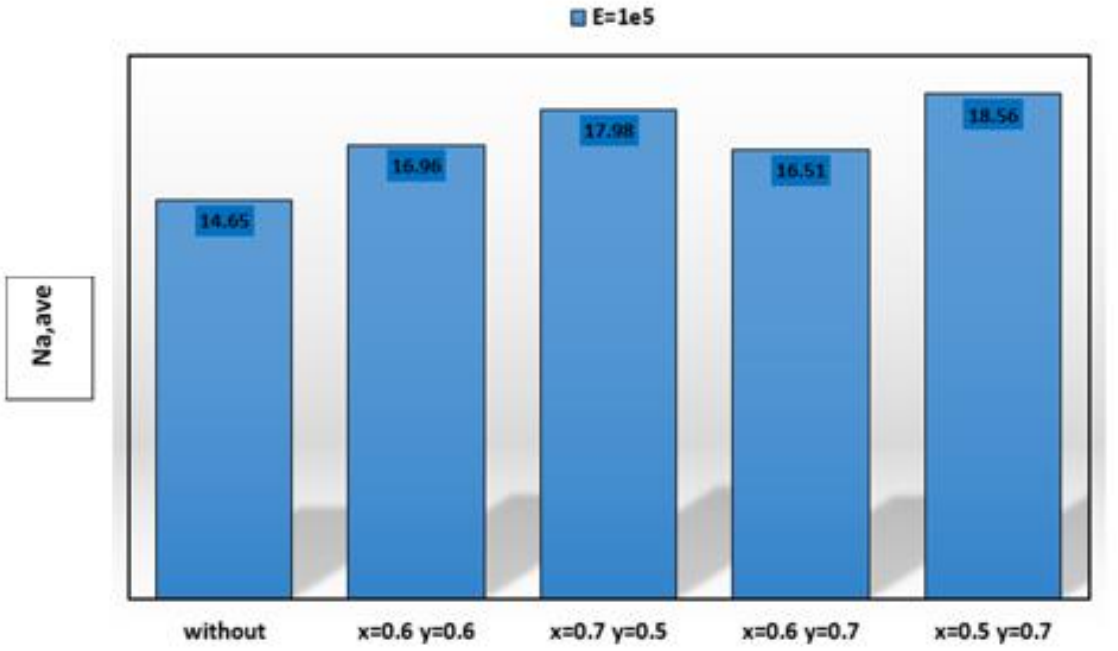
E=1e5
Na,ave
14.65
16.96
17.98
16.51
18.56
without
x=0.6 y=0.6
x=0.7 y=0.5
x=0.6 y=0.7
x=0.5 y=0.7

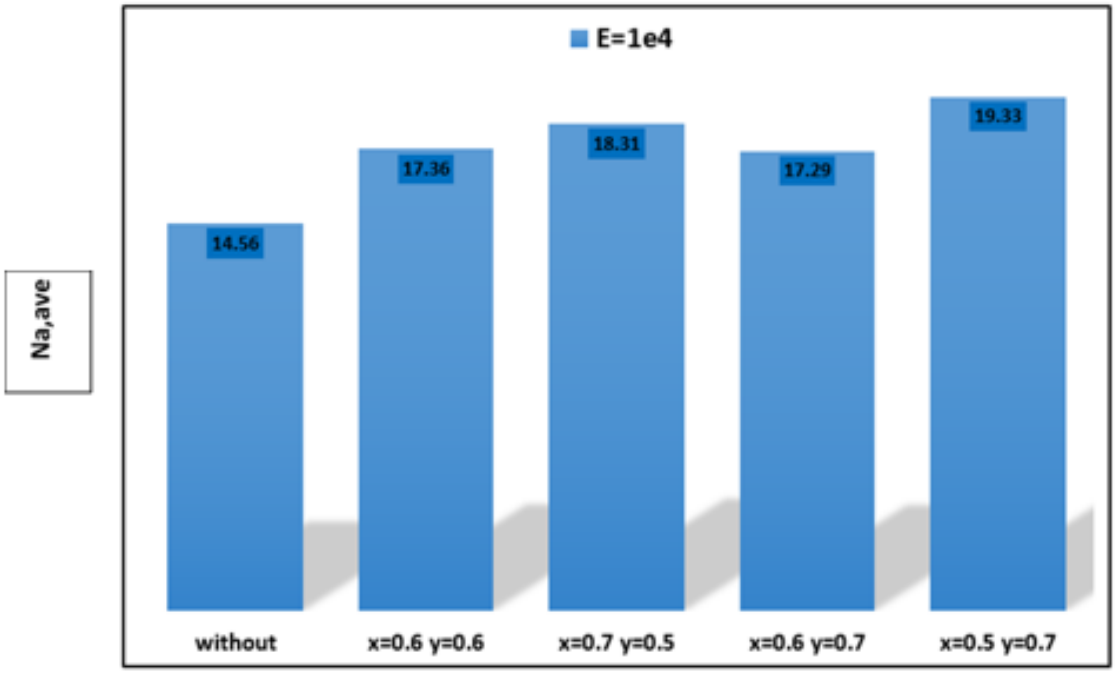
E=1e4
Na,ave
14.56
17.36
18.31
17.29
19.33
without
x=0.6 y=0.6
x=0.7 y=0.5
x=0.6 y=0.7
x=0.5 y=0.7

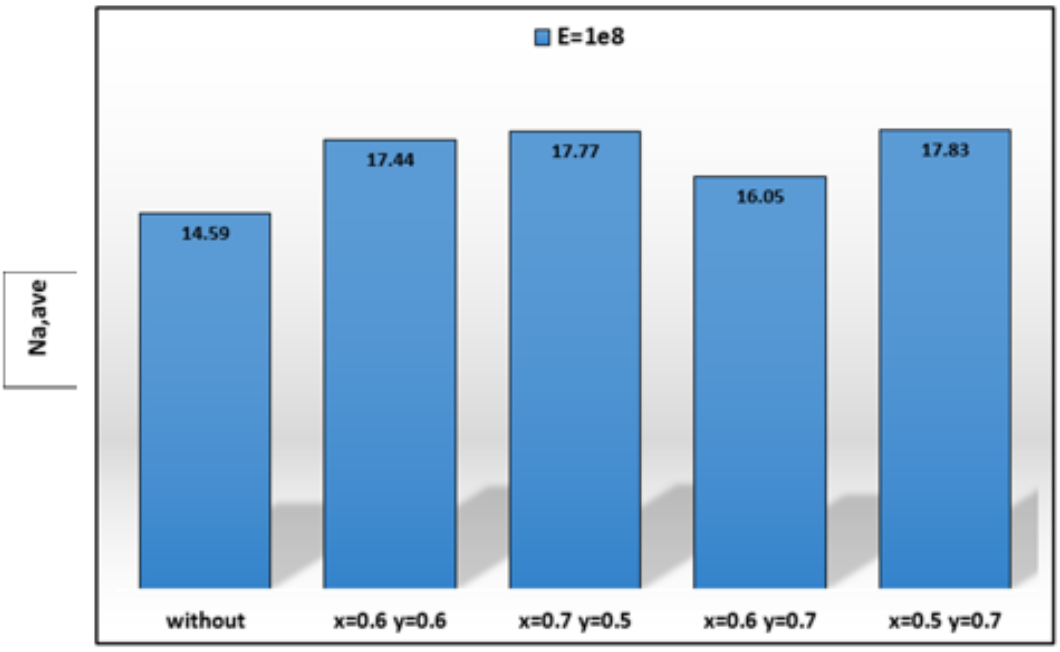

Figure (4- 36) Average Nusselt number ratio variation with for different location of hexagonal solid and E at (Re=300 , Ha = 25, γ= 45 ◦, ϕ= 0 .02).

The general case was done depending on the values and variables which is (Re=500 , ɣ=0 , Ha=60 , φ=0.06 , N=1 , $E=10^8$ at x=0.5, y=0.7). The result was 20% increased in Nu number value to the case that not contain hexagonal shape ($E=10^8$, N=3) . Also these results was compared with the researcher [31] and we found 15% increase in Nu number value.

4.3.8 Effect of entropy generation and bejan number

4.3.8.1 Sgen,T, Sgen,mu, Sgen,and Bejan number (Be).

Sgen,T Sgen,mu, and Sgen contours are shown in Figures (4-37) and (4-38) for certain conditions at Re=100, Ha = 25, ɣ= 45, and φ= 0.02. Sgen,mu decreases for all figures as E rises due to a decrease in fluid movement. While Sgen,T decreases as E rises due to increased heat transfer by convection and high fluid velocity, Sgen,T,Sgen,mu and Sgen are at their highest values at line A1's inlet point as shown in figure (4-39).

With Re=100, Ha=25, ɣ=45, and φ= 0.02 the Bejan number variation is depicted in Figure (4-40). As Be approaches 1, the irreversibility of heat transfer becomes more prominent. Whenever Be is much smaller than 1/2, the viscous effect takes over and makes processes irreversible. When Be = 1/2, the viscous effect generates the same amount of entropy as the heat transfer effect. Because Sgen,T and Sgen,mu are both equal, the more value of Be is equal to 1 at a fixed point in the elastic wall. Due to Sgen equaling zero, the value of Bejan number is also zero at the top of the line.

Table 4.1 Sgen,T Sgen,mu , Sgen and Be varation with Re and E at Ha = 25, γ= 45 ◦, φ= 0 .02 . This is due to fluid movement, which results in an increase in the Sgen,mu as Re increases. Sgen,T reduces as Re rises due to increased heat transfer by convection.

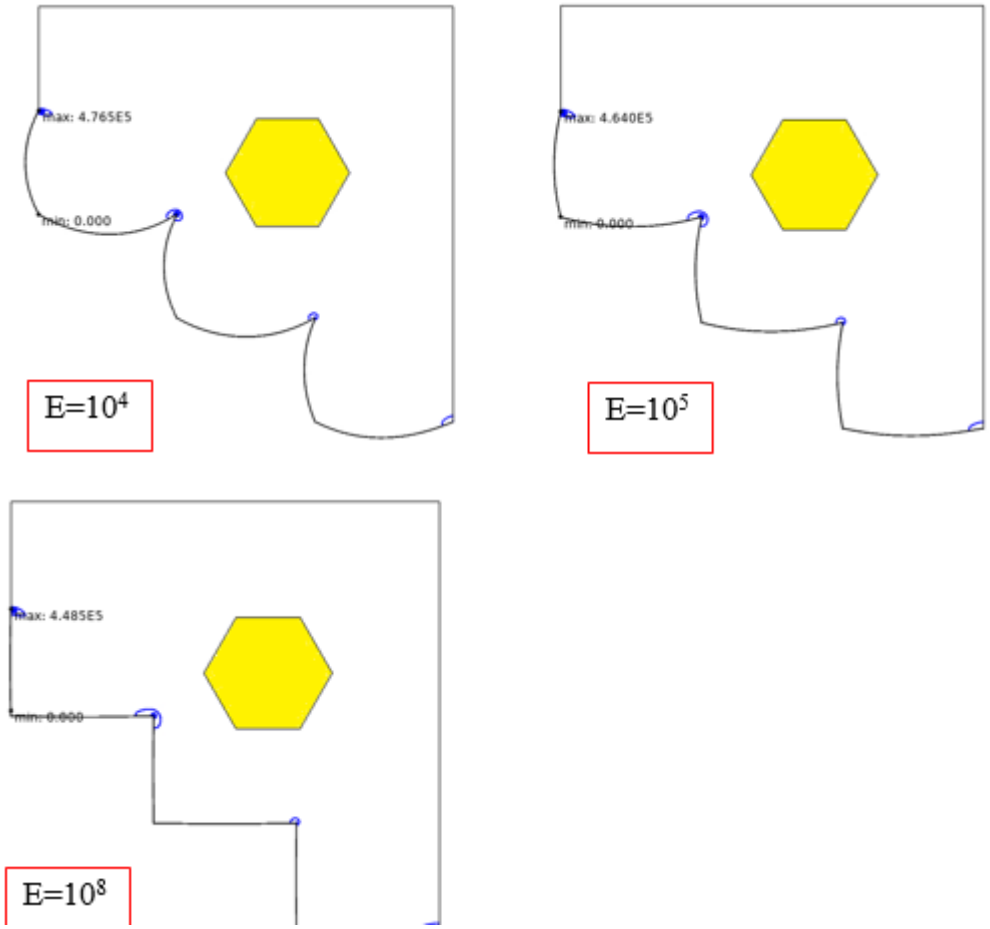

Figure (4- 37) Sgen,T variation with elastic wall E at (Re=100 , Ha = 25, γ= 45 ◦, ϕ= 0 .02).

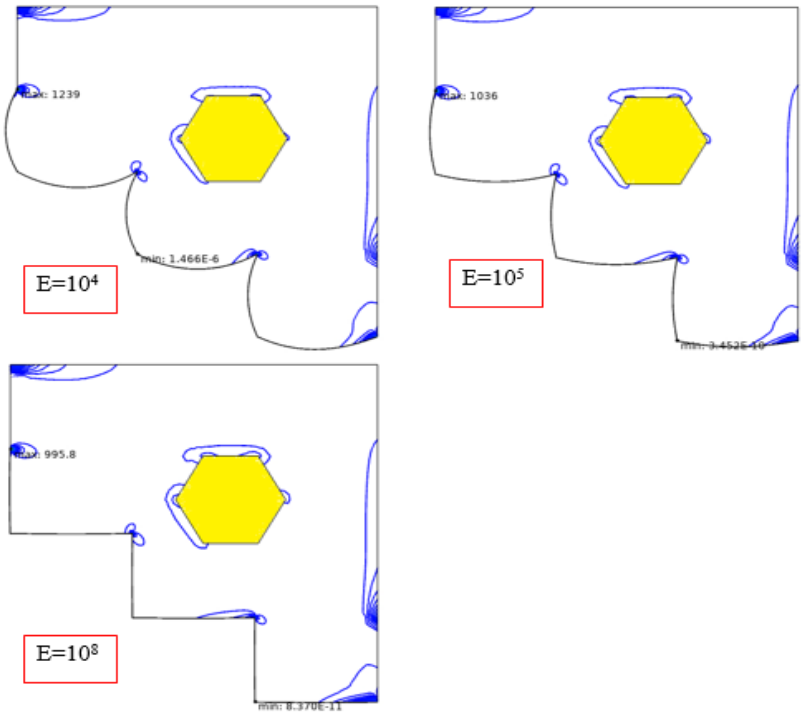

Figure (4- 38) Sge,μ variation with elastic wall E at (Re=100 , Ha = 25, γ= 45 ◦, ϕ= 0 .02).

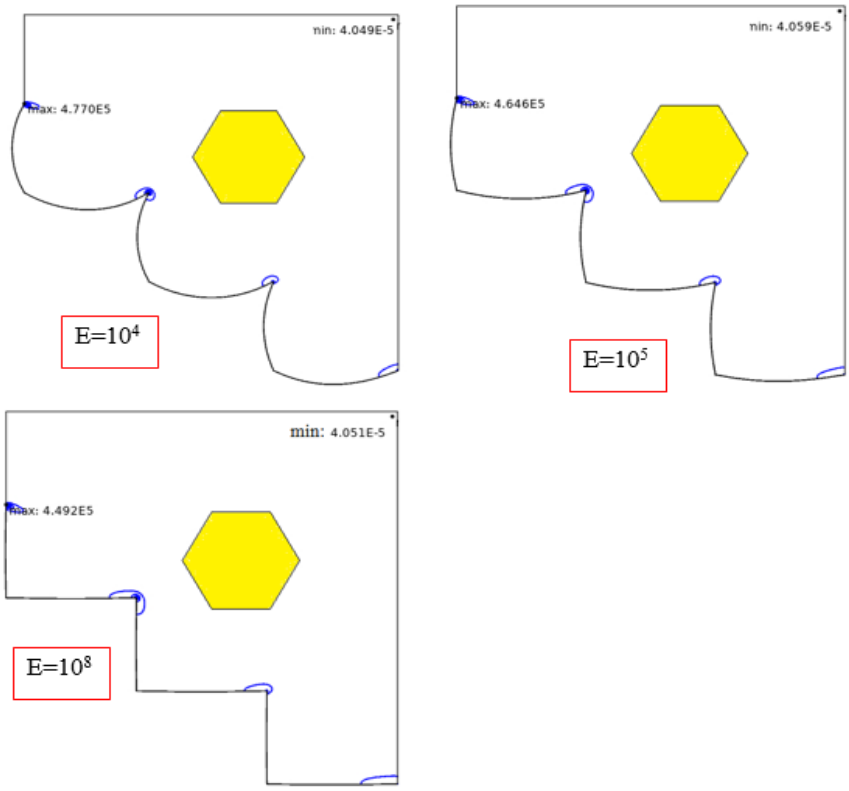

Figure (4- 39) Sgen variation with elastic wall E at (Re=100, Ha = 25, γ= 45 ◦, ϕ= 0 .02).

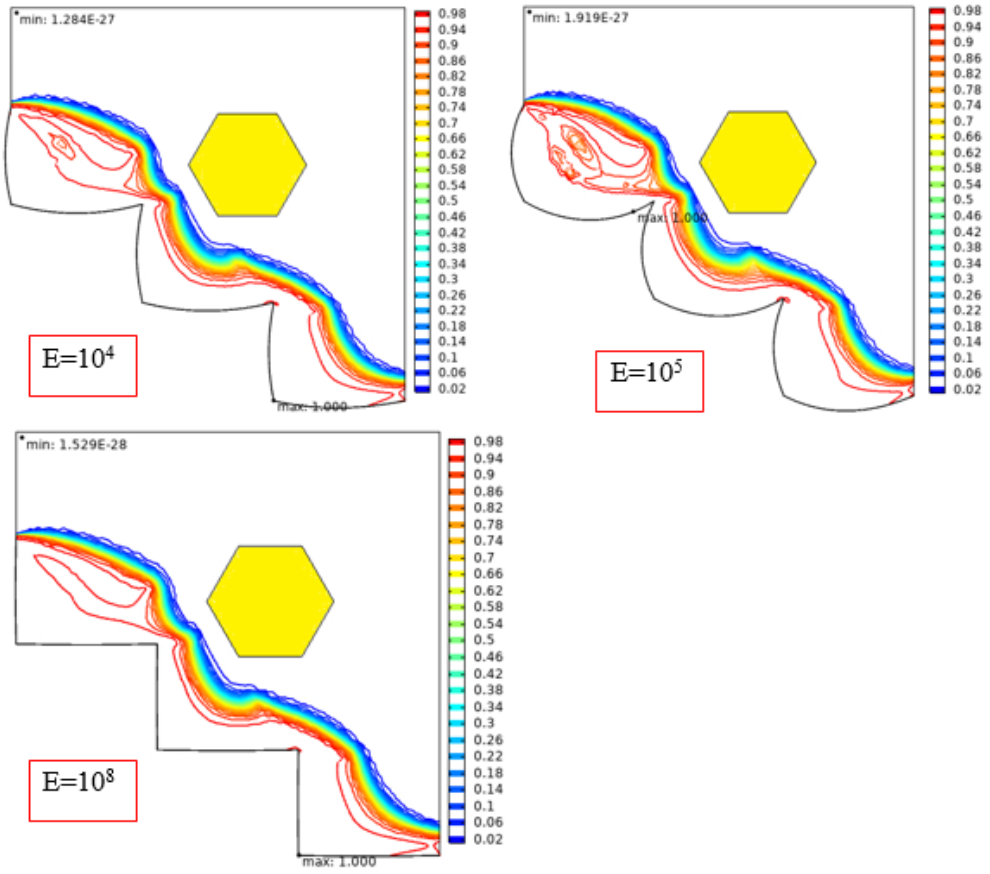

Figure (4- 40) Bejan number variation with elastic wall E at (Re=100, Ha = 25, γ= 45 ◦, ϕ= 0 .02).

Table (4- 1) Sgen,T Sgen,mu , Sgen and Be varation with Re and E at Ha = 25, γ= 45◦, ϕ= 0 .02

Table 4.1 Sgen,T Sgen,mu , Sgen and Be varation with Re and E at Ha = 25, γ= 45 ◦, ϕ= 0 .02

Re	E=1e4				E=1e5				E=1e8			
	SGE	SgeT	Sgemu	Be	SGE	SgeT	Sgemu	Be	SGE	SgeT	Sgemu	Be
100	12.219	11.745	0.47408	0.22556	12.309	11.834	0.47529	0.20417	12.460	11.981	0.47880	0.18841
300	22.610	21.960	0.64922	0.21354	21.749	21.102	0.64776	0.19285	21.404	20.754	0.65045	0.17753
500	32.056	31.278	0.77781	0.20180	30.469	29.692	0.77678	0.18553	29.755	28.976	0.77951	0.17097

Chapter Five

Conclusions and Recommendations

Chapter Five: Conclusions and Recommendations

5.1 Conclusions

The magneto hydrodynamics mixed convection of CNT-water nanofluid in a vented cavity with elastic steps like corrugation walls and hexagonal solid was numerically studied in different locations. The current study focuses on the interplay of the elastic hot wall deformation shape, fluid, and thermal fields that regulate mixed convection inside the cavity under consideration. The numerical simulation results can be used to make the following conclusions:

1. As the Reynolds number (Re) increases, the deformation of the elastic hot wall increases, providing more space for the fluid and affecting the size of the recirculation zone at the step's edges.
2. At a Reynolds number of 500, changing the elastic modulus causes both degradation and enhancement of the local Nusselt number at various locations along the hot wall; E=104 yields a larger Nusselt number.
3. As the magnetic field intensity increases, the number of vortices in the vented cavity decreases. The local Nusselt number along the hot walls closer to the inlet and outflow ports increases as the Hartmann number increases, but the magnetic inclination angle has only a little influence on the fluctuation of local Nusselt number distributions. For the same reasons, the value of Nussult number decreases at H=30 and subsequently increases as Hartman increases. In the absence and presence of a magnetic field, nanoparticle insertion to the base fluid results in average heat transfer increases of 7–7.5%.
4. Hexagonal solid at x =0.5 and y=0.7 has more value of Nussult number was 5% more the without hexagonal solid this duo to large vortices behind

the hexagonal solid and has three vortices near hot walls. Also, the amount of flowed flow under the hexagonal is higher from others.

5. Even with an increase in the number of steps from N = 1 to N = 8, a reduction in average heat transfer of around 4% is obtained, but there is only a slight increase in the average of Nusselt number at N=4, and the optimum elastic step was N=1.
6. As γ increase the Nussult number decrease the best value of γ was zero. This due to as the angle of inclination toward the flow this lead to smashing the vortices.
7. As φ increase the Nussult number increase the best value of φ was 0.06.
8. A1 has more value of Nussult number at x=0.5, y=0.7 due to large vortices generated near it.
9. The patterns of streamlines are mainly characterized by the value of Reynolds number.

5.2 Recommendations

The following topics could be good subjects for future works. Some of them were within the aims of the present thesis, but due to the absence of the time has not been calculated.

1. Studying the effects of different locations of the inlet and outlet ports. Studying the effect of Richardson number on the heat transfer.

3. Studying change the shape of cavity or using the lid-driven case by introducing a constant movement for one or two of the horizontal walls.
4.Using pure metallic nanoparticles because it has high thermal conductivity which is about 50 times larger than that of oxides nanoparticles.
5. Study the three dimensional case.
6. Studying pulsating flow and using deferent shape of solid.

REFRENCES

References

1. R., W., *Numerical Investigation of the Effect of the Baffle Length and Location on the Natural Convection in an Enclosure Filled for Different Nano-Fluids*, in *Mech.* 2017, Babylon. p. 125.
2. Rohsenow, W.M., J.P. Hartnett, and Y.I. Cho, *Handbook of heat transfer*. Vol. 3. 1998: McGraw-Hill New York.
3. Mahdi, M., *Numerical Simulation for Entropy Generation of Conjugate Heat Transfer in an Inclined Porous Enclosure*, in *Mech.* 2015, Babylon, Iraq. p. 120.
4. Garbrecht, O., S. Kabelac, and R. Kneer, *Large eddy simulation of three-dimensional mixed convection on a vertical plate*. 2017, Lehrstuhl für Wärme-und Stoffübertragung.
5. Xuan, Y. and Q. Li, *Heat transfer enhancement of nanofluids.* International Journal of heat and fluid flow, 2000. **21**(1): p. 58-64.
6. Sharifi, A., et al. *Computer-Aided simulation of heat transfer in nanofluids*. in *Proceedings of the International MultiConference of Engineers and Computer scientists*. 2012.
7. Axisa, F. and J. Antunes, *Modelling of mechanical systems: Fluid-structure interaction*. Vol. 3. 2006: Elsevier.
8. Bazilevs, Y., K. Takizawa, and T.E. Tezduyar, *Computational fluid-structure interaction: methods and applications*. 2013: John Wiley & Sons.
9. Ali, F., et al., *Entropy generation analysis of a natural convection inside a sinusoidal enclosure with different shapes of cylinders.* Frontiers in Heat and Mass Transfer (FHMT), 2018. **12**.
10. K Hamzah, H., et al., *Effect of Two Baffles on MHD Natural Convection in U-Shape Superposed by Solid Nanoparticle having Different Shapes.* Journal of Applied and Computational Mechanics, 2020.
11. Angirasa, D., *Mixed convection in a vented enclosure with an isothermal vertical surface.* Fluid Dynamics Research, 2000. **26**(4): p. 219.
12. Iwai, H., K. Nakabe, and K. Suzuki, *Flow and heat transfer characteristics of backward-facing step laminar flow in a rectangular duct.* International Journal of Heat and Mass Transfer, 2000. **43**(3): p. 457-471.
13. Abu-Mulaweh, H., *A review of research on laminar mixed convection flow over backward-and forward-facing steps.* International Journal of Thermal Sciences, 2003. **42**(9): p. 897-909.
14. Saeidi, S. and J. Khodadadi, *Forced convection in a square cavity with inlet and outlet ports.* International Journal of Heat and Mass Transfer, 2006. **49**(11-12): p. 1896-1906.

15. Abbassi, H. and S.B. Nassrallah, *MHD flow and heat transfer in a backward-facing step.* International communications in heat and mass transfer, 2007. **34**(2): p. 231-237.
16. Velazquez, A., J. Arias, and B. Mendez, *Laminar heat transfer enhancement downstream of a backward facing step by using a pulsating flow.* International Journal of Heat and Mass Transfer, 2008. **51**(7-8): p. 2075-2089.
17. Khanafer, K., et al., *Mixed convection analysis of laminar pulsating flow and heat transfer over a backward-facing step.* International journal of heat and mass transfer, 2008. **51**(25-26): p. 5785-5793.
18. Khanafer, K., *Comparison of flow and heat transfer characteristics in a lid-driven cavity between flexible and modified geometry of a heated bottom wall.* International Journal of Heat and Mass Transfer, 2014. **78**: p. 1032-1041.
19. Selimefendigil, F. and H.F. Oztop, *Control of laminar pulsating flow and heat transfer in backward-facing step by using a square obstacle.* Journal of heat transfer, 2014. **136**(8).
20. Selimefendigil, F. and H.F. Öztop, *Influence of inclination angle of magnetic field on mixed convection of nanofluid flow over a backward facing step and entropy generation.* Advanced Powder Technology, 2015. **26**(6): p. 1663-1675.
21. Gallegos, R. and R. Sharma. *Dynamic behaviour of a flexible plate behind a circular cylinder: Numerical study on the effects of blockage and cylinder size*. in *20th Australas. Fluid Mech. Conf*. 2016.
22. Mehryan, S., et al., *Analysis of fluid-solid interaction in MHD natural convection in a square cavity equally partitioned by a vertical flexible membrane.* Journal of Magnetism and Magnetic Materials, 2017. **424**: p. 161-173.
23. Selimefendigil, F. and H.F. Öztop, *Mixed convection in a partially heated triangular cavity filled with nanofluid having a partially flexible wall and internal heat generation.* Journal of the Taiwan Institute of Chemical Engineers, 2017. **70**: p. 168-178.
24. Mahalakshmi, T., et al., *MHD mixed convective heat transfer in a lid-driven enclosure filled with Ag-water nanofluid with center heater.* International Journal of Mechanical Sciences, 2018. **142**: p. 407-419.
25. Selimefendigil, F. and H.F. Öztop, *Laminar convective nanofluid flow over a backward-facing step with an elastic bottom wall.* Journal of Thermal Science and Engineering Applications, 2018. **10**(4).
26. Sabbar, W.A., M.A. Ismael, and M. Almudhaffar, *Fluid-structure interaction of mixed convection in a cavity-channel assembly of flexible wall.* International Journal of Mechanical Sciences, 2018. **149**: p. 73-83.

27. Alsabery, A., et al., *Fluid-structure interaction in natural convection heat transfer in an oblique cavity with a flexible oscillating fin and partial heating.* Applied Thermal Engineering, 2018. **145**: p. 80-97.
28. Selimefendigil, F. and H.F. Öztop, *Magnetic field effects on the forced convection of CuO-water nanofluid flow in a channel with circular cylinders and thermal predictions using ANFIS.* International Journal of Mechanical Sciences, 2018. **146**: p. 9-24.
29. Selimefendigil, F. and H.F. Öztop, *Effects of an inner stationary cylinder having an elastic rod-like extension on the mixed convection of CNT-water nanofluid in a three dimensional vented cavity.* International Journal of Heat and Mass Transfer, 2019. **137**: p. 650-668.
30. Ismael, M.A., *Forced convection in partially compliant channel with two alternated baffles.* International Journal of Heat and Mass Transfer, 2019. **142**: p. 118455.
31. Selimefendigil, F. and H.F. Öztop, *Fluid-solid interaction of elastic-step type corrugation effects on the mixed convection of nanofluid in a vented cavity with magnetic field.* International Journal of Mechanical Sciences, 2019. **152**: p. 185-197.
32. Alsabery, A., et al., *Fluid-structure interaction analysis of entropy generation and mixed convection inside a cavity with flexible right wall and heated rotating cylinder.* International journal of heat and mass transfer, 2019. **140**: p. 331-345.
33. Selimefendigil, F. and H.F. Öztop, *Forced convection in a branching channel with partly elastic walls and inner L-shaped conductive obstacle under the influence of magnetic field.* International Journal of Heat and Mass Transfer, 2019. **144**: p. 118598.
34. Selimefendigil, F. and H.F. Öztop, *Corrugated conductive partition effects on MHD free convection of CNT-water nanofluid in a cavity.* International Journal of Heat and Mass Transfer, 2019. **129**: p. 265-277.
35. Selimefendigil, F. and H.F. Öztop, *MHD mixed convection of nanofluid in a flexible walled inclined lid-driven L-shaped cavity under the effect of internal heat generation.* Physica A: Statistical Mechanics and its Applications, 2019. **534**: p. 122144.
36. Chamkha, A.J., F. Selimefendigil, and H.F. Oztop, *Pulsating flow of CNT–water nanofluid mixed convection in a vented trapezoidal cavity with an inner conductive T-shaped object and magnetic field effects.* Energies, 2020. **13**(4): p. 848.
37. Selimefendigil, F., H.F. Öztop, and N. Abu-Hamdeh, *Impacts of conductive inner L-shaped obstacle and elastic bottom wall on MHD forced convection of a nanofluid in vented cavity.* Journal of Thermal Analysis and Calorimetry, 2019: p. 1-18.
38. Selimefendigil, F., H.F. Öztop, and M. Sheikholeslami, *Impact of local elasticity and inner rotating circular cylinder on the magneto-*

hydrodynamics forced convection and entropy generation of nanofluid in a U- shaped vented cavity. Mathematical Methods in the Applied Sciences, 2020.

39. Ghalambaz, M., et al., *Controlling the natural convection flow through a flexible baffle in an L-shaped enclosure.* Meccanica, 2020. **55**(8): p. 1561-1584.
40. Yaseen, D.T. and M.A. Ismael, *Effect of Deformable Baffle on the Mixed Convection of Non-Newtonian Fluids in a Channel-Cavity.* Basrah Journal for Engineering Science, 2020. **20**(2).
41. Selimefendigil, F. and A.J. Chamkha, *MHD mixed convection of Ag–MgO/water nanofluid in a triangular shape partitioned lid-driven square cavity involving a porous compound.* Journal of Thermal Analysis and Calorimetry, 2021. **143**(2): p. 1467-1484.
42. Selimefendigil, F., D. Okulu, and H. Mamur, *Numerical analysis for performance enhancement of thermoelectric generator modules by using CNT–water and hybrid Ag/MgO–water nanofluids.* Journal of Thermal Analysis and Calorimetry, 2021. **143**(2): p. 1611-1621.
43. Jamesahar, E., et al., *Mixed convection heat transfer by nanofluids in a cavity with two oscillating flexible fins: a fluid–structure interaction approach.* Applied Mathematical Modelling, 2020. **82**: p. 72-90.
44. Bayat, J. and A.H. Nikseresht, *Thermal performance and pressure drop analysis of nanofluids in turbulent forced convective flows.* International journal of thermal sciences, 2012. **60**: p. 236-243.
45. Xuan, Y. and W. Roetzel, *Conceptions for heat transfer correlation of nanofluids.* International Journal of heat and Mass transfer, 2000. **43**(19): p. 3701-3707.
46. Drew, D.A. and S.L. Passman, *Theory of multicomponent fluids*. Vol. 135. 2006: Springer Science & Business Media.
47. Pak, B.C. and Y.I. Cho, *Hydrodynamic and heat transfer study of dispersed fluids with submicron metallic oxide particles.* Experimental Heat Transfer an International Journal, 1998. **11**(2): p. 151-170.
48. Kaviany, M., *Principles of heat transfer in porous media*. 2012: Springer Science & Business Media.
49. Ismael, M.A. and H.F. Jasim, *Role of the fluid-structure interaction in mixed convection in a vented cavity.* International Journal of Mechanical Sciences, 2018. **135**: p. 190-202.
50. Donea, J., S. Giuliani, and J.-P. Halleux, *An arbitrary Lagrangian-Eulerian finite element method for transient dynamic fluid-structure interactions.* Computer methods in applied mechanics and engineering, 1982. **33**(1-3): p. 689-723.
51. Hirt, C., A. Amsden, and J. Cook, *An arbitrary Lagrangian–Eulerian computing method for all flow speeds.* Journal of computational physics, 1997. **135**(2): p. 203-216.

52. Duarte, F., R. Gormaz, and S. Natesan, *Arbitrary Lagrangian–Eulerian method for Navier–Stokes equations with moving boundaries*. Computer Methods in Applied Mechanics and Engineering, 2004. **193**(45-47): p. 4819-4836.
53. Souli, M.h. and D.J. Benson, *Arbitrary Lagrangian Eulerian and fluid-structure interaction: numerical simulation*. 2013: John Wiley & Sons.
54. Bathe, K.J. and H. Zhang, *Finite element developments for general fluid flows with structural interactions.* International journal for numerical methods in engineering, 2004. **60**(1): p. 213-232.
55. Lewis, R.W., P. Nithiarasu, and K.N. Seetharamu, *Fundamentals of the finite element method for heat and fluid flow*. 2004: John Wiley & Sons.

الخلاصة

تبحث هذه الدراسة عدديًا في تفاعل صلد _ مائع (FSI) في التحكم على الحمل الحراري المختلط داخل تجويف مربع باستخدام جدران مرنة ساخنة متدرجة على شكل خطوات. أيضا تأثيرات زاوية المجال المغناطيسي، والشكل السداسي في مواقع مختلفة في السائل النانوي (CNT-water) برقم براندل (Pr=6.9) ، تم افتراض التدفق ثنائي الأبعاد ، نيوتوني ، غير قابل للضغط ، رقائقي وتم تحقيق الدراسة في ظل حالة غير مستقرة.

تم حل المعادلات التفاضلية الحاكمة التي تحكم المائع والصلب باستخدام طريقة العناصر المحددة (Galerkin) الموجودة ضمن تقنية اويلر - لاكرانج الاعتيادية (ALE) وذلك باستخدام الحقيبة البرمجية (COMSOL Multiphysics ver. 5.5) تمثلت معايير الدراسة ببيان تأثير كل من رقم رينولدز بين (100 و 500) ، زاوية الميل المغناطيسي بين (0 درجة و 90 درجة) ، رقم هارتمان بين (0 و 60) ، تركيز السوائل النانوية (من 0 إلى 6٪) و معامل المرونه بين (10^4 و 10^8) حيث كان العدد رايلي ثابت لكل الدراسة وقيمته $Ra=10^5$.

أوضحت النتائج بأن أفضل موقع للجسم الصلب عند (x = 0.5 ، y = 0.7) ، في هذا الموقع من

التجويف يحتوي على أكبر قيمه لرقم نسلت حيث كانت النسبة 5% اكثر من التجويف الذي لا يحتوي على جسم صلب ، وتأثير زيادة متوسط عدد نسلت مع زيادة تركيز الموائع النانوية. وكانت افضل زاوية ميل مغناطيسي عندما تساوي صفر، لان المغناطيس يكون باتجاه التدفق وهذا يؤدي الى تحطيم الدوامات . وعندما يزداد عدد هارتمان يصبح نقل الحرارة اكثر فعالية.

عند استخدام الجدار الساخن المرن يعمل على تحسين نقل الحرارة ، بحيث يكون التحسين في متوسط رقم بسلت عند استخدام الجدار الساخن المرن عند ظروف (رقم رينولد يساوي 300 ، رقم هارتمان يساوي25 ، التركيز النانوي يساوي 0.02 ومعامل المرونه يساوي 10^4) بحوالي اكثر من 22% مقارنة بالجدار الصلب، كما وجد ان متوسط رقم نسلت يزداد مع مرونة الجدار الساخن المرن.

يتم التحقيق في إنشاء الانتروبيا ورقم البيجان لحالات مختلفة. يتناقص $S_{gen,\mu}$ مع زيادة E بسبب انخفاض حركة السوائل. بينما ينخفض $S_{gen,T}$ مع زيادة E بسبب زيادة انتقال الحرارة بالحمل الحراري.

جمهورية العراق
وزارة التعليم العالي والبحث العلمي
جامعة بابل / كلية الهندسة
قسم الهندسة الميكانيكية

تداخل الصلب والمائع في الحمل المختلط لجريان مائع نانوي في تجويف بوجود جسم سداسي صلب

رسالة
مقدمة إلى كلية الهندسة – جامعة بابل وهي جزء من متطلبات نيل درجة ماجستير في علوم \ الهندسة \ الهندسة الميكانيكية \ قدرة

أعدت من قبل
حيدر نجم عبيد هجول

بأشراف
الأستاذ المساعد الدكتور حميد كاظم حمزة

2021 م ***1443 هـ***